MAREES TERRESTRES

BULLETIN D'INFORMATIONS

133

15 JUILLET 2000

Association Internationale de Géodésie

Commission des Marées Terrestres

Editeur Dr. Bernard DUCARME
Observatoire Royal de Belgique
Avenue Circulaire 3
1180 Bruxelles

BIM 133

15 Juillet 2000

VIRTANEN H.....
On the Observed Hydrological Environmental Effects on Gravity at the Metsähovi Station, Finland..
(Reprint from Cahier ECGS Vol.17)..... 10369

BOY J.-P., HINDERER J., AMALVICT M., CALAIS E.....
On the use of long records of superconducting and absolute gravity observations with special application to the Strasbourg station, France.**(Reprint from Cahier ECGS Vol.17).** 10377

MEURERS B. 10395
Gravitational effects of atmospheric processes in SG gravity data.**(Reprint from Cahier ECGS Vol.17).** ....

EL WAHABI A., DITTFELD H.-J., SIMON Z.....
Meteorological Influence on Tidal Gravimeter Drift.**(Reprint from Cahier ECGS Vol.17).** 10403

PAGIATAKIS S.D.....
Application of the Least-squares Spectral Analysis to Superconducting Gravimeter Data Treatment and Analysis.**(Reprint from Cahier ECGS Vol.17).**..... 10415

TIMOFEEV V.Y., DUCARME B., YAKOVENKO V.S., DUCHKOV A.D., SARITCHEVA Y.K., KUCHAI O.A., VANDERCOILDEN L., REVTOVA E. .....
Long-term and Tidal variation observed by tiltmeters and extensometers at the Ala-Archa Observatory (Tian Shan). 10427

TIMOFEEV V.Y., DUCARME B., SARITCHEVA Y.K., VANDERCOILDEN L.....
Tidal Analysis of Quartz-Tiltmeter Observations 1988-1998 at the Talaya Observatory (Baikal rift).... 10447

TIMOFEEV V.Y., DUCARME B., SEMIBALAMUT V., RIBUSHKIN A., FOMIN Y., VANDERCOILDEN L....
Tidal analysis of strain measurements in southwest part of Baikal rift..... 10459

LEDERER M., ZEMAN A. .....
Modelling of gravitational effects due to nonstandard atmospheric conditions. 10473

On the Observed Hydrological Environmental Effects on Gravity at the Metsähovi Station, Finland

Heikki Virtanen
Finnish Geodetic Institute
Geodeetinrinne 2, FIN-02431 Masala, Finland

Abstract

The importance of monitoring the hydrological conditions at the gravity station is demonstrated. Hydrological environmental effects have been observed to cause temporal gravity variations. Examples for years 1994 - 1999 are presented, observed by the superconducting gravimeter at the station Metsähovi, Finland. The gravity laboratory is on the bedrock. The groundwater level is recorded in the borehole nearby, its value showing a correlation with gravity residuals. In addition, the water equivalent of the snow cover has proved to be of significance when gravity is measured. An example of the observed loading effect of snow on the roof of the gravity laboratory is presented. Model calculations for gravity effects of snow cover, as a part of hydrological circulation, reveal that this effect should be noticed at station during winter conditions.

Introduction

Hydrological effects have been known to be a source of error in gravity studies for a long time (MÄKINEN, J. and TATTARI, S., 1991). The superconducting gravimeter (SG) T020 participating to the GGP project, started registering in August 1994, at the Metsähovi station, in Finland (VIRTANEN, H. and KÄÄRIÄINEN, J., 1995). The gravity laboratory is on hard bedrock on a low hill surrounded by forest and swamps. Near the building, there is a 33 m deep borehole, with a diameter of 11 cm, for monitoring the groundwater (GW). Since November 1994 the level has been measured manually, with an accuracy of 1 cm. Initially, the observations were carried out only occasionally, i.e. once or twice a month, but later, since 1996, at least once a week. In March 1998, a pressure sensor was installed in the borehole and connected to a data-acquisition system. The sampling rate is once minute, and the measuring accuracy is within a few mm. The range of the level has varied from 5 to 7 m below the ground. The minimum often seems to be in autumn, as presented in the Figure 1. The comparison with regional annual precipitation, as presented in Table 1, reveals a correlation with the level of GW. High annual precipitation causes a high level of groundwater, as in the year 1998. Correspondingly, a low annual precipitation, as in the year 1997, kept the GW level low. Gravity residuals for the years 1994 - 1999 show a correlation with the level of the water table. The water equivalent of snow cover in the winter at the beginning of the year 1999 was fairly high compared to the years 1994 -1998. The idea of studying possible gravity effects due to snow on the roof and in the neighbourhood of the laboratory arose. The results obtained, both practically and theoretically, show that this, often neglected, effect is very important at all sites where snow exists.

The effect of groundwater level

Figure 1 depicts the gravity residuals from November 1994 to February 1999. Spikes and offsets, effects of large earthquakes and other similar disturbancies were removed from the raw data (1-min). The data was detided and reduced to hourly values using ETERNA3.3 programs (WENZEL, H.,-G.,1996). For air-pressure correction the admittance of 0.30 μgal/hPa was used. The tidal model at the site was applied and for long-periodic SSA, SA, and pole tide, the value of δ=1.16 was used. The observed curve, smoothed by splines, gives the value of the groundwater level in metres. The high residuals at the beginning of 1997 due to disturbances in the helium cooling system were omitted from the calculations. The regressions give the values of 2.0±0.2 μgal/m for the admittance of groundwater level. It corresbonds roughly to a 5% porosity of the rock for a Bouguer plate equivalent of saturated rock. This value depends to some extent on the degree of polynomial fit (3rd, 5th) used for drift corrections.

There is second borehole at a distance of about 50 m, which holds the pump for the water supply of the main building in the laboratory area. The records show that the level of GW responds quickly when the pump is working. The test was carried out: 3500 litres of water was pumped out. The level in the measuring borehole, at the nearby gravity laboratory, was lowered by 2.5 m during the time lapse of two hours, but no clear effect on the observed gravity was found.

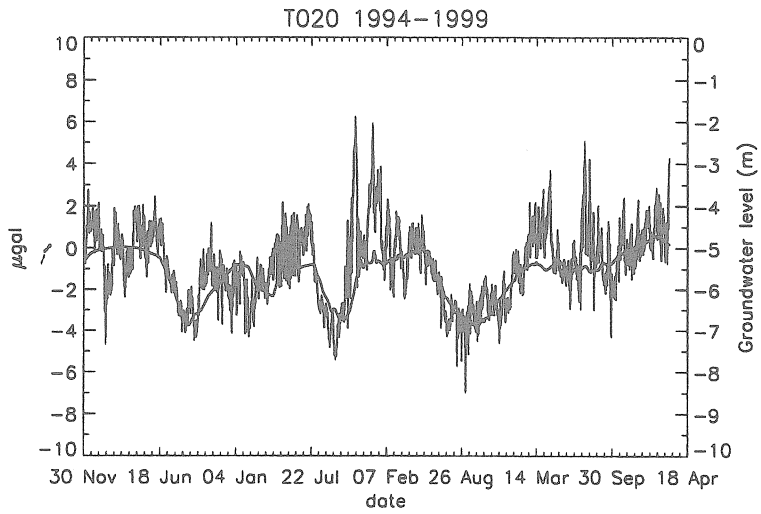

Figure 1. Tide-free, air-pressure corrected gravity recording of SG T020 in μgal at the Metsähovi station (the scale in μgal at left), compared to groundwater level in m (the scale at right).

Table 1. Regional annual precipitation (P) in mm, order of GW range (O): the minimum, maximum and the range of level of groundwater (GW) in m.

Year	P	O	GW min	GW max	GW range
1994	676		-5.43	-5.35	
1995	650	2	-6.82	-5.08	1.74
1996	679	3	-6.70	-5.43	1.27
1997	557	1	-6.96	-5.13	1.83
1998	728	4	-5.90	-5.00	0.90
1999				-4.84	

The effects of snow loading

In February 1999 precipitation reached 200 - 300 % of the seasonal mean in the regional area of Metsähovi. Thus the water equivalent (WE) of the snow was above the normal level. Figure 2. depicts the regional WE of the snow cover measured at the distance of about 30 km from Metsähovi (Oulunkylä, Helsinki), taken from Monthly Hydrological Report of Finnish Environmental Institute (MHR, 1994 - 1999). The snow fell in relatively short period. Roofs were, in general, endangered by a high load of snow. The severe conditions initiated the idea of carrying out studies of snow loading on the roof of the SG laboratory and on the surrounding area. The roof, consisting of four slopes, has a total area of 225 m^2. On 9th March 1999, four lines were measured across the slopes, from four points midway between the corners and the top of building. In total, 24 points were measured on the roof. The special instrument was borrowed from the Finnish Meteorological Institute. The device is a simple balance, which gives, directly, the WE in mm of the snow column detached from roof. In addition, the heights of snow cover were obtained. The snow was distributed over the roof fairly smoothly, and the thickness of the snow cover varied from 50 to 70 cm, with a WE of from 80 to 120 mm. In the final result, the mean WE was 107 mm, which gave a total mass of 23 tons of snow loading. The work continued on 15 March in the terrain surrounding the laboratory. On that day the snow was dropped from the roof by caretakers, without our special research plan.This gave a chance, however, to observe directly and reliably the effect of snow loading. The results of this big mass transfer are shown in Figure 3. The curve represents the tide-free and air-pressure corrected recording for 15 March 1999. The duration of the work of snow removing was four hours, starting at 8 o'clock. The work progress is clearly seen, including lunch- and coffee breaks. The observed gravity increased and the total effect on gravity was 2.3 μgal. To verify these results, model calculations were needed. The roof covers an horizontal area of 12 × 16 m. The height varies from 2.5 to 6.5 m above the ground. The mesh models are shown in Figure 4. Every grid point includes a block of water, with dimensions of 50 × 50 × 10.7 cm. In addition, the fallen snow has been taken into account, lying at 1 m distance from the building, the uppermost part modelled as 0.36 m below the floor. The gravity-sensing unit (GSU) locates asymmetrically with respect to the midpoint of the roof, and 0.3 m above the ground. The sums of the gravity effects were calculated for 1280 water blocks, whose midpoints were on the mesh. This simple model gives a result, for the snow on the roof, of 1.95 μgal, and 0.35 μgal for the fallen snow. The signs of the effects were

opposite, thus the total effect was 2.30 μgal which is fully compatible with observation. A suitable model is useful for reducing both future and past data.

Snow cover was also partially mapped in the neighbourhood of the laboratory building. A rather sparse irregular grid consisting of 30 points, extended to 25 m distance from the building. The thickness of snow varied from 40 to 80 cm, and the WE from between 60 -and 120 mm. The values for the snow thickness were accurate, but the horizontal and vertical coordinates were estimated. The vertical height differences of the terrain near the gravity laboratory were - 1.5 - 0 m. This local model was extrapolated to a distance of 50 m, where the heights were taken from the digital heigt map of the National Land Survey of Finland. The total range of heights was from 49 to 57 m, the height of the gravity-sensing unit being 56 m. This approximate calculation of the gravity effects of snow cover gives a result of 0.4 μgal.

To estimate the theoretical effect of snow loading for a wider area, the digital height map of the National Land Survey of Finland was used as an aid. In this map the mean height for 25 × 25 m blocks are given. The gravity effects for these blocks were summed. The results show that a total gravity effect from 100 mm WE can reach up to 0.4 μgal, at distances from 50 m to 1 km. The heights varied from 42 to 70 m, most values were below GSU. This estimation shows that, in total, the observed gravity should increase by about one μgal from the snow cover.

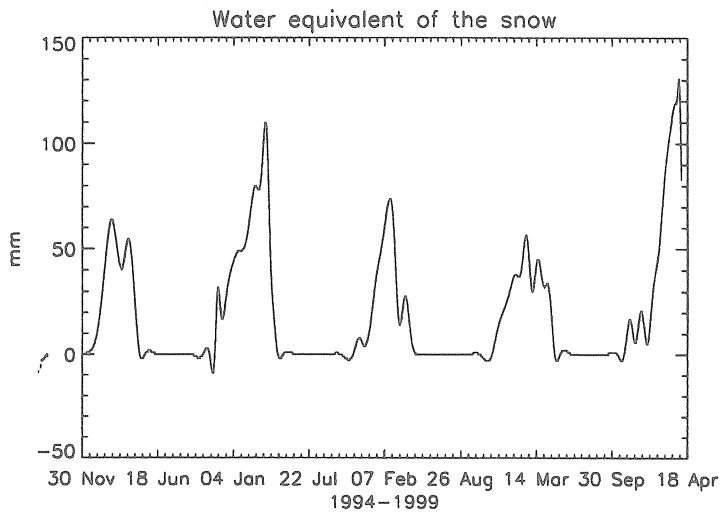

Figure 2. Regional water equivalent of the snow for years 1994 - 1999, taken from *Monthly Hydrological Report of Finnish Environmental Institute.*

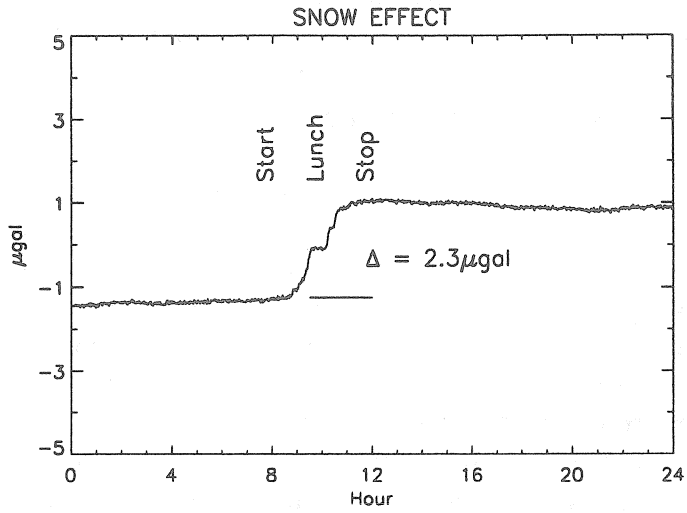

Figure 3. Gravity effect of removing the snow from roof on 15 March 1999.

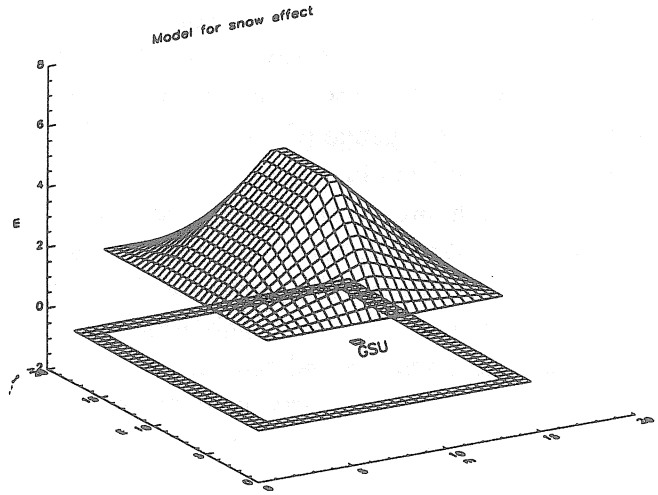

Figure 4. The mesh model for the gravity laboratory calculation of the snow-loading effect.

Conclusions

After removing known effects on gravity, such as tides, polar motion and air-pressure, the residual curve clearly shows a correlation with the observed groundwater level. This means that the level of the groundwater indicates the variations in the mass of bedrock or of the soil of the surrounding terrain. The gravimeter stands on a small hill, on the hard bedrock. If this long-periodic water variation is modelled using the Bouguer-plate, it gives a value for the porosity of the rock of about 5% or 100 mm water. This is a relative high value for water content in the bedrock, which is exposed for a distance of 15 m around the SG. The pumping test indicates, that the groundwater is in the aquifers in the bedrock in this area.

The terrain is sloping down 5 m at distances of about 50 m from the station and then slowly rising. It is observed that the contribution of soil moisture could be as important as the variation of the groundwater level on the gravity measurements (MÄKINEN, J. and TATTARI, S.,1991). In Finland, the annual effect can rise up to 10 μgals. This means that the heights of the terrain and the soil moisture should be mapped in detail, up to a distance of about 100 - 200 m from the gravity station. Also, where the terrain is swampy, larger areas should be studied. The water level seems to be at a minimum in autumn, because of evaporation during the summer. If there is plenty of rain, the level will high. It is necessary to know the correlation with the soil moisture in the terrain around and with the water level in the borehole. To monitor soil moisture regularly, some access tube should be established. It is possible that the borehole will also be a good indicator of soil moisture. Thus, the level of groundwater could be related to gravity reductions directly.

The effect of snow loading on the roof can be calculated accurately and the WE measurements carried out. The effect can be over 2 μgal, even though in normal winters the snow will melt more quickly on the roof than on the surrounding terrain. The properties of snow in the neighbourhood of the gravity laboratory should be studied in detail every year for at least up to a distance of 50 m. The local detailed digital height map is needed for this purpose.

In Table 1, only regional rainfall values are presented. Probably the values correlate with local precipitation. However, local rainfall measurements are necessary. Heavy local precipitation has been observed to have an influence on soil moisture and groundwater for some hours. The observed gravity has changed several μgals (CROSSLEY et.al, 1998, PETER et. al, 1995). At the end of May 1999, registering of rainfall at the Metsähovi station was started. The tipping-bucket type of rain gauge (CASELLA 10000E) is capable, with a 10 sec sampling rate, of measuring 72 mm of rain in an hour.

The performance of SGs makes the hydrological models necessary. The nature of these phenomena are periodic, annual or semi-annual, thus effecting the measurements strongly, e.g. long periodic tidal waves. The well-equipped gravity station needs the mapping of heights and knowledge of the hydrological conditions in the neighbourhood. This concerns most of stations. In addition, the weather conditions, groundwater level and soil moisture should be monitored regularly. The local recharge and discharge mechanism, for rainfall and snowfall should be modelled. The effects of an exceptional snowfall should be investigated at relevant stations.

Acknowledgements

Special thanks to senior research scientist Jaakko Mäkinen from the Finnish Geodetic Institute. He was the initiator of snow-loading measurements, and carried out practical studies on the roof and on the terrain around the laboratory. In addition, he has given valuable guidance on the hydrological effects on gravity variations.

References

CROSSLEY, D, XU, S., Van DAM., T, 1997:, Comprehensive Analysis of 2 years of SG Data from Table Mountain, Colorado, *Proceedings of the Thirteenth international Symposium on Earth Tides, Edited by B. Ducarme, P. Pâquet, Brussels 1998*

MHR, *Monthly Hydrological Report, Finnish Environment Institute, Hydrology and Water Management Division, 1994 - 1999, Helsinki*

MÄKINEN, J., 1991: The influence of variation in subsurfafe water storage on observed gravity, *Proceedings of the Eleventh International Symposium on Earth Tides, Helsinki 1989, edited by J. Kakkuri, pp 457-471, E. Schweizerbartst'sche Verlagsbuchhandlung, Stuttgart 1991.*

PETER, G., KLOPPING, F., BERTIS, K., 1995: Observing and Modeling Gravity Changes Caused by Soil Moisture and Groundwater Table Variations with Superconducting Gravimeters in Richmond, Florida, U.S.A, *Cahiers du Centre Européen de Géodynamique et de Séismologie, Volume 11, pp. 147-158, Luxembourg 1991.*

WENZEL, H.-G., 1996: *Earth Tide Data processing Package ETERNA3.3, Black Forest Observatory, Schiltach, Karlsruhe.*

VIRTANEN, H. and KÄÄRIÄINEN, J., 1995: The installation of and first results from the superconducting gravimeter GWR20 at the Metsähovi station, *Rep. Finn. Geod. Inst. 95:1, Helsinki.*

On the use of long records of superconducting and absolute gravity observations with special application to the Strasbourg station, France

Jean-Paul Boy[1], Jacques Hinderer[1], Martine Amalvict[1] and Eric Calais[2]
[1]EOST-IPGS (UMR 7516 CNRS-ULP) 5 rue Descartes 67084 Strasbourg France
[2]CNRS (UMR Geoscience Azur) Sophia-Antipolis 250 rue Einstein 06560 Valbonne France

Abstract

This paper is a report mainly devoted to the gravimetric station near Strasbourg (France) where both superconducting and absolute gravimetry measurements are performed. After nine years of continuous recording (1987-1996), the superconducting gravimeter (SG) T005 was replaced by a GWR compact instrument model CO26 in July 1996. We show the first results obtained with the new data series and compare them to the previous 3000 day SG T005 record. We present here some analyses of superconducting gravimeter data which are now classical with SGs : determination of the Earth's response to polar motion in terms of gravimetric factors (amplitude and phase lag), of Free Core Nutation (FCN) parameters (eigenfrequency and quality factor) and detection of signals in the quart-diurnal band. The comparison between SG T005 and SG CO26 results clearly reveals the quality improvements of the newer GWR instruments and this allows to launch more precise studies of the Earth's response to various excitation sources like body tides, ocean and atmospheric loading, polar motion over a wide spectral range (from quar-diurnal tides to the Chandler component of the Earth's rotation). Our new tidal determinations are in agreement with the ones from

SG T005 3000 day record but exhibit a significant reduction of instrumental perturbations such as noise level and long term drift. We also show that a repetition of precise absolute gravity measurements superimposed onto continuous SG recording provides useful information in the challenging problem of the determination of sub-centimetric vertical displacement. The special case of the CERGA station near Grasse (France) where absolute gravimetry is collocated with permanent GPS is also presented.
Key words: Superconducting gravimeter, polar motion, Free Core Nutation, tides, absolute gravimetry, GPS.

1 Introduction

In February 1987 a superconducting gravimeter (SG), model GWR T005, was installed in an old fort near Strasbourg (France) (called J9 station) where a long tradition of relative gravity measurements was already existing. During more than 9 years, gravity, pressure and other parameters were recorded without levitation loss or important perturbations (no large gaps or offsets) at a 5 minute sampling rate from September 1987 to May 1996. This long record allows observations of polar motion effects on gravity (Loyer *et al.*, 1999) in agreement with an elastic Earth model (Dehant *et al.*, 1999) and with simple oceanic pole tide models (Agnew and Farrell, 1978). Many improvements of atmospheric corrections using global pressure data (Boy *et al.*, 1998a, b) instead of a local barometric admittance correction allow a good characterisation of the Earth's response to long period body tides and a validation of oceanic models (Schwiderski, 1980; Lyard *et al.*, 1998).

In July 1996 the older instrument was stopped and replaced without large gap by a newer compact SG model at the same place to further extend the 9 year series. Strasbourg station belongs to the GGP network (see Crossley et al. 1999 for an updated review) and the acquisition system was upgraded to be in agreement with GGP standards at 1 min sampling. We have 2 years of data without major perturbations such as offsets from July 1996 to April 1998 and this will allow us to compare gravity observations from SG CO26 to the previous 9 year record of SG T005.

We will separate three different frequency domains in the comparison of both instruments:

- Long period band where we investigate in particular instrumental drift and polar motion induced effects;
- Diurnal band where we study the differences in terms of gravimetric tidal factors; an inversion of Free Core Nutation parameters allows to

quantify those variations;

- Quar-diurnal band where we look for short period tidal gravity effects of small amplitude and begin a new study of non-linear effects on gravity measurements which may be caused by non-linear ocean loading.

In section 2, we show some preliminary characteristics of the new superconducting gravimeter, especially improvements in instrumental noise and drift reduction.
In section 3, we compare a previous retrieval of polar motion gravimetric factors (Loyer *et al.*, 1999) based on the 3000 day analysis of SG T005 data to a two year analysis of SG CO26 record.
In section 4, other long period contributions are examined and we discuss the potential use of long term gravity observations in tectonogravimetry. In addition to the Strasbourg station, we also present preliminary results from the CERGA station (Grasse, France) where permanent GPS is collocated with (repeated) absolute gravimetry.
In section 5, the inversion of Free Core Nutation parameters allows us to compare both instruments; SG T005 data are analysed using two year subsets and a whole 3000 day duration and SG C026 data using a 508 day long record.
In section 6, we investigate the quar-diurnal band in order to compare higher frequency records and to start a preliminary study of non-linear contributions to surface gravity originating possibly in the oceans.

2 Some preliminary characteristics

In this section, we present some characteristics of new SG models. The installation of SGs more than two decades ago was a high improvement in gravity recording. In fact, even good mechanical gravimeters such as Lacoste-Romberg instruments have a drift larger than 10 $nm\ s^{-2}$ (1 microgal) per day. This is obviously a problem for the determination of long period gravity variations and classical spectrum analyses could not be applied most of the time beyond the fortnightly tide. Figure 1 shows the drift behaviour of SG CO26 (top) and SG T005 (bottom).

The compact model is characterised by a very low drift (less than 10 nm/s^2 per year) which is confirmed by absolute gravity measurements using an absolute gravimeter FG5 206. The SG T005 had a much larger drift, but which could fortunately be easily modeled as an exponential decaying function with

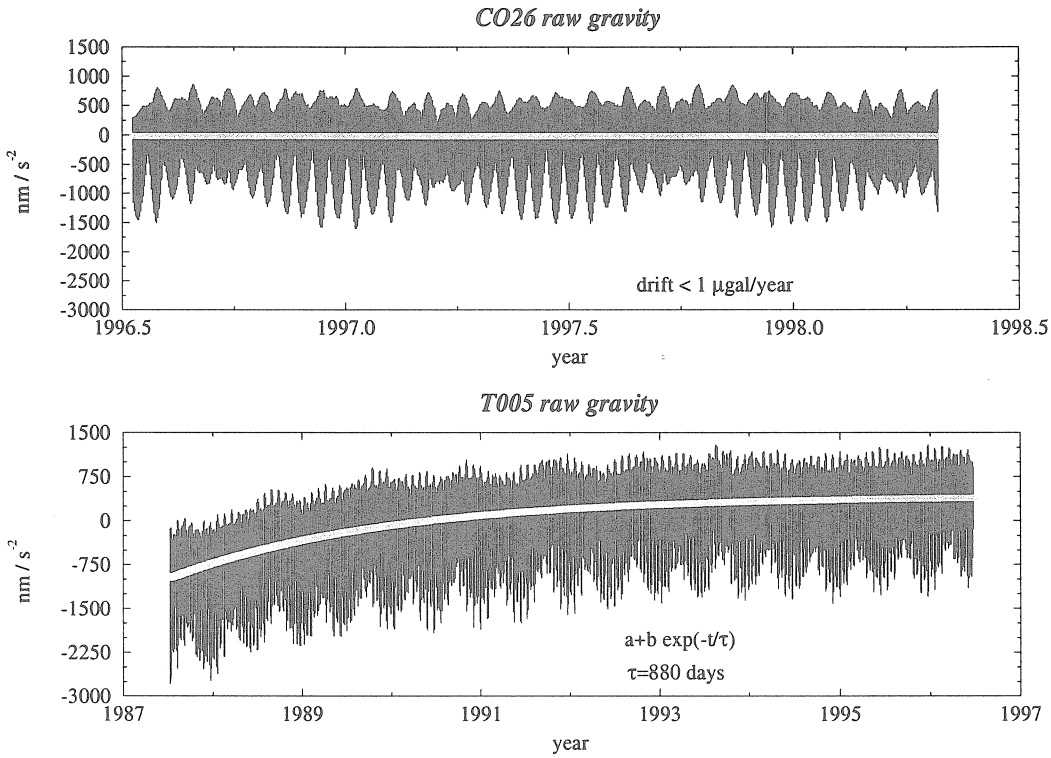

Figure 1: Instrumental drift of SG T005 and SG CO26.

a time constant τ found to be equal to 880 days.

$$d(t) = a + b \exp \frac{t - t_0}{\tau} \tag{1}$$

where a = 401.03 nm/s^2 and b = -1278.32 nm/s^2. The long period stability of SG CO26 allows a better modelisation of long period gravity changes, especially long period tides, polar motion effects, hydrogeology or tectonically induced secular effects. Such a low drift may even allow to detect in the future the Bradley wave of 18.6 year period.

The other high improvement of our newer compact SG is the reduction of instrumental noise as shown in Figure 2.

The spectrum of gravity residues after classical corrections (drift, tides and air pressure) shows a noise reduction of:

- a factor 10 for periods exceeding 10 days,
- a factor larger than 3 for periods smaller than 1 day.

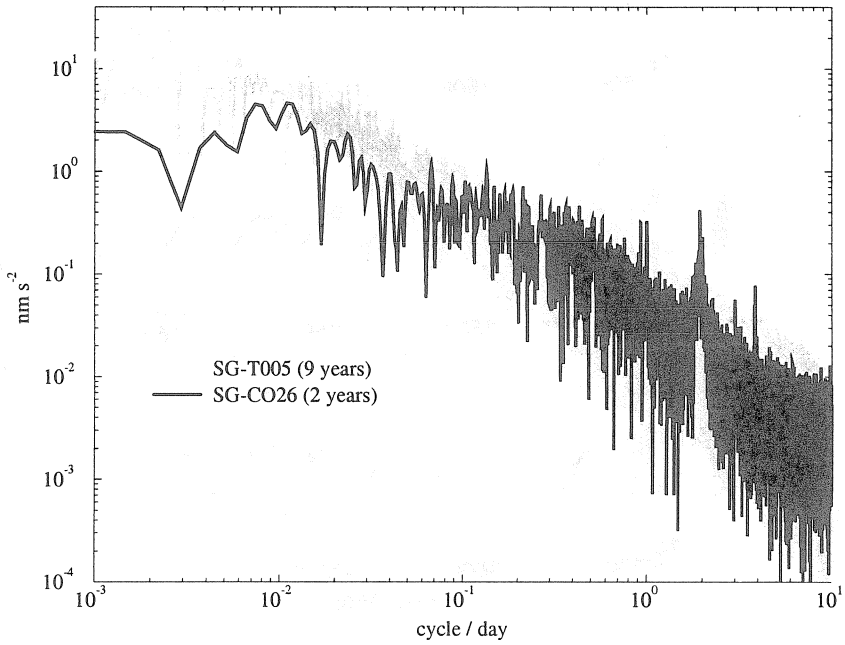

Figure 2: Spectrum of gravity residues (after correction of drift, tides and air pressure) for SG T005 and SG CO26.

In the intermediate frequency band, there is no apparent significant improvement of noise reduction for the compact SG. The higher quality of gravity measurements with newer models of SG allows a better estimation of tidal parameters, especially of the small degree 3 and 4 body waves (Hinderer et al. 1998a), and brings better conditions to the search for core modes (Slichter triplet for example) (see Jensen et al. 1995).

3 Gravity variations induced by polar motion

In a previous paper (Loyer *et al.*, 1999), we have determined the Earth's response to polar motion effects with the help of the pole gravimetric factors (amplitude and phase). Figure 3 shows gravity residues after tidal, global air pressure corrections and modelised polar motion effects and Figure 4 shows the variations of the gravimetric factors (δ, κ) according to the length of the data used for the estimation.

The adjusment of gravimetric factors (amplitude and phase lag) are found

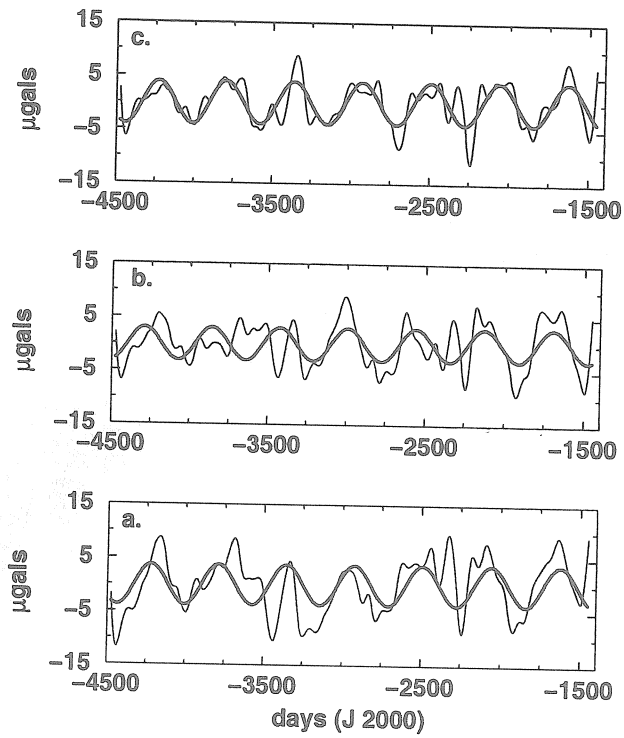

Figure 3: Gravity residues of SG T005 after tidal and air pressure corrections and predicted gravity change induced by polar motion (from Loyer *et al.*, 1999): (a) fit of Sa, Ssa and Chandler; (b) same as (a) + fit of long period tides; (c) same as (b) + fit of additional long period signals

equal to $\delta = 1.19 \pm 0.1$ and $\kappa = 22^o \pm 5^o$. The theoretical factors for an elastic Earth are equal to 1.16 for the amplitude and 0^o for the phase shift. Taking into account a static model of oceanic pole tide (Agnew and Farrell, 1978), the amplitude factor increases to 1.185 and the phase lag is less than 0.5^o. The adjusted amplitude factor is hence in agreement with the value predicted by the static model but not the phase lag and this fact points on an unknown additional contribution. It should be mentioned that the important phase lag which is observed cannot be due to the anelastic response of the Earth or to the oceanic polar tide which is not far from static equilibrium. This phase lag may be rather due to unmodelled gravity changes present in the long period range and possible candidates are changes in the water table level or rainfall.

In the Strasbourg station, in addition to the continuous recording of relative gravity by SG CO26 every 1 min, we also have regular series of mesurements of absolute gravity from AG FG5, model 206. Every month, we record absolute gravity during one week with a typical rate of one set every 15 min

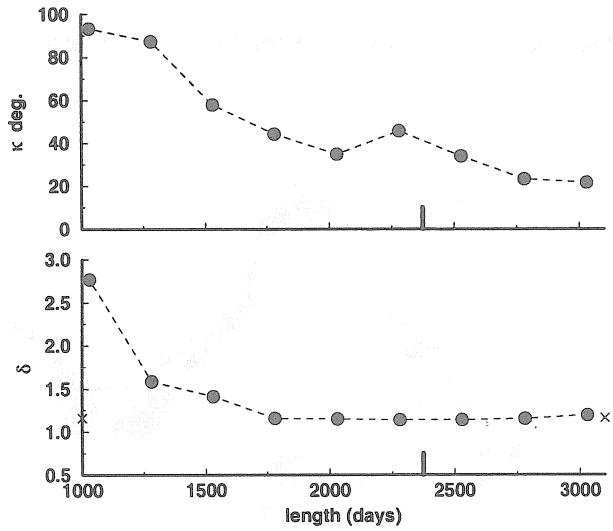

Figure 4: Variations of the gravimetric factors according to the length of data used for the estimation (from Loyer *et al.*, 1999).

consisting of 25 drop every 15 sec; this regular parallel recording is done for investigating the stability in time of the SG calibration factor (see Hinderer et al. 1998b) and to determine the SG instrumental drift which is shown to be very small (say less than a few microgal per year). Figure 5 shows AG and SG residues corrected for tides and air pressure, superimposed onto the theoretically predicted polar motion gravity induced effects using a gravimetric factor of 1.185 in amplitude and 0^o for the phase lag in order to take into account the static pole tide (see Agnew and Farrell 1978).

Despite a shorter duration as for the SG T005 record, there is a better agreement between gravity observations and theoretical polar motion effects. As shown by Figure 4, there are long period perturbations on the SG T005 gravity residues which are not present in SG CO26 ones. These differences may be due to a different response of GWR electronics or sensor to temperature or humidity changes between the older and newer SG. However, despite the agreement, it is still difficult to determine the polar motion gravimetric factors for SG CO26 and, as already discussed, this is due to the limited time span presently available. In fact, the convergence of the amplitude factor and phase lag is only reached after a 2000 day duration (Figure 3), which is the minimum time needed to separate the annual from the Chandlerian component of 435 day period. In fact, the presence of drift and noise can even further increase this duration.

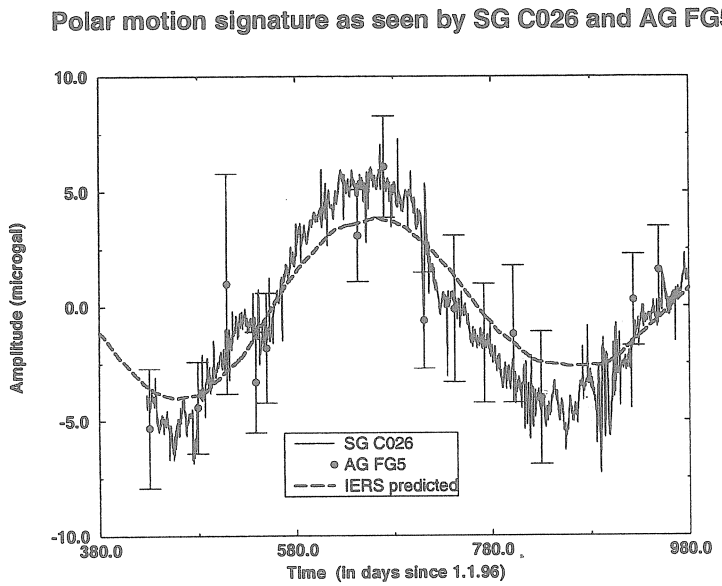

Figure 5: Comparison of SG CO26 and AG FG5 206 gravity residues corrected from tides and pressure.

4 Other long period gravity contributions

In addition to the study of the gravity changes induced by long-period tides and polar motion, the very low drift of SGs enables us to investigate other long term contributions of environmental effects (rainfall, hydrogeology including soil moisture and water table level changes) with strong seasonal and possibly secular components; we refer the reader to recent papers on this subject (Bower and Courtier 1998; Crossley et al. 1998).

Another subject of interest is the potential use of long gravity records (SG + AG) to investigate elevation changes due to tectonics or volcanic activity. Knowing that the standard vertical gravity gradient amounts to 3 microgal/cm, the observation of precise gravity changes at the microgal level can be translated in terms of uplift or subsidence at the sub-centimetric level (provided that no other mass tranfer occurs during the deformation). Figure 6 shows the superimposition of AG and SG in Strasbourg after subtraction of the same polar motion contribution exhibited in Figure 5. One can see that both types of measurements have a scatter of the order of 1-2 microgal and lie within the range ± 3 microgal corresponding to ± 1cm mentioned above. Of course, this is just an example of stability since the tectonic changes in the Rhine Graben are known to be presently sub-millimetric. The figure simply indicates the potential use of long term gravity measurements

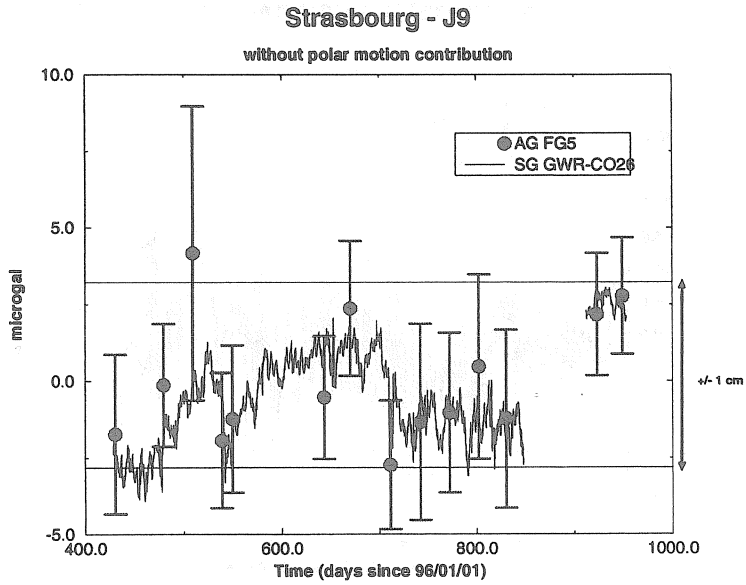

Figure 6: Long term gravity changes as seen by SG CO26 and AG FG5 206 after removal of polar motion contribution

in tectonogravimetry.

The other example concerns the space geodesy station (CERGA) near GRASSE in the southern part of France, where continuous measurements of permanent GPS are available together with regular AG measurements (roughly every 3 months). Figure 7 shows the series of AG observations at two different sites only separated by about 200 m (gravimetric station (G) and Lunar Laser Ranging station (L)) after conversion in vertical displacement using a (measured) vertical gravity gradient of -0.296 microgal/mm, as well as the vertical component of the GPS. It appears that the scatter of the vertical displacement in the GPS determination is slightly above 1 cm (SD = 12.1 mm) and is therefore comparable to what is seen by the AG in terms of gravity (SD (point G) = 8.8 mm and SD (point L) = 9.8 mm). Both techniques have their own advantages and disadvantages but they are clearly complementary and should be used in collocation in all tectonic problems exhibiting a significant vertical component. It is worth to mention here that our gravity values seem to confirm changes in vertical position obtained from laser ranging to the Moon (LLR) or to satellites (SLR) (see Nicolas et al. 1999); the intercomparison between GPS, laser telemetry and absolute gravimetry is still under investigation.

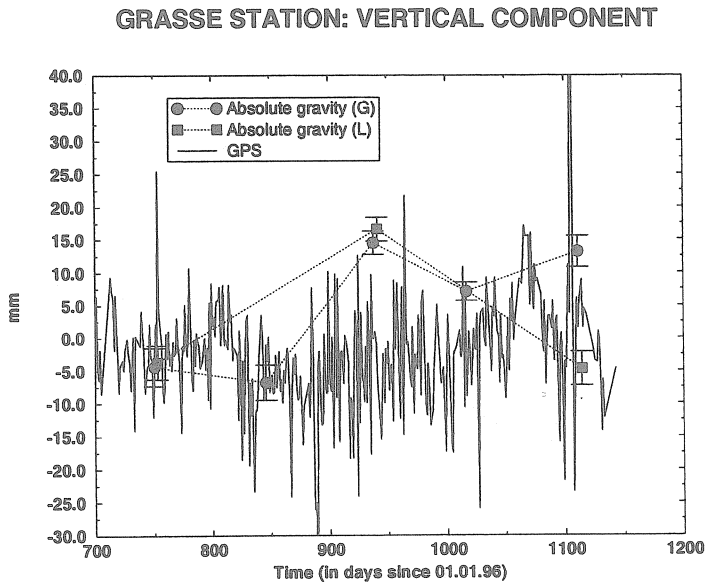

Figure 7: Long term stability in gravity (FG5-206) and vertical GPS in Grasse, France (gravity is transformed in vertical displacement by using the measured free air gravity gradient)

5 Diurnal tidal waves and Free Core Nutation

Superconducting gravimeters allow to determine with high precision the parameters of the Free Core Nutation (Richter *et al.*, 1995). However instrumental, atmospheric and oceanic perturbations perturb the inversion of these parameters (Florsch and Hinderer, 1998). The high quality of SG CO26 must improve the determination of the FCN parameters. Gravity data from SG T005 and SG CO26 are both analysed by the same processing programme ETERNA 3.30 (Wenzel, 1996). Gravimetric factors (amplitude and phase lag) are used in the inversion of FCN eigenfrequency and strength (Equation 2).

Figure 8 and 9 show the gravimetric factors (amplitude δ and phase lag κ) for diurnal tidal waves O_1, P_1, K_1 and Ψ_1 respectively for the following time intervals (Hinderer *et al.*, 2000):

- successive two year analyses of SG T005 data,
- the 3000 day analysis of SG T005,
- the two year analysis of SG CO26.

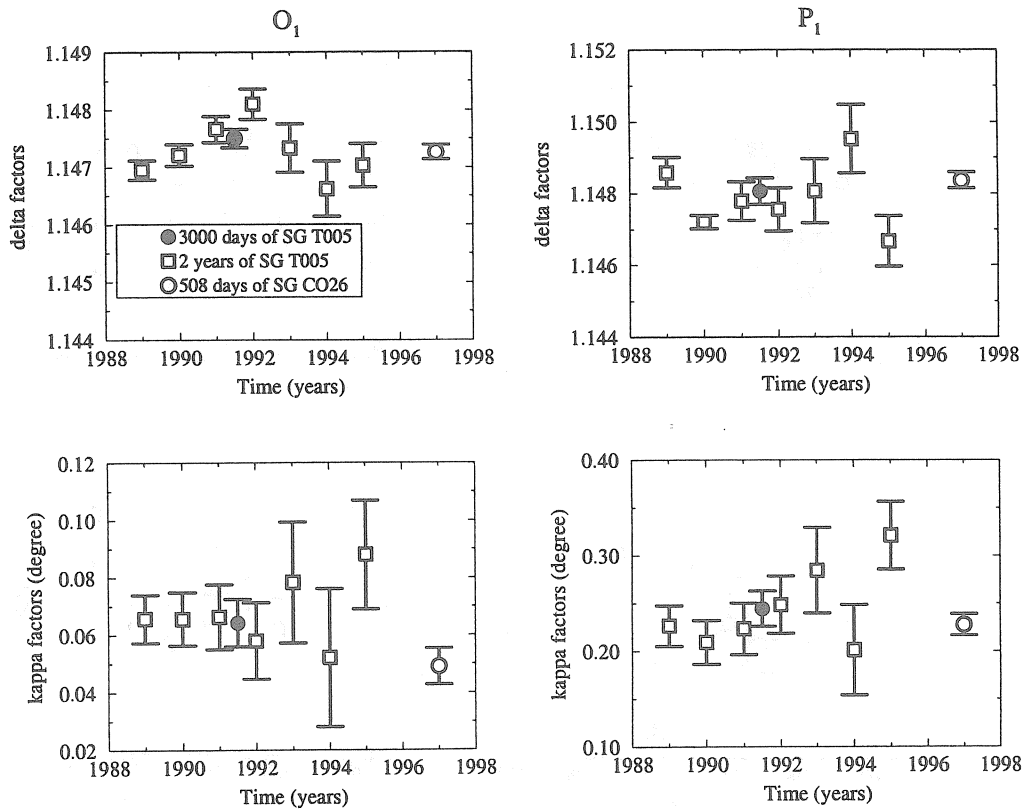

Figure 8: Time variations in gravity tides (O_1 and P_1) (from Hinderer *et al.*, 2000).

As shown in previous figures, there is a significant noise reduction (here in term of errors bars) for the 2 first years of SG CO26 gravity records. Variations of gravimetric factors $\tilde{\delta}$ as a function of frequency σ are equal to (Neuberg *et al.*, 1987):

$$\tilde{\delta}(\sigma) = \delta_2 + \frac{\tilde{A}}{\sigma - \tilde{\sigma}_{fcn}} \tag{2}$$

where $\tilde{\sigma}_{fcn}$ and $\tilde{A}$ are respectively the complex eigenfrequency and the resonance strength of the Free Core Nutation.

Figure 10 and 11 show respectively the time variations of Free Core Nutation eigenperiod and quality factors.

Inversions of SG T005 and SG CO26 gravity records lead to similar results when account is taken of the errors bars. However, the smaller error bars in the gravimetric factors relative to the new data series allow as expected a more precise estimation of FCN parameters.

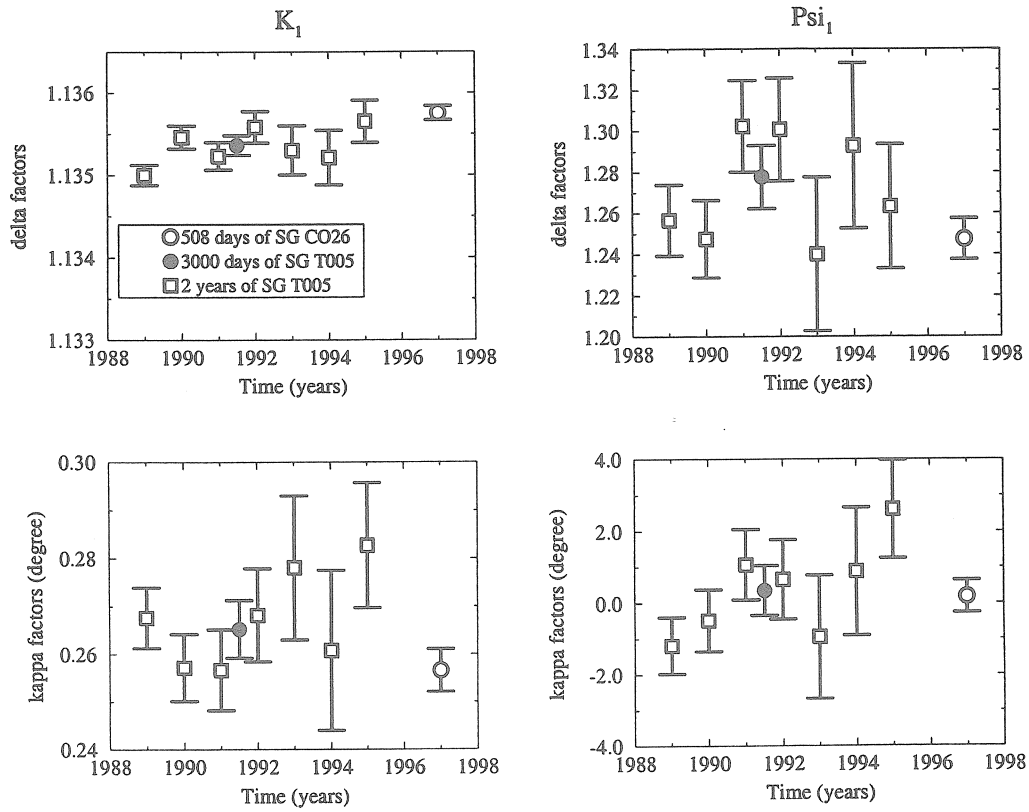

Figure 9: Time variations in gravity tides (K_1 and Ψ_1) (from Hinderer *et al.*, 2000).

6 Quar-diurnal tidal waves

Florsch et al. (1995) could achieve one of the first attempts to observe quar-diurnal tidal waves in a 6 year record (1987-1992) of SG T005, as well as in the SG data from Cantley station in Canada. However the high noise level present in SG T005 had first to be strongly reduced by a careful removal of perturbations (like spikes) existing in the quar-diurnal tidal band. This was needed by the fact that M_4 amplitude is smaller than 0.1 nm/s^2 and was right at the level of instrumental noise. The lower noise content of SG CO26 (Figure 2) led us to start a new investigation in this tidal band. Figure 12 shows respectively the gravity spectrum for SG T005 and SG CO26 (corrected for air pressure with an admittance close to -3.5 nms^{-2}/hPa) and theoretical body tides using degree 4 gravimetric factors (Dehant *et al. 1999*) . Notice that no specific corrections were applied to SG CO26 data instead of the strong despiking needed for SG T005 data. However, despite the difference in the duration of the two records (two years for C026 and nine

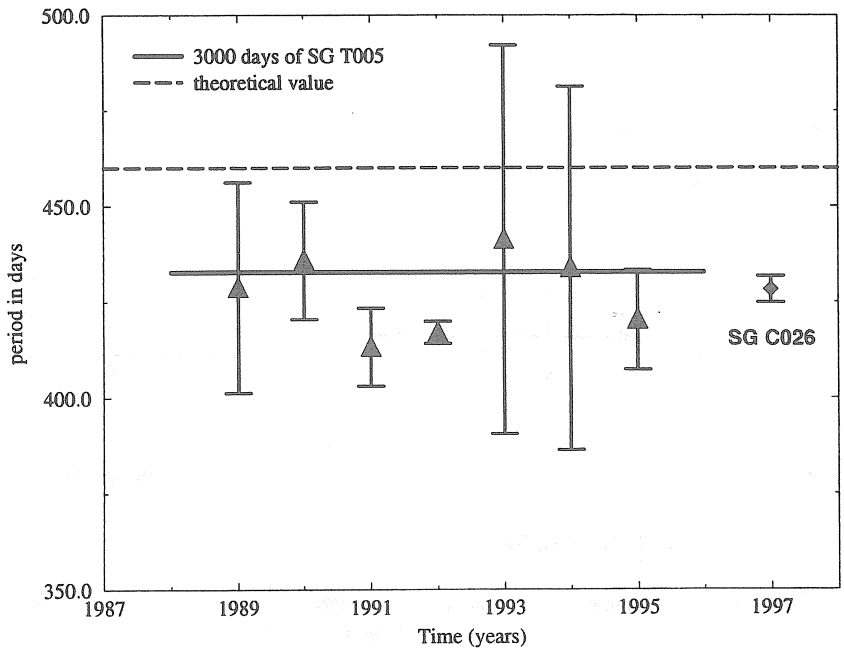

Figure 10: Time variations of FCN period (from Hinderer *et al.*, 2000).

years for T005), the achieved noise levels are almost similar.

Major waves (N_4, M_4 and S_4) are retrieved with an anomalistic amplitude for S_4 and M_4. For S_4, it is clearly due to the influence of the fourth harmonic of solar wave S_1 of thermal origin which cannot be corrected by the same barometric admittance as the meteorological continuum as shown by Crossley *et al.* (1995)(see also Boy *et al.*, 1998a); for the other tidal wave, it could be due to the influence of non-linear oceanic waves. Indeed a peak at 0.164 cycle per hour (6.098 hours) caused by a non-linear combination of M_2 and S_2 of oceanic origin is favoured for the moment.

7 Conclusion

Our first results from the analysis of two years of SG CO26 are globally in agreement with the results found from our previous long record of SG T005. However the strong reduction of instrumental drift (less than 10 $nm\ s^{-2}$ per year) and the lower level in noise (3 times smaller in diurnal and sub-diurnal bands, 10 times smaller for periods exceeding 10 days) allow us to estimate

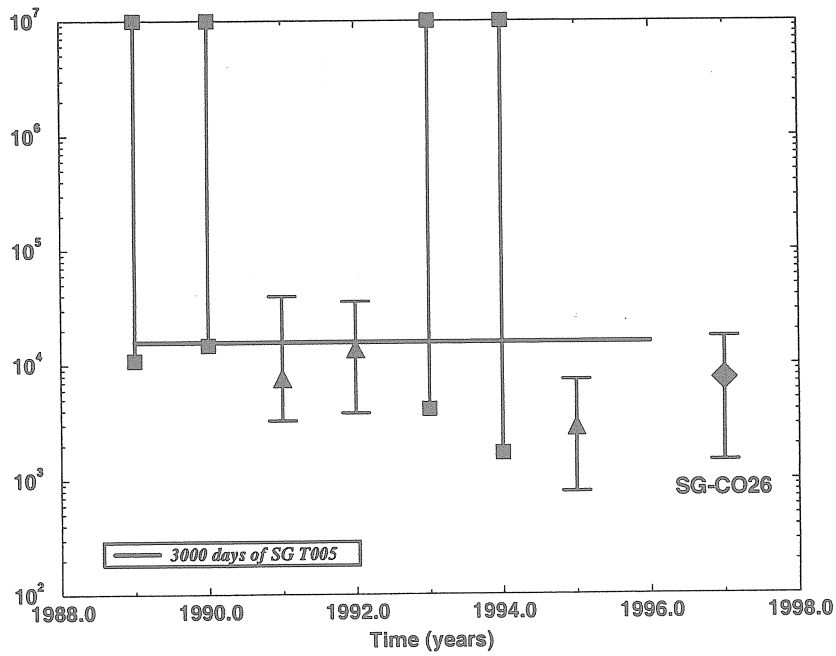

Figure 11: Time variations of FCN quality factor (from Hinderer *et al.*, 2000).

with much higher accuracy solid Earth tidal parameters (elastic deformation, phase lag) and to test more optimally oceanic models (Baker, 1998). The previously existing long period perturbations are no longer present in the new SG C026 series and this leads to a better restitution of gravity effects induced by polar motion. However, the existing two year duration is not yet sufficient to allow the separation of annual and Chandler components (6.5 years are needed) in order to estimate quantitatively the Earth's response to this long-period geodynamic forcing. We have also shown that thanks to the extremely low drift component of SG C026, both AG and SG measurements are very valuable to study the gravity stability in time. It is shown that for the Strasbourg station, our scatter in gravity residues (after removing all known corrections) leads to a sub-centimetric level in terms of vertical displacement (after conversion using the free air gradient). A similar experiment at the space geodesy station (CERGA) also confirms that AG measurements indicate a scatter comparable to the one present in the vertical component of GPS measurements suggesting that both techniques should be used at collocated stations. Inversion of the Free Core Nutation parameters show similar results for both SG records but the lower noise of the compact

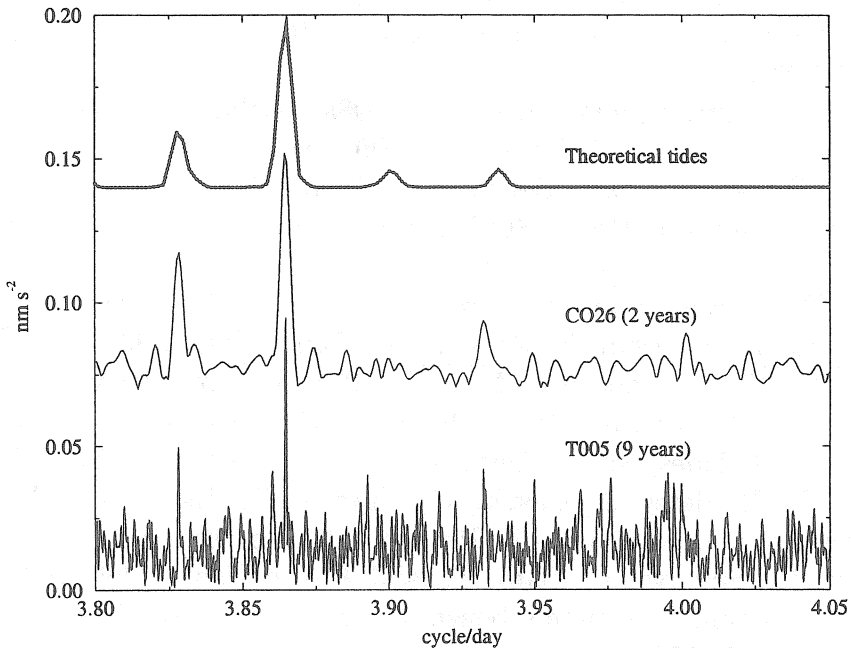

Figure 12: Quar-diurnal waves observed by both instruments and theoretical tides

model induces a better determination of tidal waves and hence a more accurate inversion of the eigenfrequency and quality factor of the FCN. In the quar-diurnal band, the identification of degree 4 tidal signals is facilitated by the lower noise content of SG C026 but there are obviously non-linear signals present which were already seen in the older series and of unknown origin for the moment. The improvement of recent GWR superconducting gravimeters allows now to start more precise studies in a wide frequency band ranging from yearly phenomena to hourly ones. In particular, in the sub-daily band, the effort will be devoted to the investigation of non-linear oceanic effects and to the detection of core modes including the Slichter triplet, especially by taking advantage of the stack of the numerous records available from the GGP network.

References

Agnew, D. C. and Farrell, W. E., 1978, Self-consistent equilibrium ocean tides, *Geophys. J. astr. Soc.*, 55, 171-181.

Baker, T. F., 1998, Tidal gravity observations and Earth tides models, *Proc.13th Int. Symp. Earth tides*, Brussels, eds. P. Pâquet and B. Ducarme, 287-294.

Bower, D. R., and Courtier, N., 1998. Precipitation effects on gravity measurements at the Canadian absolute gravity site, Phys. Earth Planet Int., **106**, 353-369.

Boy, J.P., Hinderer, J., and Gégout, P., 1998a. Global atmospheric loading and gravity, Phys. Earth Planet Int., **109**, 161-177.

Boy, J.P., Hinderer, J., and Gégout, P., 1998b. The effect of atmospheric loading on gravity, in Proc. 13th Int, Symp. Earth Tides, eds. B. Ducarme and P. Pâquet, Brussels, 439-446.

Crossley, D., Jensen, O. and Hinderer, J., 1995, Effective barometric admittance and gravity residuals, *Phys. Earth Planet. Inter.*, 90, 221-241.

Crossley, D., Su Xu , and van Dam, T., 1998. Comprehensive analysis of 2 years of SG data from Table Mountain, Colorado, in Proc. 13th Int, Symp. Earth Tides, eds. B. Ducarme and P. Pâquet, Brussels, 659-668.

Crossley, D., Hinderer, J., Casula, G., Francis, O., Hsu, H.-T., Imanishi, Y., Jentzsch, G., Käriänen, J., Merriam, J., Meurers, B., Neumeyer, J., Richter, B., Shibuya, K., Sato, T., and T. van Dam, 1999. Network of Superconducting gravimeters benefits a number of disciplines, EOS, **80**, No 11, 121, 125-126.

Dehant, V., Defraigne, P., and Wahr, J. M., 1999, Tides for a convective Earth, J. Geophys. Res, **104**, B1, 1035-1058.

Florsch, N. and Hinderer, J., 1998, Estimation of the Free Core Nutation Q factor from tidal analysis, *Proc.13th Int. Symp. Earth tides*, Brussels, eds. P. Pâquet and B. Ducarme, 315-322.

Florsch, N., Hinderer, J. et Legros, H., 1995, Mise en évidence d'ondes de marées quart diurnes de quelques pico-g d'amplitude l'aide de gravimètres supraconducteurs, *C. R. Acad. Sci. Paris*, T321, serie IIa, 279-285.

Hinderer, J., Boy, J.P., and Legros, H., 1998a. A 3000 day registration of the superconducting gravimeter GWR T005 in Strasbourg (France), in Proc. 13th Int, Symp. Earth Tides, eds. B. Ducarme and P. Pâquet, Brussels, 617-624.

Hinderer, J ., Amalvict, M., Florsch, N., Francis, O., and Mäkinen, J., 1998b. On the calibration of superconducting gravimeters with the help of absolute gravity measurements, *Proc.13th Int. Symp. Earth tides*, Brussels, eds. P. Pâquet and B. Ducarme, 557-564.

Hinderer, J., Boy, J. P., Defraigne, P., Roosbeek, F. and Dehant, V., 2000, Are the Free Core Nutation parameters variable in time ?, *Phys. Earth Planet. Inter.*, **117**, 37-49.

Jensen, O., Hinderer, J. and Crossley, D., 1995. Noise limitations in the core-mode band of superconducting gravimeter data, Phys. Earth Planet.

Int., 90, 169-181.

Loyer, S., Hinderer, J. and Boy, J. P., 1999, Determination of the gravimetric factor at Chandler period from Earth's orientation data and superconducting gravimetry observations, *Geophys. J. Int.*, 136, 1-7.

Lyard, F., Biancale, R. and Schwintzer, P., 1998, A new long period ocean tide model. Application to the satellite orbit determination and global gravity field model, *Proc.13th Int. Symp. Earth tides*, Brussels, eds. P. Pâquet and B. Ducarme, 519-519.

Neuberg, J., Hinderer, J. and Zürn, W., 1987, Stacking gravity tide observations in Central Europe for the retrieval of the complex eigenfrequency of the nearly diurnal free wobble, *J. Roy. astr. Soc.*, 91, 853-868.

Nicolas, J., Exertier, P., Bonnefond, P., Berger, Boudon, Y., Walch, J.J., Barlier, F., Calais, E., Hinderer, J., Crtaux, J.F., Boucher, C., and Haase, J., 1999. Collocation experiments at CERGA, IUGG99, Birmingham, UK, July 1999.

Richter, B., Wenzel, H. G., Zürn, W., Klopping, F., 1995, From Chandler wobble to free oscillations: comparison of cryogenic and other instruments in a wide period range, *Phys. Earth Planet. Inter.*, 91, 131-148.

Schwiderski, E. W., 1980, On charting global ocean tides, *Rev. Geophys. Space Phys.*, 18, 243-268.

Wenzel, H. G., 1996, The nanogal software: Earth tide data processing package ETERNA 3.30, *Bull. Inf. Marees Terr.*, 124, 9425-9439.

Gravitational effects of atmospheric processes in SG gravity data

Bruno Meurers
Institute of Meteorology and Geophysics
University of Vienna

Abstract

Some typical case studies of short term (< 120 min) gravity residual variations are investigated by comparing the air pressure signal and the residual gravity in high temporal resolution. Most of these events are connected with heavy rainfall and atmospheric processes characterized by high vertical convection activity. After almost perfect removal of even very short (< 20 min) pressure perturbations by applying a frequency independent admittance factor, a typical behavior of the gravity residuals can be observed. A common feature is a sudden gravity decrease followed by a very slow return to the previous level. Two models of vertical mass transport are used to explain the observations roughly.

Introduction

Atmospheric signatures can be detected very clearly in high quality gravity records. Gravity variations of different origin have already been interpreted e.g. by Müller and Zürn (1983) or Neumann and Zürn (1999). High temporal resolution records offer the possibility to observe gravitational effects of even very short term atmospheric processes. At the GGP station in Vienna a data set covering a period longer than 3 years is now available obtained by the super-conducting gravimeter GWR C025, that is operating since August 1995. Because of the very small and linear drift of this instrument the data is especially suited for investigating such effects. Selected short term variations in gravity and air pressure channels lasting for some hours to less than 10 min have been investigated in that respect.

Data base and processing

The GWR C025 is installed on a concrete pillar in the base floor of a huge building belonging to the Central Institute for Meteorology and Geodynamics in Vienna. The institute's building is founded in tertiary sediments (loess-like clay) that form a flat topography in its immediate vicinity. The base is situated about 7-8 m below mean surface level. Thus the gravimeter sensor position is below the soil layer that can be penetrated by water after heavy rain. Unfortunately there is no ground water level sensor available in the vicinity of the station. On the other hand a lot of meteorological parameters are permanently monitored, among others precipitation data in high temporal resolution (1 min). The corresponding data acquisition system is separated by only few tens of meters from the gravity site as part of a semiautomatic climate station (TAWES). Both, the threshold - for detecting precipitation - and the precision are 0.1 mm. Precipitation events of less amount are indicated only by a specific code. The data set of GWR C025 is acquired by using the high resolution gravity channel (HR-GRAV) sampled with 1 Hz and the pressure transducer output sampled with 0.1 Hz, respectively.

Gravity residual and air pressure data have to be investigated at 1 min intervals in order to detect gravity effects of even very short term atmospheric processes. For that purpose the raw data was calibrated and decimated to 1 min samples by applying appropriate numerical FIR

filters offered by the ETERNA v3.3 software (Wenzel 1996). Based on Tamura's (1987) tidal potential the gravity data set was detided using the tidal parameters derived from the analysis of hourly data that cover a three years' interval. In order to obtain the 1 h data set several preprocessing steps were performed based on the software packages ETERNA v3.3 (Wenzel 1996) and Tsoft (Vauterin 1997). Preprocessing consisted of degapping, despiking, destepping and decimating to 1 h samples. Despiking and destepping was done automatically. Thresholds of 2 and 5 nms^{-2} respectively have been applied for spike and step detection. Manual offset corrections were necessary only in three cases of known instrumental origin. The earth tide model for the Vienna station is very well defined now. It does not differ significantly from the results obtained previously (Meurers 1998).

In a second step, air pressure effects were removed from the gravity residuals by applying an admittance factor of $-3.533\,nms^{-2}/hPa$. This factor results from tidal analysis by assuming a pressure admittance factor that is constant within the tidal band. Of course, the air pressure admittance function is frequency dependent and perhaps not constant in time. Nevertheless, this method is well suited to investigate short term effects.

Case studies

A big amount of air pressure signatures have been investigated so far by comparing air pressure and residual gravity in high temporal resolution. In most cases a narrow correlation can be found even for pressure variations of less than 1–2 h duration. Generally their gravity response is almost perfectly controlled by the mean admittance factor mentioned above, although such events are often caused by very local meteorological processes which we do not expect to cause loading effects. Only sometimes a slightly higher factor is needed to remove the air pressure effect more effectively. A typical example of a cold front passage has been reported in Meurers (1999).

In addition, we found a lot of events showing very systematic residual perturbations with no or only weak correlation to air pressure variations. Three examples are shown in Figs. 1-3 comparing air pressure with gravity residuals before and after air pressure effect correction using the constant admittance factor.

The air pressure variation is quite different in these examples. In Fig. 1, air pressure is almost constant, only few perturbations of less than 1 h duration and in the order of less than 0.5 hPa can be observed. In contrast, Figs. 2 and 3 show short term pressure variations of different magnitude (up to 2 hPa) superimposed to long term trends. In all cases the air pressure effect can be perfectly removed by applying the frequency independent admittance model. In the examples shown above - and in several other cases - the gravity residuals obtained after air pressure correction show similar behavior. It is characterized by a steep residual decrease during a time interval of a few tens of minutes only. Afterwards, the residuals need some hours to return back to the previous level. A common feature of all these atmospheric events is the occurrence of heavy rainfall that was mostly connected with thunderstorms above or near the station. Another characteristic is a distinct time shift of 10 to 30 minutes between the drop of the residual curve and the begin of rainfall. The magnitude of the residual decrease (offset) is obviously well correlated with the amount of total rain fall connected with these events. This can be seen in Fig. 4. It has to be considered, of course, that only one rainfall monitoring station is perhaps not sufficient to characterize the amount of precipitation in the region, where the atmospheric process took place. This could be one reason for the scatter seen in Fig. 4.

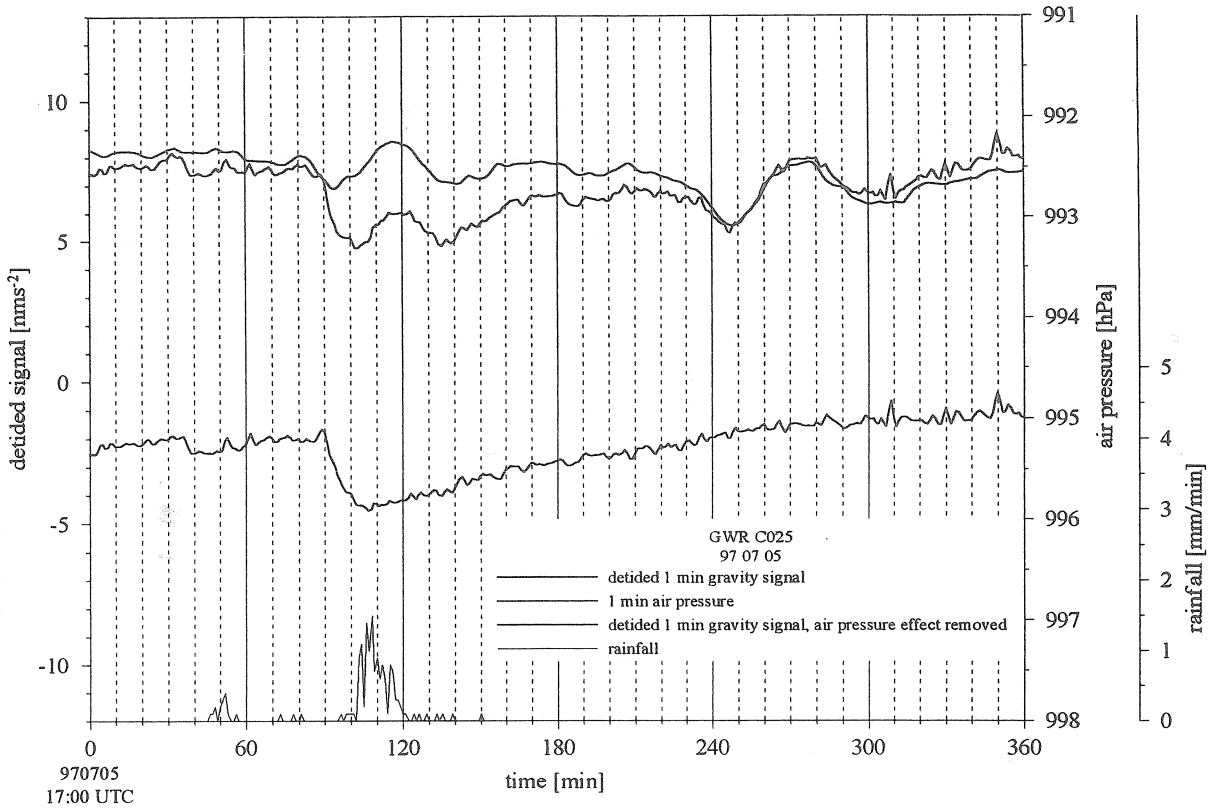

Fig. 1: Gravity residuals and air pressure observed by GWR C025 and rainfall(18-19h) in Vienna on 1997 07 05.

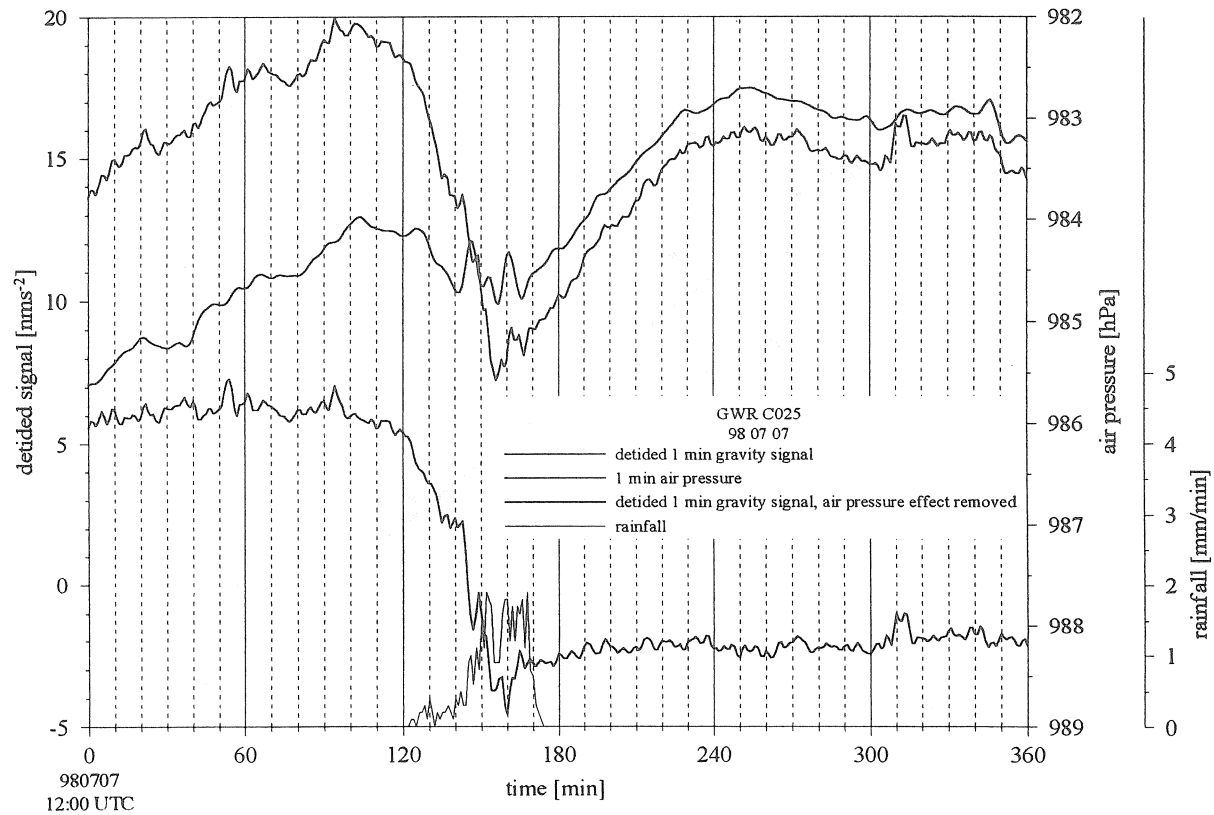

Fig. 2: Gravity residuals and air pressure observed by GWR C025 and rainfall(14:00) in Vienna on 1998 07 07.

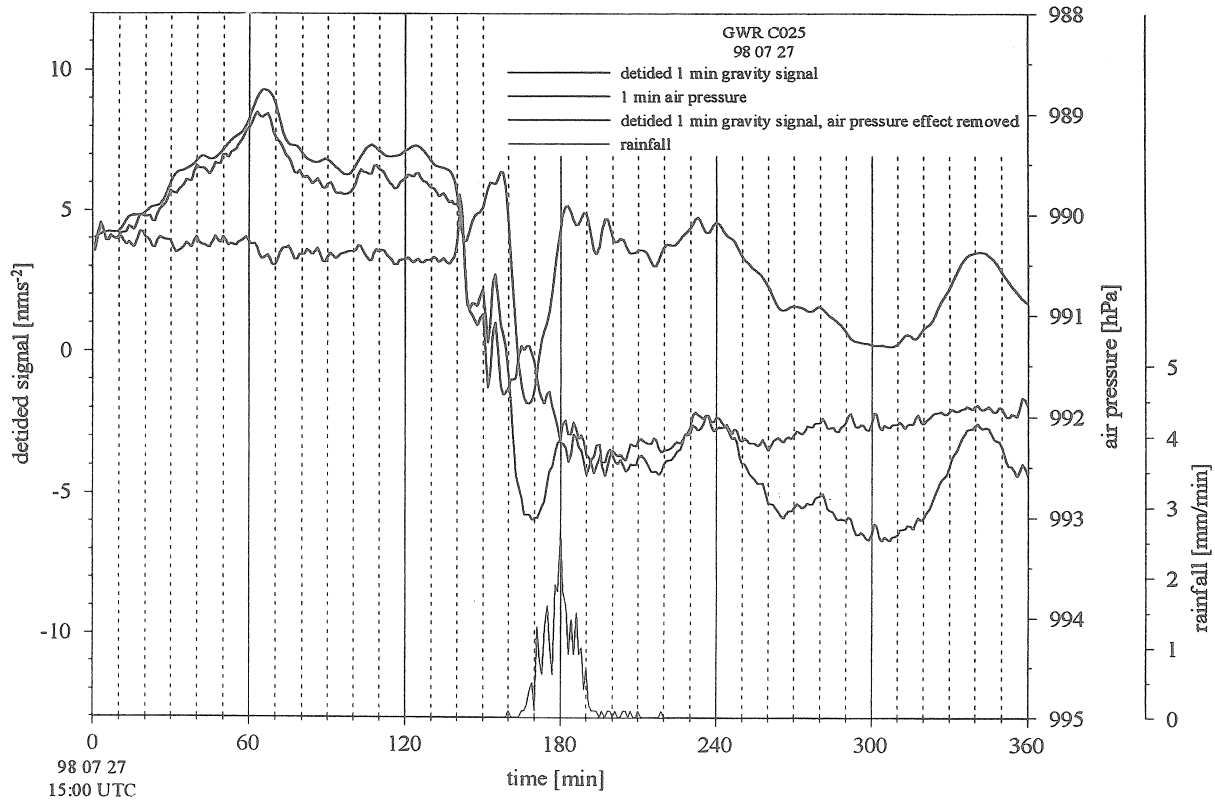

Fig. 3: Gravity residuals and air pressure observed by GWR C025 and rainfall(17:45) in Vienna on 1998 07 27.

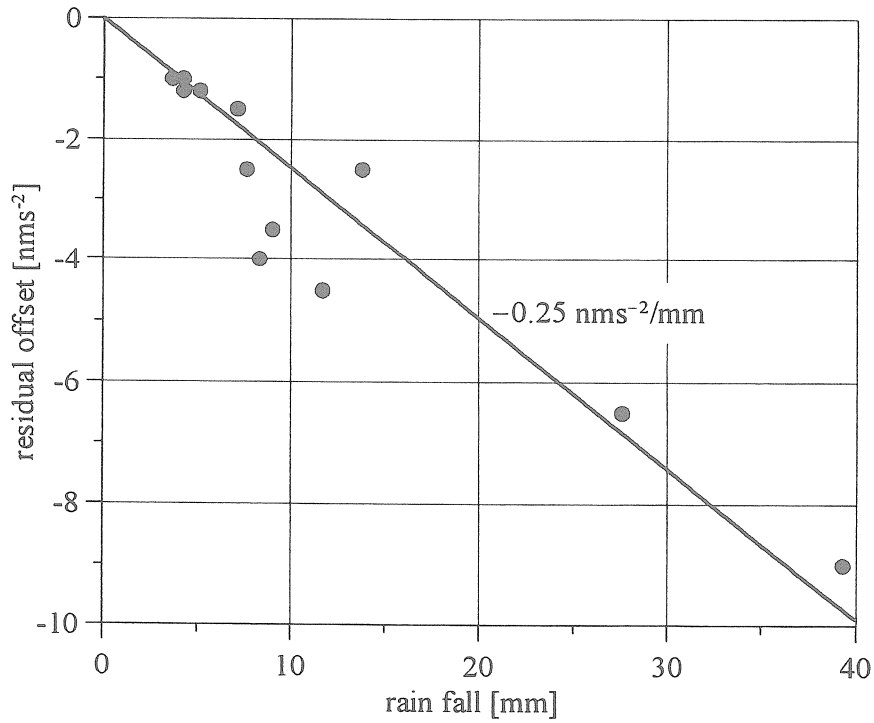

Fig. 4: Relation between gravity residual offset and total precipitation amount.

Interpretation

The gravity signals discussed above are most likely caused by vertical mass redistribution that has only small or even no air pressure effect. The fact that those events are mostly connected with thunderstorms or very heavy short term rainfall indicates atmospheric processes with a high amount of vertical convection activity. In order to give a rough estimate of the gravity effects, two very simple models have been developed that assume vertical mass flow either by air mass exchange or by water transport down to the ground.

- *Gravity effect of vertical air mass exchange without pressure variation*

The first model consists of two homogeneous cylindrical cells filled with air of different density. Both cylinders have the same radius r and vertical dimension h. At an initial state the air density is $\rho_0 + \delta\rho/2$ within the upper layer and $\rho_0 - \delta\rho/2$ within the lower layer, respectively. Therefore, the exchange of both air masses results in a density change of $-\delta\rho$ in the upper and $+\delta\rho$ in the lower layer.

In a coordinate system with positive z-axis pointing upwards, the gravity effect of a homogeneous vertical cylinder at the center of its lower surface is given by

$$g = 2\pi G\rho\left(h_2 - h_1 + \sqrt{h_1^2 + r^2} - \sqrt{h_2^2 + r^2}\right)$$

where h_2 is the height of the upper surface, h_1 the height of the lower surface and ρ the density of the cylinder. With $h = h_2 - h_1$, $h_2 = 2h$ and $h_1 = h$ for the upper cell and $h_2 = h$ and $h_1 = 0$ for the lower cell, the corresponding contributions are

$$g_u = -2\pi G\delta\rho\left(h + \sqrt{h^2 + r^2} - \sqrt{4h^2 + r^2}\right) \quad \text{and} \quad g_l = 2\pi G\delta\rho\left(h + r - \sqrt{h^2 + r^2}\right)$$

respectively. Then, the total gravity effect δg of the vertical mass transport is

$$\delta g = g_l + g_u = 2\pi G\delta\rho\left(r + \sqrt{4h^2 + r^2} - 2\sqrt{h^2 + r^2}\right)$$

The gravity effect as function of the cell radius r is shown in Fig. 5 for two models which differ in their vertical extent. In the example given here, the density contrast is $1.26 \cdot 10^{-3}$ kgm^{-3} corresponding to an isothermal air pressure variation of 1 hPa only. For a realistic horizontal size (e.g. r between 1 and 3 km) the gravity effect is similar to the one observed in the real case studies if the density contrast is properly adjusted by a factor of 2 – 10. This yields to a density contrast that is still quite reasonable.

- *Gravity effect of vertical water mass transport*

The second model (Fig. 6f) estimates roughly the gravity effect of redistribution of water in the atmosphere. Again, it consists of two homogeneous cylindrical cells with radius r. At an initial state a certain amount of water is distributed as vapor in the upper cell between the heights h_1 and h_2. All water is transported as precipitation down to the earth surface and remains there as a cylindrical layer of radius r and height h_0. The gravity sensor is assumed to be located at the center of the water layer's lower surface.

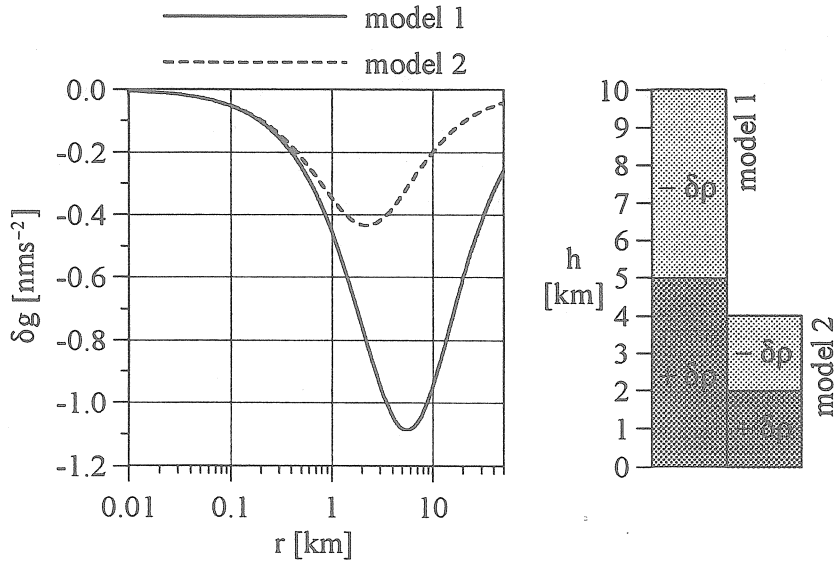

Fig. 5: Estimate of the gravity effect of a vertical air mass exchange.

As the total water mass is $m_w = \pi r^2 h_0 \rho_w$, the mean density of water and vapor within the upper cell amounts to:

$$\rho_v = \frac{m_w}{\pi r^2 (h_2 - h_1)} = \rho_w \frac{h_0}{h_2 - h_1}$$

The upper and the lower cylinder therefore contribute to the gravity at the gravimeter's sensor position (Figs. 6d and 6a) by

$$g_u = 2\pi G \rho_v \left(h_2 - h_1 + \sqrt{h_1^2 + r^2} - \sqrt{h_2^2 + r^2} \right) \quad \text{and} \quad g_l = 2\pi G \rho_w \left(h_0 + r - \sqrt{h_0^2 + r^2} \right)$$

If the gravimeter is housed in a building, the close surrounding modeled by a small disk with radius r_i around the sensor position does not contribute to gravity g_l. However, this small disk contributes most to the Bouguer plate effect. Its gravity effect g_i (Fig. 6b) has to be subtracted. If the sensor is not located immediately beneath the water layer but at a distance d downwards, then the following equation holds for the total gravity effect δg:

$$\delta g = g_l - g_i - g_u = 2\pi G \rho_w \times$$
$$\left[\sqrt{d^2 + r^2} - \sqrt{(h_0 + d)^2 + r^2} - \frac{h_0}{h_2 - h_1} \left(\sqrt{(h_1 + d)^2 + r^2} - \sqrt{(h_2 + d)^2 + r^2} \right) \right.$$
$$\left. - h_0 - \sqrt{d^2 + r_i^2} + \sqrt{(h_0 + d)^2 + r_i^2} \right]$$

Again, sign and order of magnitude of the gravity effect match observations, once a certain geometry is assumed, i.e. if the sensor is located not too close to the water layer. However, this model shows even that gravity effects of opposite sign are possible, but only for unreasonable cell sizes or if the gravity sensor is located in immediate vicinity of the lower surface of the water layer. In the latter case only the upper cylinder contributes to the gravity effect as long as a small inner disc has to be disregarded due to the station configuration. It has to be stressed,

that these results are very sensitive to the assumed geometry, and reliable estimates can only be given if the layer topography with respect to the sensor location is modeled in more detail.

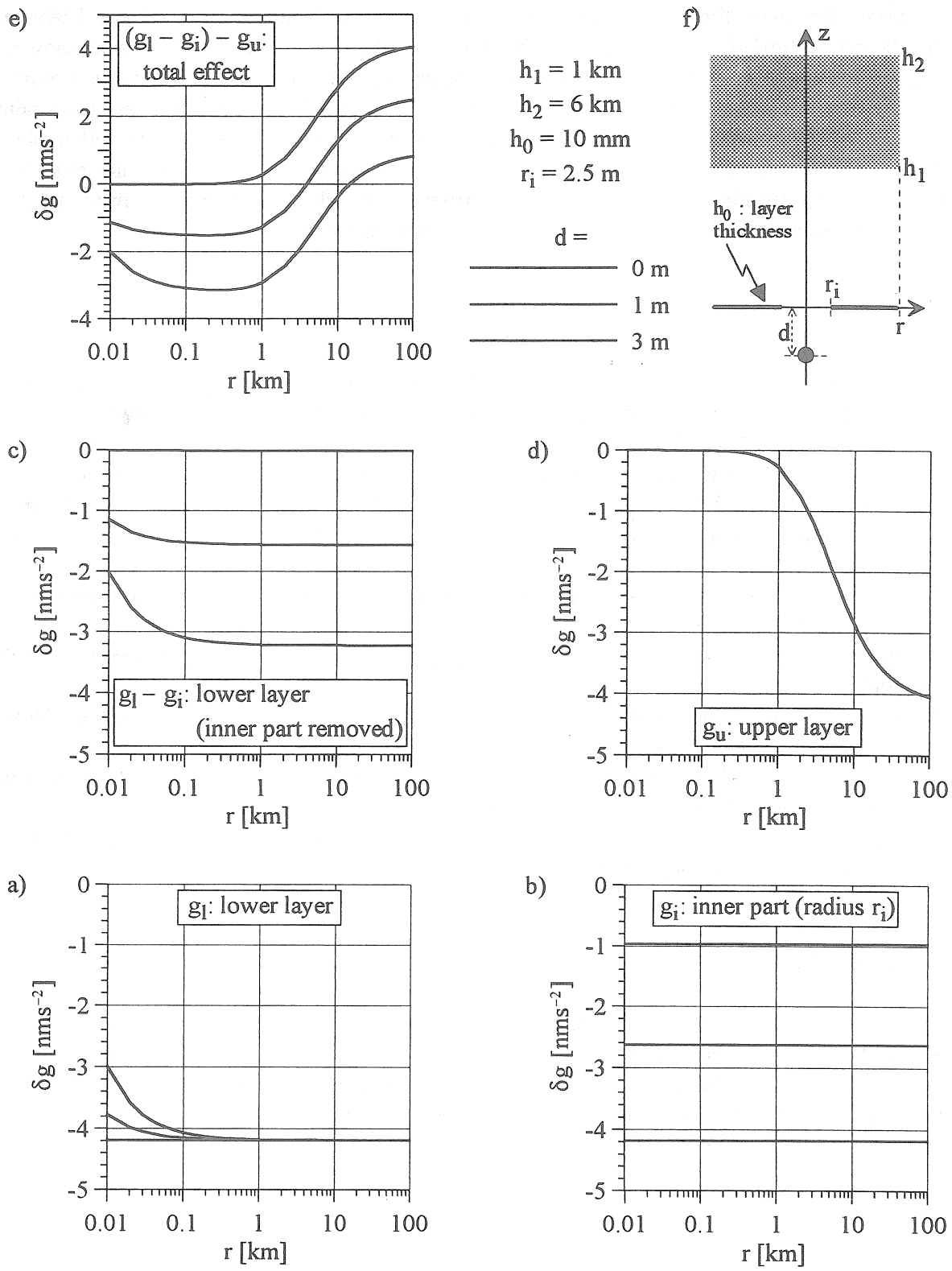

Fig. 6: Estimate of the gravity effect of vertical water mass transport. Water, equally distributed in a cylindrical cell of radius r between heights h_1 and h_2, is transported vertically down due to condensation and rain fall into a layer of thickness h_0. (a): Gravity effect of the water layer after rainfall. (b): Considering the gravimeter's surrounding, the gravity of a circular disk of radius r_i does not contribute. (c): Gravity effect of the water layer after rainfall taking (b) into account. (d): Gravity effect of the water distributed in the air before rainfall. (e): Total gravity effect at sensor position d. (f): Model geometry.

Conclusion

Both models presented above are in principle able to explain the amount of observed gravity decrease. However, the fact that the drop of gravity residual occurs 10 to 30 min before rain fall, favors vertical air convection to be the most probable interpretation. Increasing convective activity intensifies the process of water condensation and, additionally, enlarges the volume of the involved air mass. The correlation between the amount of residual offset and total rainfall can be possibly contributed to this fact. However, the presented models are rather simple. More detailed ones can be developed only if more meteorological parameters are available in the station surrounding. Nevertheless, this investigation will be continued in order to detect other influences of atmospheric processes not considered up to now.

References

Meurers, B., 1998: Gravity monitoring with a superconducting gravimeter in Vienna. In: Ducarme, B., Paquet, P. (eds): Proceedings of the 13th International Symposium on Earth Tides, Brussels 1997, 625-634.

Meurers, B., 1999: Air pressure signatures in the SG data of Vienna. In: Ducarme, B., (ed): Proceedings of the Working Group on "Analysis of Environmental Data for the Interpretation of Gravity Measurements", Jena, 1999. Bulletin d'Informations Mareés Terrestres, in press.

Müller, T. and Zürn, W., 1983: Observation of gravity changes during the passage of cold fronts. J. Geophys., 53, 155 - 162.

Neumann, U. and Zürn, W., 1999: Gravity signals from waves in the atmosphere and their modeling. Bulletin d'Informations Mareés Terrestres, in press.

Tamura, Y., 1987: A harmonic development of the tide-generating potential. Bulletin d'Informations Mareés Terrestres, 99, 6813-6855.

Vauterin, P., 1997: Graphical interactive software for the analysis of earth tide information. 13th International Symposium on Earth Tides, Brussels.

Wenzel, H.-G., 1996: The nanogal software: Earth tide data processing package ETERNA 3.30., Bulletin d'Informations Mareés Terrestres, 124, 9425-9439.

Acknowledgement

The author wishes to thank P. Melichar (head of dept.), N. Blaumoser, M. Göschke, S. Haden and R. Steiner from the Geophysical Department of the Central Institute for Meteorology and Geodynamics in Vienna for their cooperation. Rainfall data was made available by the Climatological Division of the same institute which is gratefully acknowledged.

METEOROLOGICAL INFLUENCE ON TIDAL GRAVIMETER DRIFT

A. EL WAHABI, H.-J. DITTFELD[a] and Z. SIMON[b]

Observatoire Royal de Belgique
Avenue Circulaire 3, Bruxelles, B-1180 Belgique
(E-mail : Abdelbar.Elwahabi@oma.be)

Abstract

Lately, the interest of measuring gravity on volcanoes has been increasing. However, the spring gravimeters we use are strongly influenced by the Earth tides and the meteorological parameters. So, it is necessary to remove their effects in order to obtain reliable gravity residuals which could be related to some geophysical phenomena such as the volcanic activity.

The effect of the Earth tides can be modelised precisely and then removed easily. The influence of the atmospheric pressure has been removed using a single regression coefficient which is normally close to -0.3 microgal/mbar. Generally, continuous gravity recordings show a large annual variation of the drift as a common feature, with a magnitude ranging from hundreds of microgals to a few mgals. This drift usually presents for the LCR gravimeters an obvious correlation with temperature variations and a negative correlation with air humidity measurements, both with a large phase lag. In the case of Askania gravimeters, we point out the fact that the humidity presents a positive correlation with the gravity data.

Previously, it has been suggested that the external temperature is the origin of this apparent drift. But, the experiment of Bastien et al (1990) in a controlled environment has shown that the air humidity may be directly responsible for the gravimeters drift as well. Moreover, in some stations (Pecny, Potsdam) where the temperature is controlled with an accuracy of ± 0.1°C, tidal gravimeters still show large annual variations in their drift. Finally, another spring gravimeter installed in a mine (Walferdange) where the temperature and the humidity are very stable shows only a linear drift.

All these examples led us to consider that the air humidity is one of the major meteorological parameters affecting the drift of the spring gravimeters.

I. Introduction

When studying gravity measurements in volcanic areas, we have always to cope with the fact that the gravity changes due to volcanic activity are very small compared to other geophysical or instrumental effects. Therefore, several corrections are needed to get reliable gravity residuals susceptible to reflect the volcanic effect.

(a) Geoforschungszentrum Potsdam, Telegrafenberg A 17- D14473 - Potsdam – GERMANY (E-mail : ditti@gfz-potsdam.de).

(b) Research Institute of Geodesy, Topography and Cartography, CZ25066 - Zdiby 98 – Praha-vychod.

Many effects influence gravity measurements; they can be :

- instrumental effects such as :
  - temperature and/or relative humidity,
  - atmospheric air pressure if it is not well compensated by the gravimeter.
- geophysical effects such as :
  - Earth tides,
  - atmospheric air pressure,
  - rainfall and snow,
  - water table,
  - geology of the area.
- volcanic effects through variations of elevation or changes in mass/density.
- a coupling effect tilt/apparent gravity : the tilt variations induce an instrumental effect on the gravimeters producing apparent gravity changes.

II. Order of magnitude

Volcanic activities produce gravity changes of some tens of microgals. If we want to detect those effects, we have to correct the data with a precision of at least 10 μgal. This corresponds to :

- 4% of the Earth Tides,
- 30 mbar of air pressure variations,
- 3 cm of elevation,
- attraction of a 10 cm thick rock layer.

On what concerns the temperature and the humidity, they cause an instrumental effect on spring gravimeters which can reaches an amplitude of about one mgal as a mean value on yearly period. The tilt effect is negligible if the gravimeter is properly adjusted; if not, the tilt can have a non linear effect.

III. Earth tides effect

We first analyse the Earth tides effect (Eterna, Wenzel 1996) which can be thus modelised with high accuracy and removed efficiently from the gravity measurements. If we are only interested in long period gravity variations, we can use a low-pass filtering.

IV. Air pressure effect

Considering the fact that, for the final residuals, we are looking for a precision of about 1 μgal for a period of one day, a simple linear regression using the local pressure (see table 1) is sufficient to correct the air pressure effect. We notice that the regression coefficient is near to –0.3 μgal/mbar except for the LCR3 and LCR8 where it is very high indicating that these gravimeters are not well compensated any more for air pressure variations and this probably because the pressure seals are not more airtight (El Wahabi et al, 1997; 1998).

	LCR ET19 (Schiltach)	LCR G365 (Potsdam)	LCR D002 (Potsdam)	ASK Gs223 (Pecny)	LCR G008 (Uccle)	LCR G003 (Etna)
Regr. Coef.	-0.303	-0,395	-0,321	-0,364	-1,882	-2,015
RMS error	± 0.0027	± 0.0015	± 0.0031	± 0.0035	± 0.0317	± 0.0371

Table 1 : Pressure regression coefficients in µgal/mbar (computed using Eterna Software). They are around –0.3 µgal/mbar except for the LCR3 and LCR8 which present obvious anomalies for air pressure.

V. Temperature and humidity effects

The relative humidity is closely dependent on the temperature. Therefore, it is difficult to separate their effects on gravimeters. Moreover, these effects depend on the frequency band which can be divided in three parts : short, medium and long periods.

1. Short periods

By short periods, we mean the periods from some minutes to a few hours. A typical example of a quick change of the temperature can be the switching on or off of the viewing lamp of gravimeters. This induces some perturbations due to the fact that the thermostat of the gravimeter needs a certain time to adjust itself. Fortunately, this takes only some minutes and so has no significant influence.

2. Medium periods

By medium periods, we mean the periods from some days to a few weeks, and for this band of frequencies, unfortunately, we have no example. For this reason, we decided to make an experiment in the fundamental station of the Royal Observatory of Belgium in order to study the temperature and humidity influences on spring gravimeters. The station, which is in the cellar, is thermostatised while the humidity is not controlled. Some exchanges of air masses are possible, especially, when opening the station door. We have at our disposal, a LaCoste & Romberg G8 and high precision pressure and temperature/humidity sensors. Our objectives are the following :

- the determination of the transfer function of the couple temperature/humidity between inside and outside the station,
- the study of the gravity changes with the temperature variations in a stable humidity environment,
- the study of the gravity changes with the humidity variations in a temperature controlled environment,

- the study of the correlation between temperature and humidity for each frequency band to decide which parameter is more suitable to determine the transfer function for the gravimeter responses.

As first results, we can notice in the figure 1 a large temperature perturbation (an increase of about 4°C) during three days (around 18 November 1998) to which corresponds a gravity residuals variation with a change in the slope following immediately after the steep fall of the temperature. This suggests a link between the gravity change and the corresponding temperature perturbation.

Another example given on the figure 2 shows a large perturbation in the temperature, a decrease of about 5°C, which is also correlated to the gravity residuals with a phase lag. Comparing the temperature and the relative humidity records, there is no clear correlation between these two parameters. We notice indeed, during the beginning of March 1999, a large increase in the relative humidity of about 11% in one day while the temperature remains stable and no significant change appears in the gravity residuals. However, in the middle of March, a decrease of relative humidity appears to be anti-correlated with the man made temperature perturbation. As a conclusion, it seems that the temperature has an effect on spring gravimeters for medium periods while the humidity might need more time to influence the gravimeter response.

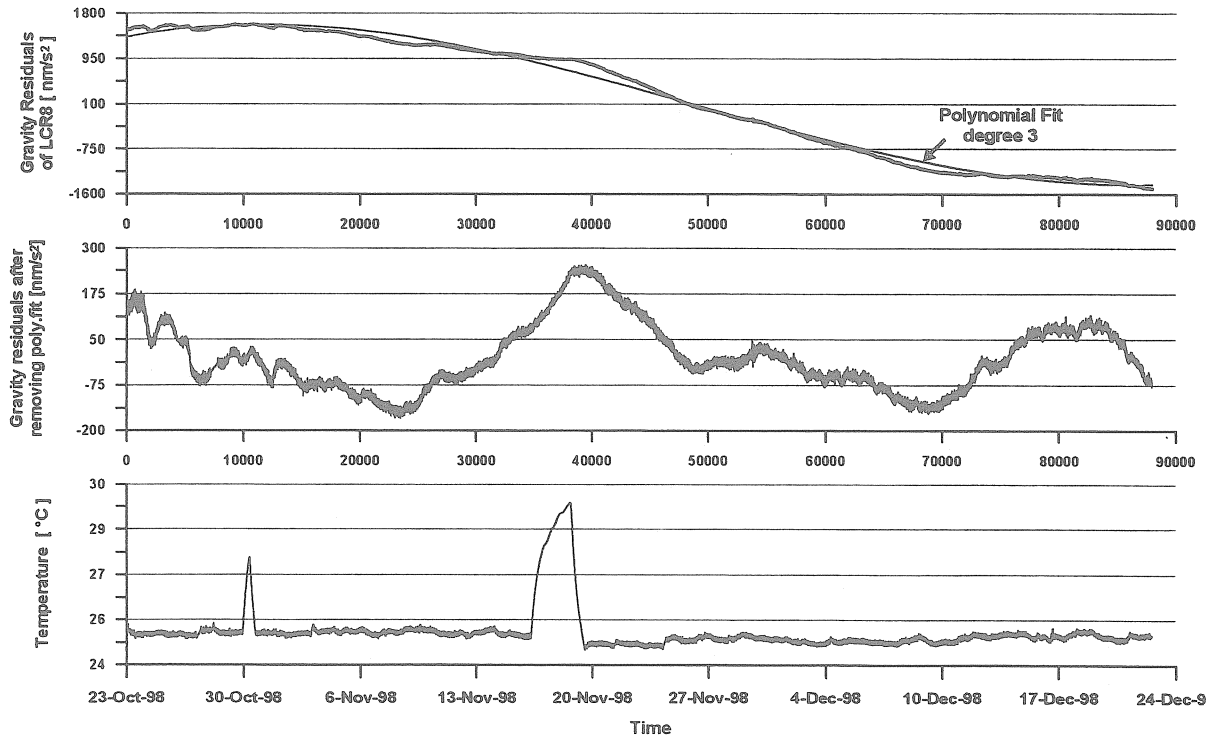

Figure 1 : Illustration of the LCR G8 drift with temperature variations in Brussels. From top to bottom : gravity residuals after removing the Earth tides and air pressure effects, gravity residuals reduced by a polynomial fit and temperature records with a big man made perturbation.

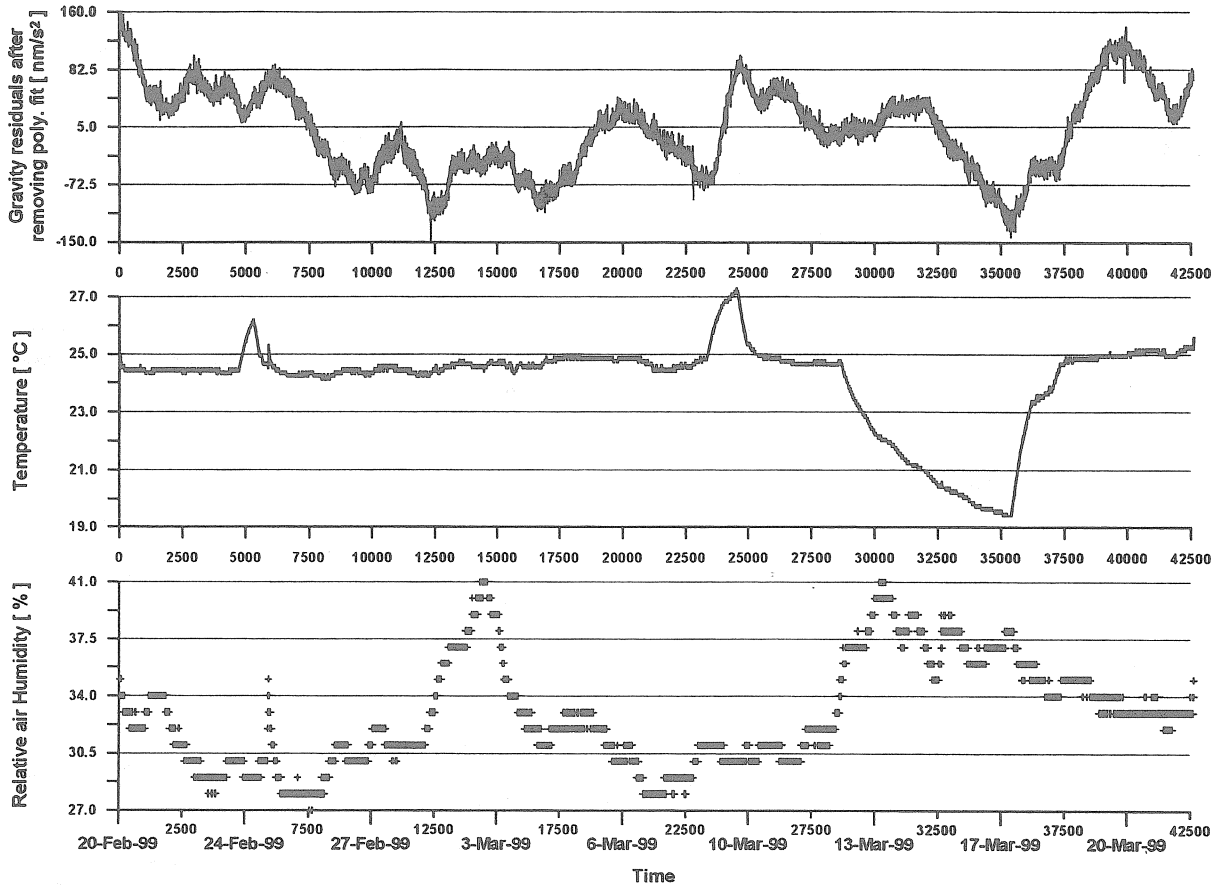

Figure 2 : Illustration of the LCR G8 drift with temperature and relative humidity variations in Brussels. From top to bottom : gravity residuals after removing the Earth tides and air pressure effects (also reduced by a polynomial fit), temperature records and relative air humidity measurements.

3. Long periods

Usually by long periods, we mean the periods of several months and especially the yearly cycles. We shall hereafter call the drift the non tidal apparent gravity variations after removing the pressure effect. Generally, the recordings of spring gravimeters present an annual oscillation of the drift which is correlated with the temperature and the relative humidity variations. The question is now to determine whether both of the two parameters are responsible of this drift or only one of them and, in this latter case, which one. The answer will be illustrated by means of the following examples.

The first one came from Centuripe, a station in the Etna area (Sicily), where the LaCoste Romberg (LCR) G3 was installed in September 1992. The obvious annual periodicity, that we see in the gravity residuals, is perfectly correlated with the temperature records (see figure 3). However, during the beginning of the measurements, the gravity residuals show a large perturbation (see figure 3 and 4) which coincides with the setting of a door in the station room. We think that the door could have limited the air circulation between inside and outside so that a new regime set in the air and heat exchanges. Looking at the station room temperature, no significant perturbation was recorded for the same period proving the fact that the drift perturbation was not due to the temperature effect (El Wahabi et al., 1997; 1998).

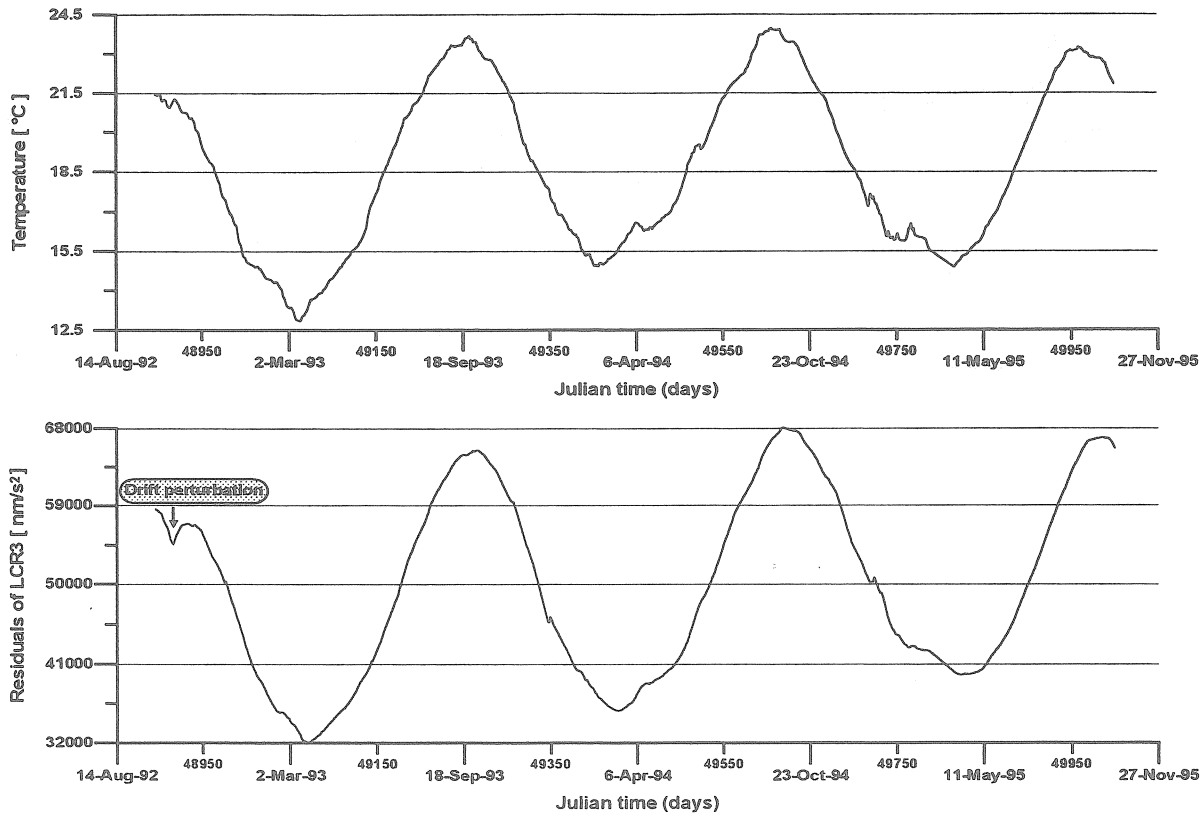

Figure 3 : Illustration of the LCR G3 annual oscillation with temperature variations in Centuripe. From top to bottom : temperature and gravity residuals after removing the Earth tides and air pressure effects.

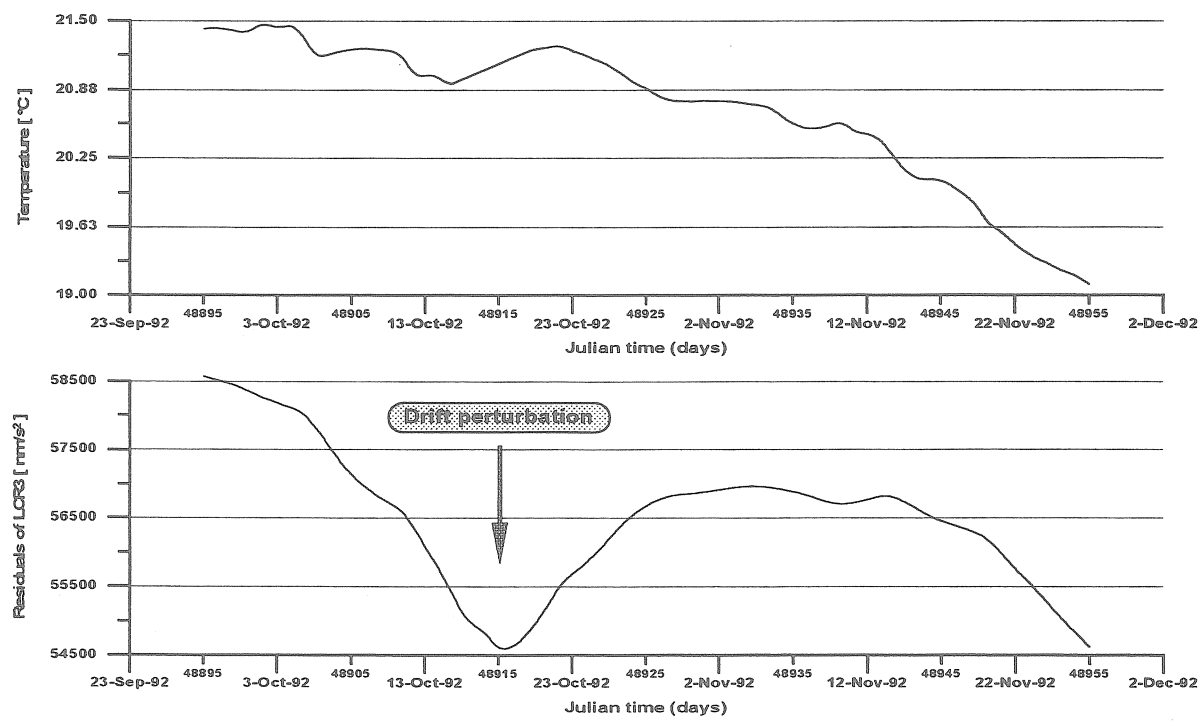

Figure 4 : Illustration of the LCR G3 drift perturbation with temperature variations in Centuripe (initial part of figure 3). From top to bottom : temperature and gravity residuals after removing the Earth tides and air pressure effects.

Now, comparing the annual oscillation of the same gravimeter, the LCR G3, in two different stations (Centuripe in Sicily and Lanzarote in the Canary Islands), we see in the figure 5 that the drift amplitude is more than twice bigger in Centuripe than in Lanzarote. Therefore, the annual periodicity is due to the environment where we put the gravimeters.

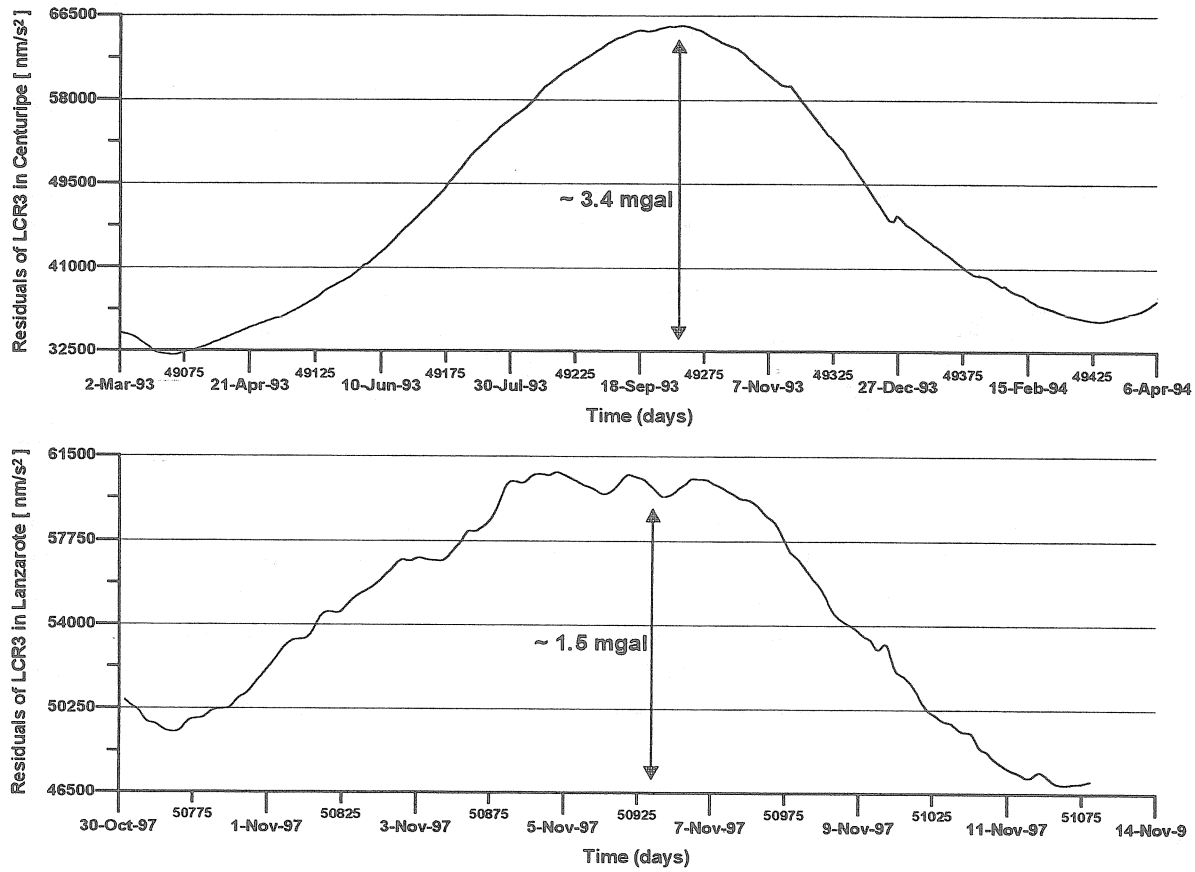

Figure 5 : Illustration of the LCR G3 annual periodicity in Centuripe (Top) and in Lanzarote (Bottom). In Centuripe the gravimeter had more than twice the drift amplitude recorded in Lanzarote.

In the other station in the Etna area, Serra-la-Nave, the LCR G8 was installed in January 1992. Due to a lack of heating power, the station room was imperfectly thermostatised. We decided later, in June 1994, to lower the thermostat. The result was a drop of the mean temperature in the station from 23 °C to 19 °C (see figure 6). This strong variation was not noticeable in the drift curve of the LCR G8, so that the room temperature was not the responsible parameter of the annual oscillation (El Wahabi et al., 1998). A cross-correlation shows a phase lag of about 44 days between the temperature outside the station (in the open air) and the temperature inside the station which itself is leading the gravity signal by about 25 days. The station is thus acting like a low-pass filter between the temperature outside and inside the station, as well as the gravimeter which is also acting like a low-pass filter between the temperature excitation in the station and the gravity response.

Looking now at the residuals of the gravimeters LCR/ZLS G385 (see figure 7) and LCR D2 (see figure 8) which are installed in Potsdam station, we see clearly an anti-correlation with the relative humidity while the temperature is stabilised in a range of ±0.1 °C. The phase difference between gravity and relative humidity signals is close to 180 degree.

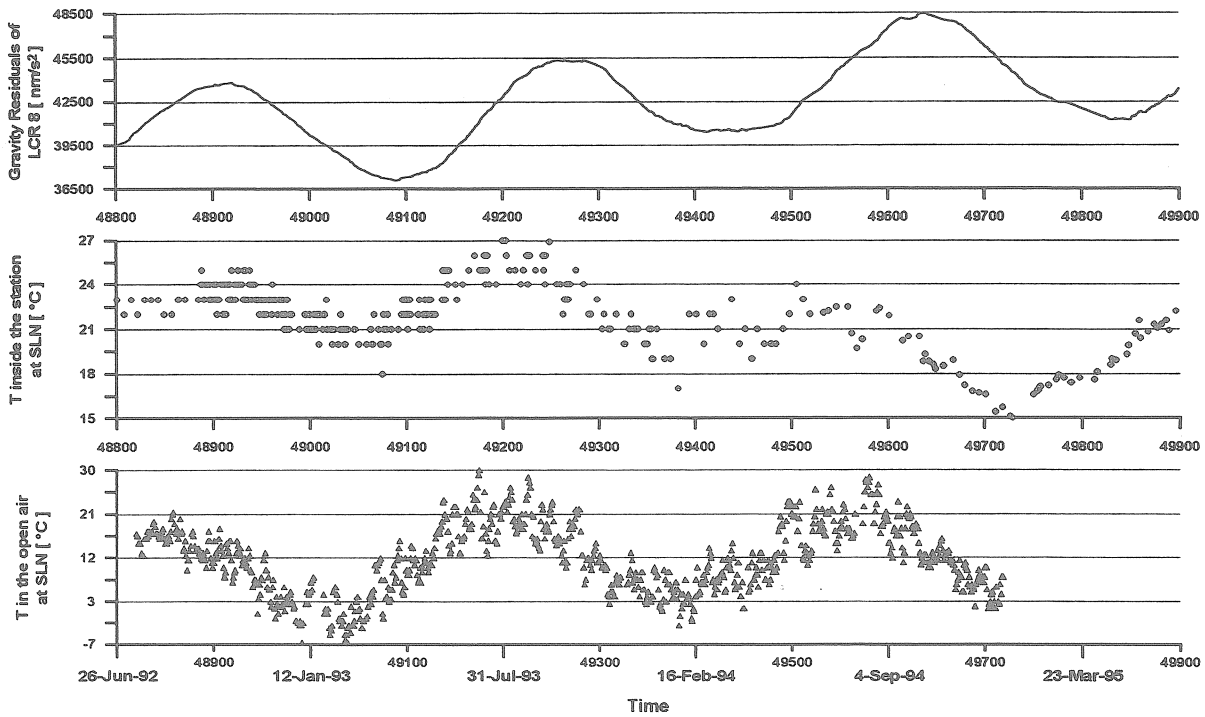

Figure 6 : Illustration of the LCR G8 annual periodicity with temperature variations in Serra-La-Nave. From top to bottom : gravity residuals after removing the Earth tides and air pressure effects, the temperature recorded in the station room and the temperature recorded in the open air. The phase lag between the temperature outside and inside the station is about 44 days; and between the inside temperature excitation and the gravimeter response is about 25 days.

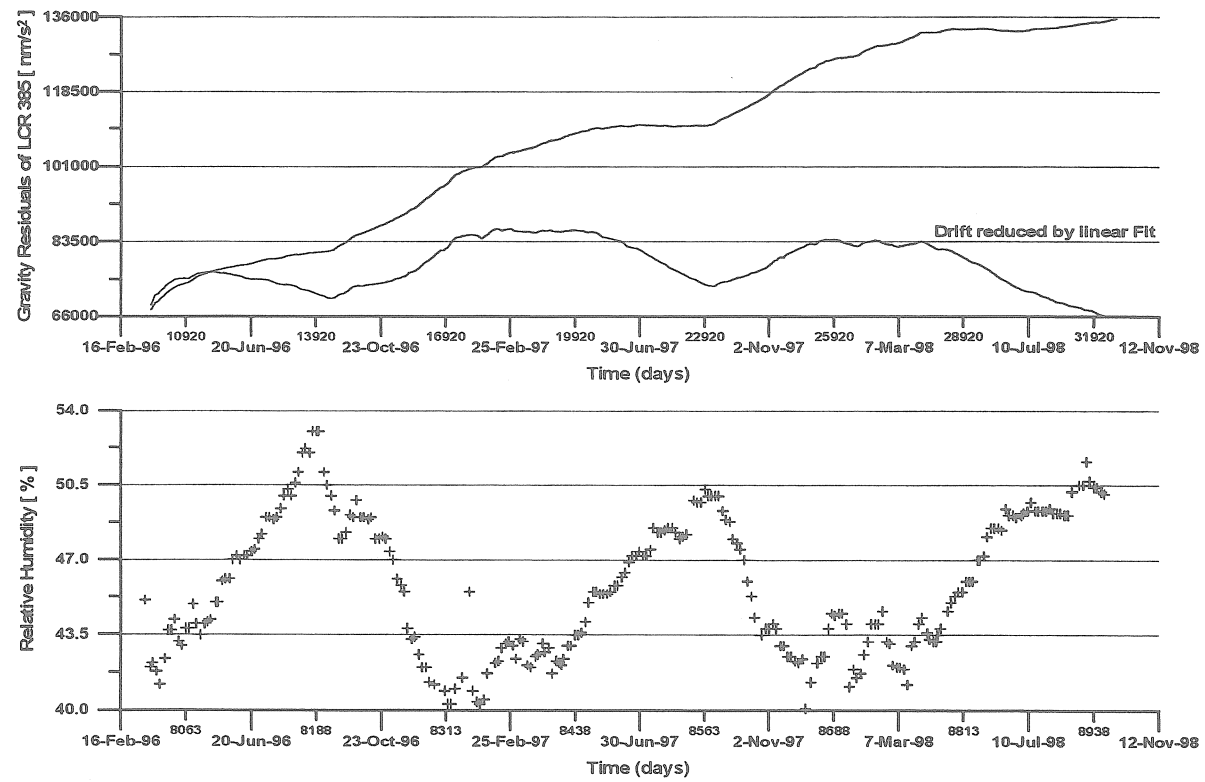

Figure 7 : Illustration of the LCR/ZLS G385 annual drift (Top) with humidity variations (Bottom) in Potsdam. The temperature is stabilised at 25°C ± 0.1°C. The lower curve on the top graph shows the annual drift reduced by a linear fit.

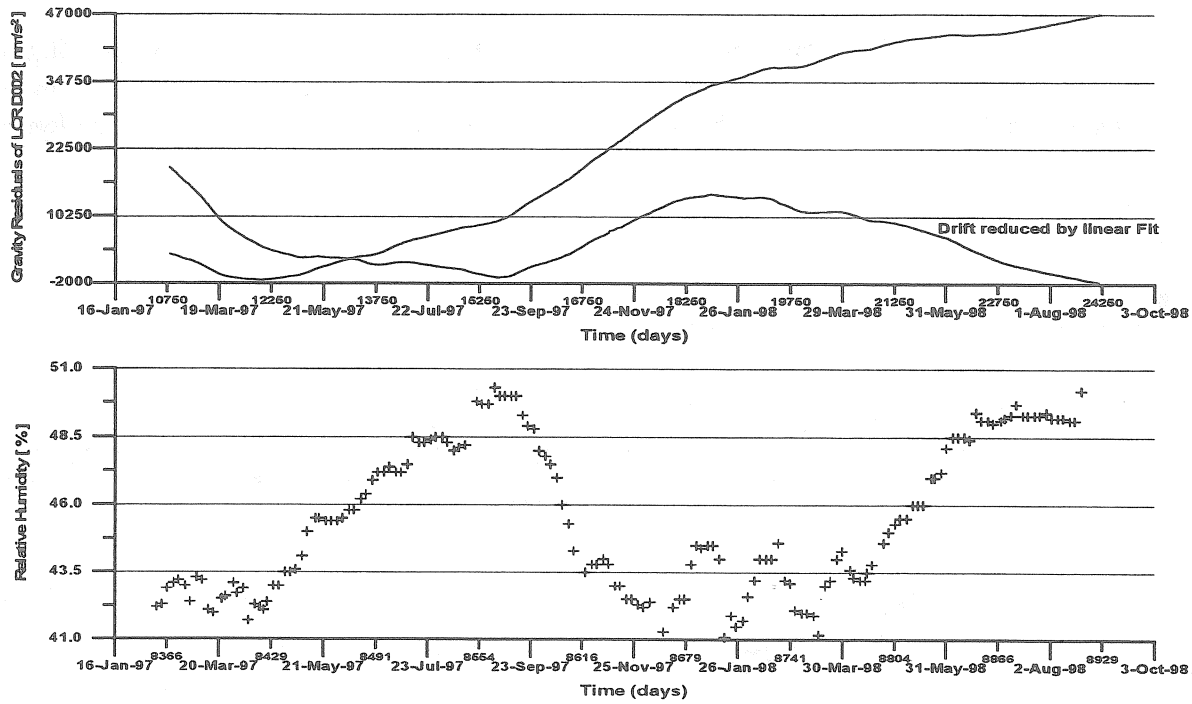

Figure 8 : Illustration of the LCR D2 annual drift (Top) with humidity variations (Bottom) in Potsdam. The temperature is stabilised at 25°C ± 0.1°C. The lower curve on the top graph shows the annual drift reduced by a linear fit.

Some examples of Askania gravimeters come from Pecny, Potsdam and Walferdange stations. In Pecny, where the station is thermostatised with a precision of ±0.1 °C, the gravity residuals of the Askania 228 show a correlation –instead of an anti-correlation like in the case of LCR gravimeters– with the air humidity and a large apparent phase lag of about three months (see figure 9).

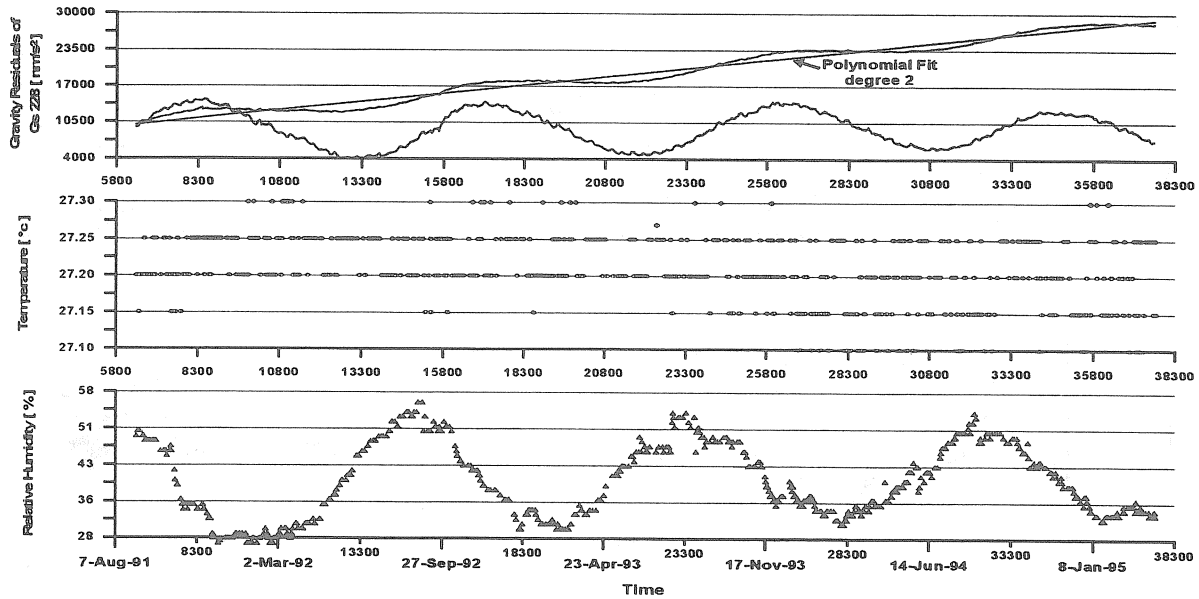

Figure 9 : Illustration of the Askania Gs 228 annual periodicity with temperature and humidity variations in Pecny. From top to bottom : gravity residuals after removing Earth tides, temperature and humidity records. The lower curve on the top graph shows the annual drift reduced by a polynomial fit.

The Askania 222 in Potsdam presents the same feature as the previous one (see figure 10). In 1989, an experiment has been made in Potsdam by putting the Askania 222 in an air-sealed container. Afterwards, the annual oscillation disappeared completely (see figure 11).

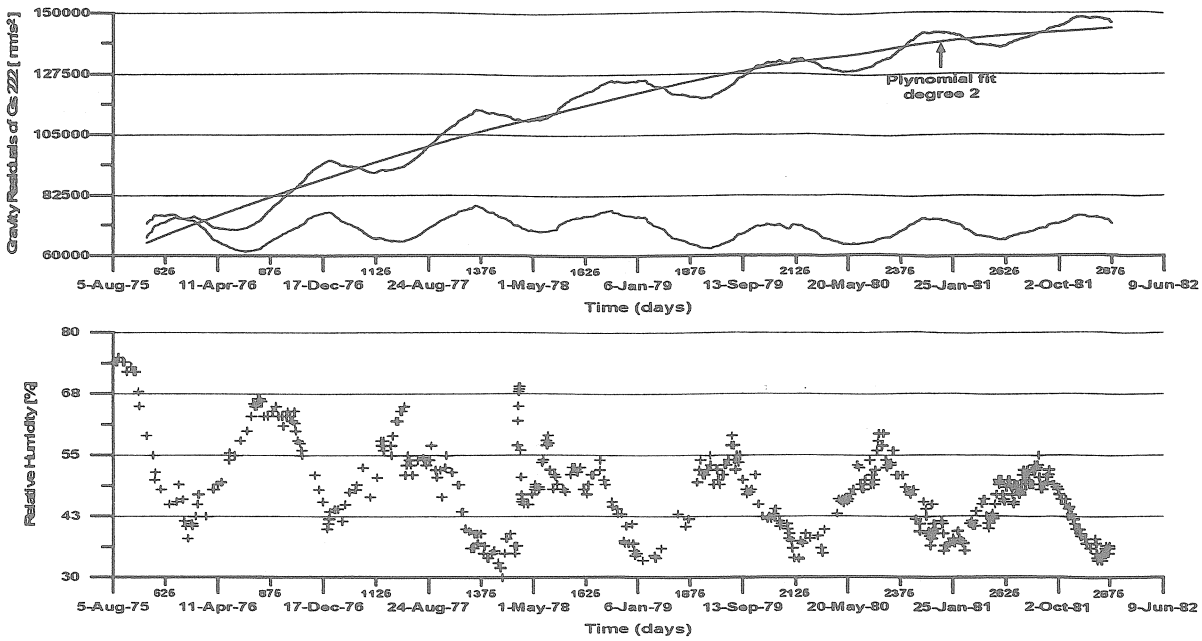

Figure 10 : Illustration of the Askania Gs 222 annual periodicity (Top) with humidity Variations (Bottom) in Potsdam. The temperature is stabilised at 25°C ± 0.1°C. The lower curve on the top graph shows the annual drift reduced by a polynomial fit. The temperature is controlled with an accuracy of ±0.1 °C.

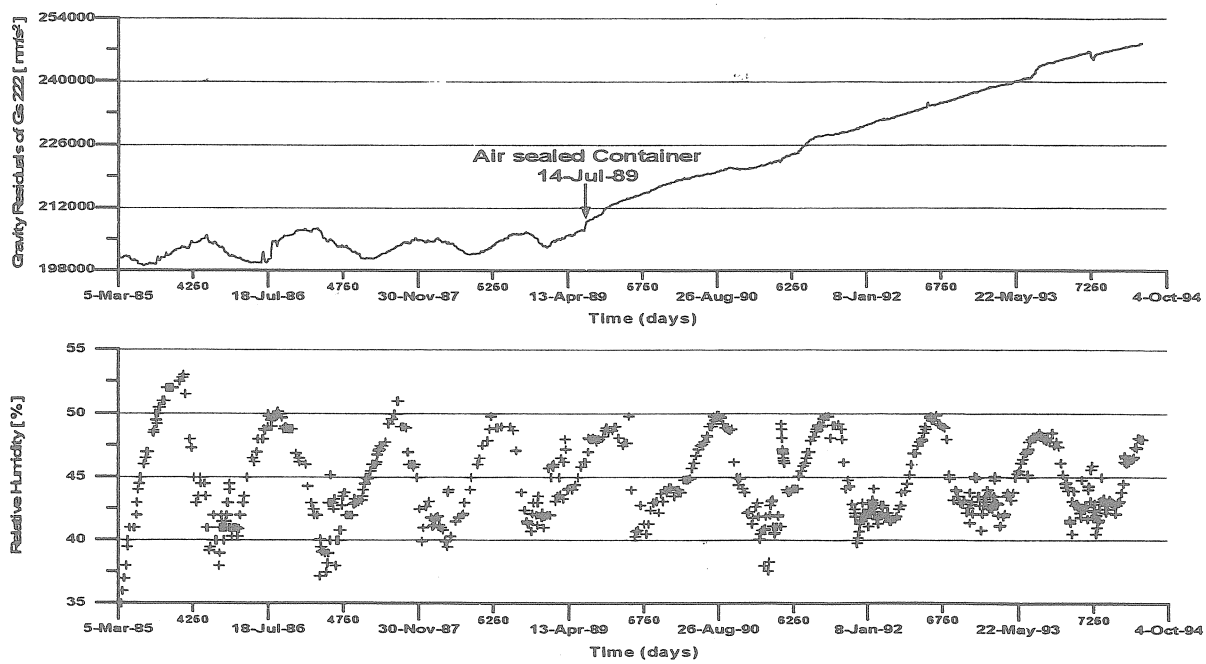

Figure 11 : Illustration of the Askania Gs 222 annual oscillation (Top) with humidity variations (Bottom) in Potsdam. The temperature is stabilised at 25°C ± 0.1°C. After putting the gravimeter in an air sealed container (14 July 1989), the annual drift disappeared.

In Walferdange, the Askania 191/BN01 was installed in the mine where the temperature and the humidity are very stable around 11°C and 80% respectively. The gravity residuals show only a linear drift (see figure 12) proving that one of these two meteorological parameters or both of them are responsible for the annual oscillation.

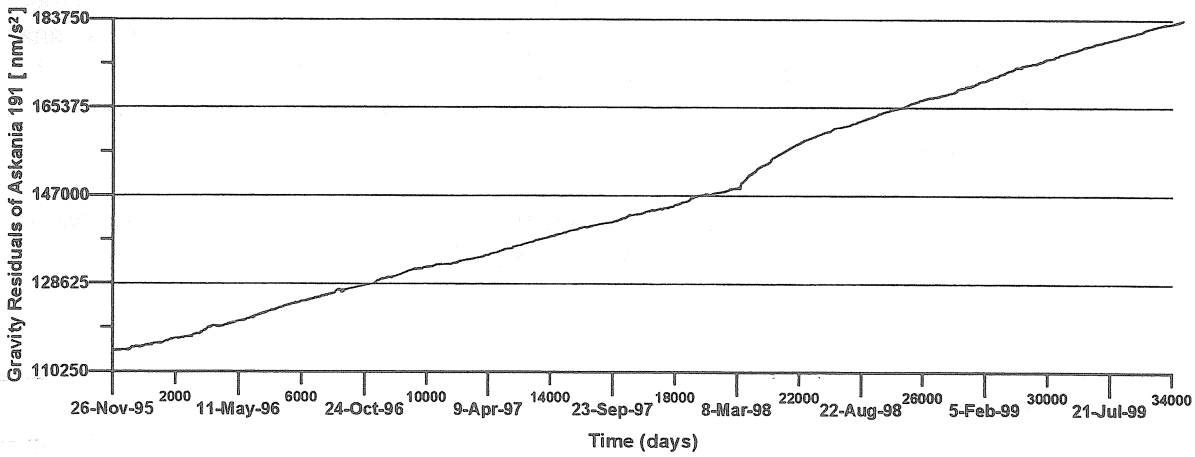

Figure 12 : Illustration of the Askania Gs 191/BN01 drift in the mine of Walferdange. The Earth tides and the air pressure effect are removed. No annual component is visible.

Bastien and Goodacre (1990) made an experiment with the LCR ET12. They put the gravimeter in a temperature controlled environment with low and high humidity level. The result is that the annual drift apparently disappeared during the period of the experiment with opposite quasi-linear drift rates for low and high humidity level (see figure 13).

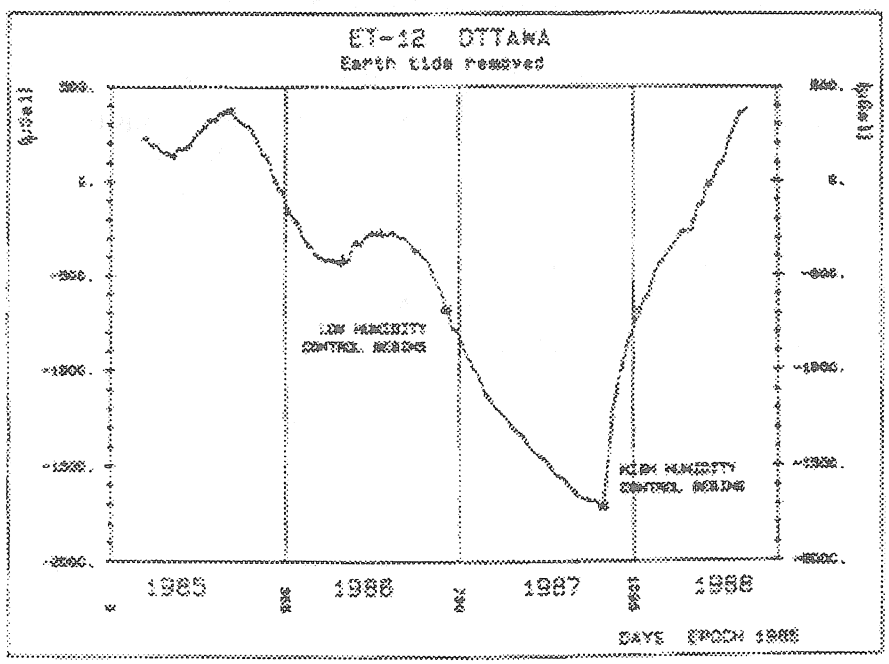

Figure 13 : Illustration of the LCR G12 annual periodicity in Ottawa. The drift behaviour between 1985/1987 disappears after putting the gravimeter in controlled environment.

VI. Conclusions

With these examples, we see clearly that the humidity has an effect on spring gravimeters for long period variations. It should be noticed that all the gravimeters are equipped with the capacitive transducers and, therefore, the humidity can indeed change the dielectric constant of the air. However, Askania gravimeters are completely sealed against pressure variations and the LCR gravimeters are sealed with dry inert gas inside. There should thus be no direct influence of humidity on the capacitance, while most of the electronic parts are exposed to the humidity changes.

When monitoring the gravity on volcanoes, we have to record in addition at least three other parameters : the air pressure, the temperature and the relative humidity.

Acknowledgements

We are first very grateful to Prof. P. Pâquet for his help and encouragements. We thank Prof. B. Ducarme as well for his valuable advice and support. We acknowledge also Mr. M. Hendrickx for his help. Many thanks go to Mr. N. d'Oreye for providing the data of Askania 191.

References

Bastien R. and Goodacre A.K., 1990, The effect of humidity variations on long-term tidal gravity recordings, Bull. Inf. Marées Terrestres, 106, p. 7506-7510.

El Wahabi A., Ducarme B., Van Ruymbeke M., d'Oreye N. and Somerhausen A. , 1998a, Continuous gravity observations at Mount Etna (Sicily) and correlations between temperature and gravimetric records, Cahiers du Centre Européen de Géodynamique et de Séismologie, Vol.14, p.105-120, 1997.

El Wahabi A., Ducarme B., Van Ruymbeke M., d'Oreye N. and Somerhausen A. , 1998b, Four years of continuous gravity observations at Mount Etna (Sicily), Proceedings of the 13th International Symposium on Earth Tides, p.477-479, 1998.

Wenzel H.-G., 1996, The nanogal software : Earth tide data processing package : Eterna 3.3, Bull. Inf. Marées Terrestres, 124, p. 9425-9439.

Application of the Least-squares Spectral Analysis to Superconducting Gravimeter Data Treatment and Analysis

Spiros D. Pagiatakis
Natural Resources Canada, Earth Sciences, Geodetic Survey Division, 615 Booth Street, Ottawa, Ontario, Canada K1A 0E9
e-mail:pagiatakis@geod.nrcan.gc.ca; Tel.:613 995 8720; Fax: 613 992 1468.

Abstract: Data collected from a superconducting gravimeter contain spikes, gaps, datum shifts (offsets) and other disturbances. Data sampling rates are usually higher than required and filtering is the usual procedure that is followed for their decimation. Spikes, gaps and datum shifts are not desirable in the data and often are removed following techniques that are not rigorous and based on intuition. More importantly, the acquired data series are non-stationary by virtue of having variable noise levels; yet, they are assumed stationary when they are cast in a spectral analysis scheme. In this paper a rigorous method is presented for the analysis of the superconducting gravimeter data, based on the parameterisation of unknown quantities in a least-squares scheme, followed by statistical testing and evaluation of the solution. It is shown that there is no need to de-gap and de-spike the data, or pre-process noisy segments due an earthquake. An example is given by analysing a five-day-long series from the Canadian Superconducting Gravimeter Installation (CSGI), in Cantley, underlining the advantages of the approach.

1. Introduction

The Global Geodynamics Project (GGP), an international program of observations of temporal variations of the gravity field of the Earth, is co-ordinating the operation of a network of 16 superconducting gravimeters (SG) around the globe, for the purpose of studying a range of important phenomena, such as Earth tides, ocean tide loading, core nutations and core modes. The SGs sample the gravity field every 1-10 s with a precision of one nGal and they are frequently calibrated with absolute gravimeters. The GGP has been scheduled for six years (1997-2003) and data from all stations are being sent to the International Centre of Earth Tides (ICET) in Brussels for further distribution to the scientific community. More details on the GGP can be found in Crossley et al., (1999).

Similar to any other experimental series, the SG data are not continuous due to instrumental failures. Power failures usually introduce short gaps, while the presence of spikes is not unusual. Furthermore, advances in instrument development and our better understanding of the operation of the SG have resulted in improvements in the accuracy of the data and will continue to improve over the life span of the GGP. Precipitation, hydro-geological processes, earthquakes and other disturbances (helium refills, maintenance, calibration, system upgrades) alter significantly the quality and the characteristics of the series, introducing variable noise levels and datum shifts (offsets). Thus, SG time series collected over long periods will be non-stationary by virtue of being unequally weighted.

The majority of the researchers are using almost exclusively fast Fourier transform (FFT) algorithms for the determination of the power spectrum of the SG series. The FFT approach is computationally efficient and produces, in general, reasonable results for a large class of

signal processes (Kay and Marple, 1981). However, there are many inherent limitations in the FFT techniques, the most prominent being the requirement that the data be equally spaced and equally weighted (e.g. Press et al., 1992). Pre-processing of the data is inevitable in these cases. De-gapping, de-spiking, de-trending and smoothing noisy segments of the data (earthquakes) are part of the routine before an analysis is initiated. Any "data massaging" is subjective, non-rigorous, non-unique and, in general, unsatisfactory.

In order to avoid unnecessary data pre-processing that may corrupt or obliterate the useful information hidden in the series (signal), the Least Squares Spectral Analysis (LSSA) is used in this study as an alternative to the classical Fourier methods. LSSA was first developed by Vanícek (1969; 1971) to bypass all inherent limitations of Fourier techniques, providing the following advantages: (a) systematic noise (coloured or other) can be rigorously suppressed without producing any shift of the existing spectral peaks (Taylor and Hamilton, 1972), (b) time series with unequally spaced values can be analysed without pre-processing (Maul and Yanaway, 1978; Press et al., 1992), (c) time series with an associated covariance matrix can be analysed (Steeves, 1981, Pagiatakis 1999) and (d) rigorous statistical testing on the significance of spectral peaks can be performed (Pagiatakis, 1999).

In this paper, a brief overview of the LSSA is presented and applied on a segment of the SG series obtained from the Canadian Superconducting Gravimeter Installation (CSGI). The interested reader can find additional details on the LSSA in Pagiatakis (1999).

2. Overview of the Least-squares Spectral Analysis

An observed time series can be considered to be composed of *signal*, a quantity of interest, and *noise*, and an unwanted quantity that distorts the signal. The noise can be *random* or *systematic*. An idealised concept of random noise is the *white noise*, which is completely uncorrelated possessing constant spectral density and it may or may not follow the Gaussian distribution. In practice, we usually deal with *non-white random noise*, a band-limited random function of time. Systematic noise, is noise whose form may be describable by a certain functional form; it can be periodic (*coloured*), or non-periodic. Non-periodic noise may include datum shifts (offsets) and trends (linear, quadratic, exponential, etc.) and renders the series *non-stationary*, that is, it causes the statistical properties of the series to be a function of time.

An observed time series is considered to be represented by $f(t)0$,, where , is a Hilbert space. The values of the series have been observed at times t_i, i=1,2 ...m; here, we do not assume that t_i are equally spaced. We assume, however, that the values of the time series possess a fully populated covariance matrix C_f, that metricises ,.

One of the main objectives of LSSA is to detect periodic signals in f, especially when f contains both, random and systematic noise. Thus, time series f can be modelled by g as follows:

$$g = \mathrm{M}x \tag{1}$$

where $\mathrm{M}=[\mathrm{M_s}|\mathrm{M_n}]$ is the Vandermonde matrix and $x^{\mathrm{T}}=[x_s|x_n]^{\mathrm{T}}$ is the vector of unknown parameters. Subscripts $[_s]$ and $[_n]$ refer to the signal and noise, respectively. Matrix M specifies the functional form of both signal and (systematic) noise. We must emphasise here that the

distinction between signal and noise is subjective, therefore, the partitioning of M and x is arbitrary. We wish to determine the model parameters, such that the difference between g and f (residuals) is minimum in the least-squares sense. Using the standard least-squares notation (e.g. Vanícek and Krakiwsky, 1986) we can write:

$$\hat{r} = f - \hat{g} = f - \Phi(\Phi^{\mathrm{T}} C_f^{-1} \Phi)^{-1} \Phi^{\mathrm{T}} C_f^{-1} f . \qquad (2)$$

In the above equation, $\hat{g}$ is the orthogonal projection of f onto the subspace Sδ,, generated by the column vectors of M. It follows from the *projection theorem* (Oden, 1979) that $\hat{r} \perp \hat{g}$. This means that f has been decomposed into a signal $\hat{g}$ and noise $\hat{r}$ (residual series).

In order to find something similar to spectral value, we have to compare $\hat{g}$ to the original series. This can be achieved by projecting orthogonally $\hat{g} \in \mathrm{S}$ back onto ,, and comparing the norm of this projection to the norm of f. Hence, we can obtain a measure (in terms of percent) of how much of $\hat{g}$ is contained in f. This ratio is smaller than unity and can be expressed as follows:

$$s = \frac{\langle f, \hat{g} \rangle / |f|}{|f|} = \frac{\langle f, \hat{g} \rangle}{|f|^2} = \frac{f^{\mathrm{T}} C_f^{-1} \hat{g}}{f^{\mathrm{T}} C_f^{-1} f}, \quad \in (0,1), \qquad (3)$$

So far, we have not specified the form of the signal through base vectors that form M. In spectral analysis, it is customary to search, among others, for periodic signals that are expressible in terms of sine and cosine base functions. Thus, we can assume a set of spectral frequencies $\Omega = \{T_i;\ i = 1,2,\ldots\ k\}$, each defining a different subspace S spanned by M (Wells et al., 1985)

$$\mathrm{M} = [\cos \omega_i t, \sin \omega_i t], \quad i = 1,2, \quad \ldots, \quad k \qquad (4)$$

and the orthogonal projection of f onto S will be different for each $T_i \in \Omega$. We must emphasise here that each frequency $T_i \in \Omega$, is tried independently from the rest. Then the least-squares spectrum is defined by [Pagiatakis, 1999; Eqs. (5) and (10)]

$$s(\omega_i) = \frac{f^{\mathrm{T}} C_f^{-1} \hat{g}(\omega_i)}{f^{\mathrm{T}} C_f^{-1} f} = \left[1 + \frac{Q_n}{Q_s} \right]^{-1}, \qquad i = 1,2,\ldots,k, \qquad (5)$$

where Q_n and Q_s are the quadratic forms of the noise and signal respectively.

At this point, it is expedient to re-examine equation (1) and the partitioning of matrix M. $\mathrm{M_s}$ may include trigonometric base functions (Eq. (4)) to describe the periodic components of the series, or other, such as *random walk*, *autoregressive* (AR), *moving average* (MA), and *autoregressive moving average* (ARMA) (Jenkins and Watts, 1968; Gelb, 1974). When the calculation of the least-squares spectrum is carried out, there will be a simultaneous least-squares solution for the parameters of the process. This, indeed, is a rigorous approach to the problem of hidden periodicities: the parameters of the assumed linear system driven by noise are determined simultaneously with the amplitudes and phases of the periodic components and with other parameters, that describe systematic noise.

Equation (5) gives the least-squares spectrum in percentage variance and it is equivalent to a periodogram, or amplitude spectrum. However, Eq. (5) can be further developed into other

forms to provide the researcher with more familiar spectral representations, such as power spectral density (PSD) in decibels (dB) or in units^2/frequency, where "units" signifies the units of the time series values. Following Pagiatakis [1999], the least-squares power spectral density in decibels is given by [ibid., Eq. (11)]

$$PSD_{LS} = 10 log_{10}\left[\frac{s}{1-s}\right], \text{(dB)}. \tag{6}$$

Solving Equation (5) with respect to Q_s and dividing by the frequency f, the classical least-squares spectrum can be transformed into a least-squares PSD in units^2/frequency

$$PSD_{LS} = \frac{Q_n}{f}\left[\frac{s}{1-s}\right], \text{ (units}^2\text{ / frequency)}. \tag{7}$$

The least-squares *PSD* given by (6) and (7) is equivalent to the one determined from the FFT method, when the series is equally spaced and equally weighted. Evidently, (6) and (7) can be used to calculate power spectra of any series, without resorting to FFT and its stringent requirements.

What follows is a thorough and rigorous analysis of the SG series from the CSGI, using software LSSA v5.0. This software is based on LSSA v1.0 (Wells and Vaníček, 1978) and LSSA v2.0 (Wells et. al., 1985). Statistical evaluation of the results of this analysis are based on **Theorem 3** and **Theorem 4** as developed by Pagiatakis (1999) and on other classical statistical tests found in geodetic methodology (e.g. Mikhail, 1976; Vaníček and Krakiwsky, 1986).

3. CSGI Data Analysis

As it is mentioned in the introduction, similar to any other experimental series, the SG data from the CSGI possess short gaps, spikes, datum shifts (offsets), earthquake disturbances, and atmospheric and hydrological effects. The latter effects introduce increased noise in short time scales, which occasionally can reach many tens of μGal. Figure 1 shows a sample of typical daily records from the Canadian Superconducting Gravimeter Installation (CSGI). On a "quiet" day, the noise level is usually low, reaching an RMS scatter of a few tenths of μGal (Fig. 1a). Atmospheric disturbances, such as heavy precipitation or abrupt change of the atmospheric pressure, increase the noise to several μGal (Fig. 1b), or even to several tens of μGal (Fig. 1c). Human disturbances are also possible, despite the extreme care taken by the personnel when, for instance, transferring liquid helium (Fig. 1d), or repairing certain components of the installation (e.g. cold head replacement). Very often, the record is severely saturated with non-gravity signals, such as those originating from an earthquake (Fig. 1e). Power fluctuations or short interruptions, or sometimes other unknown causes may force the data acquisition system (DAS) to a re-boot. Re-booting of the DAS takes usually a few minutes and this is the cause of short data gaps.

It is our tenet that when such time series are used to detect minute changes of the Earth's gravity field and in particular those originating from deep interior processes (e.g. core motions), the series have to be treated with great respect! Any pre-processing, such as

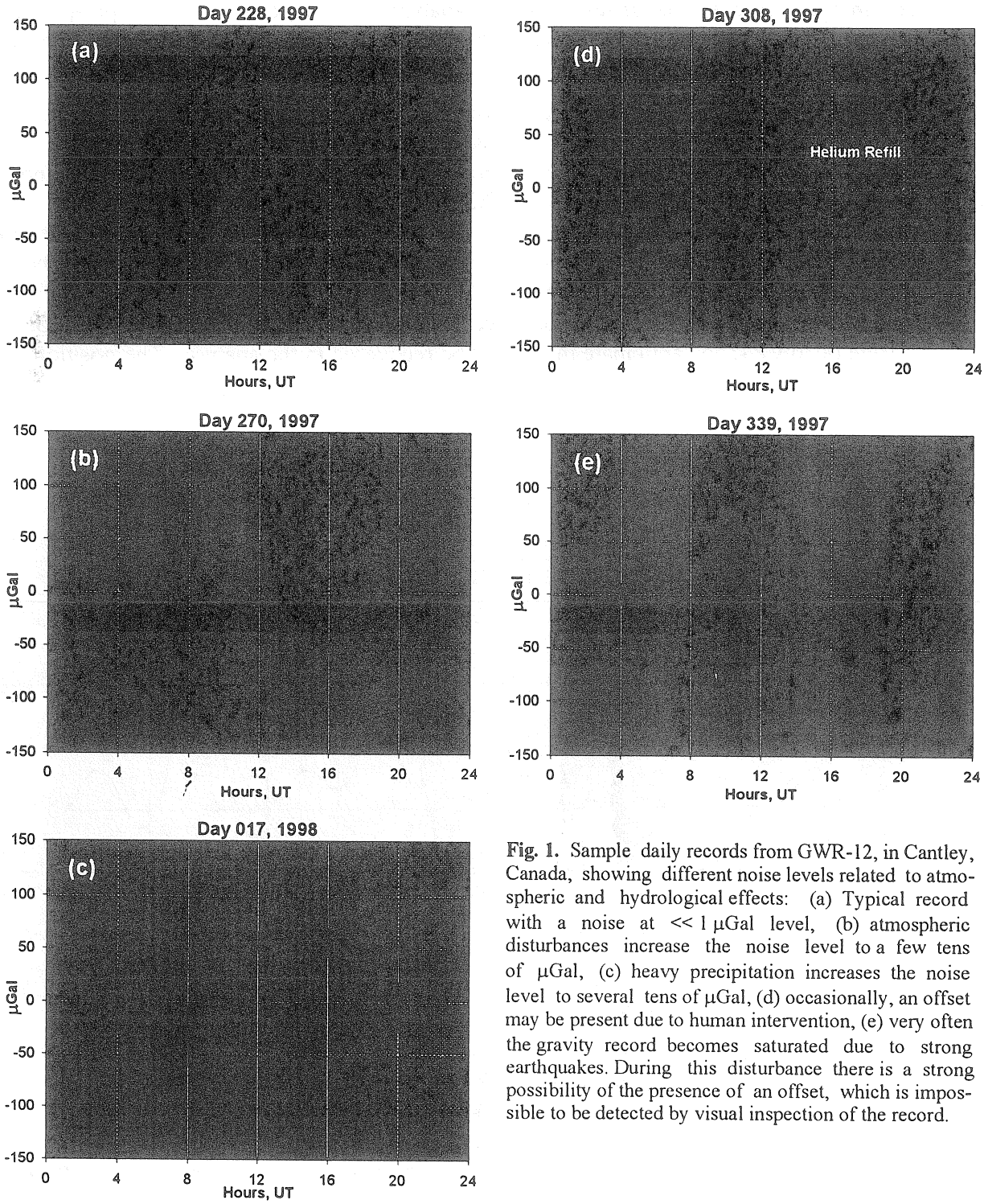

Fig. 1. Sample daily records from GWR-12, in Cantley, Canada, showing different noise levels related to atmospheric and hydrological effects: (a) Typical record with a noise at << 1 µGal level, (b) atmospheric disturbances increase the noise level to a few tens of µGal, (c) heavy precipitation increases the noise level to several tens of µGal, (d) occasionally, an offset may be present due to human intervention, (e) very often the gravity record becomes saturated due to strong earthquakes. During this disturbance there is a strong possibility of the presence of an offset, which is impossible to be detected by visual inspection of the record.

editing, de-gaping, de-spiking, and de-trending, or ignoring the variable noise levels, may obscure or suppress nanogal level signals, yet very important for the studies of the Earth's deep interior. Hence, the series must be analysed as recorded with no pre-processing. Traditional FFT methods are not offered for such an analysis for the reasons outlined in the introduction.

In order to demonstrate our rigorous approach, we select a five-day record from the CSGI, shown in Fig. 2. This record possesses almost all the characteristics usually found in a SG time series. The presence of a nearly two-minute gap renders this segment essentially unequally spaced. Variable noise levels throughout the series require variable weights; simply it is not suitable to assign the same weight to all the series values when their noise level varies significantly (cf. Fig. 1). In addition, the presence of an earthquake (day 339) and other smaller disturbances may have introduced an offset that cannot be detected by a simple visual inspection of the record. Furthermore, we introduce an artificial offset of +1 μGal after t=8169h (arrow #4) and anticipate that it will be recovered in the analysis. The positions of the

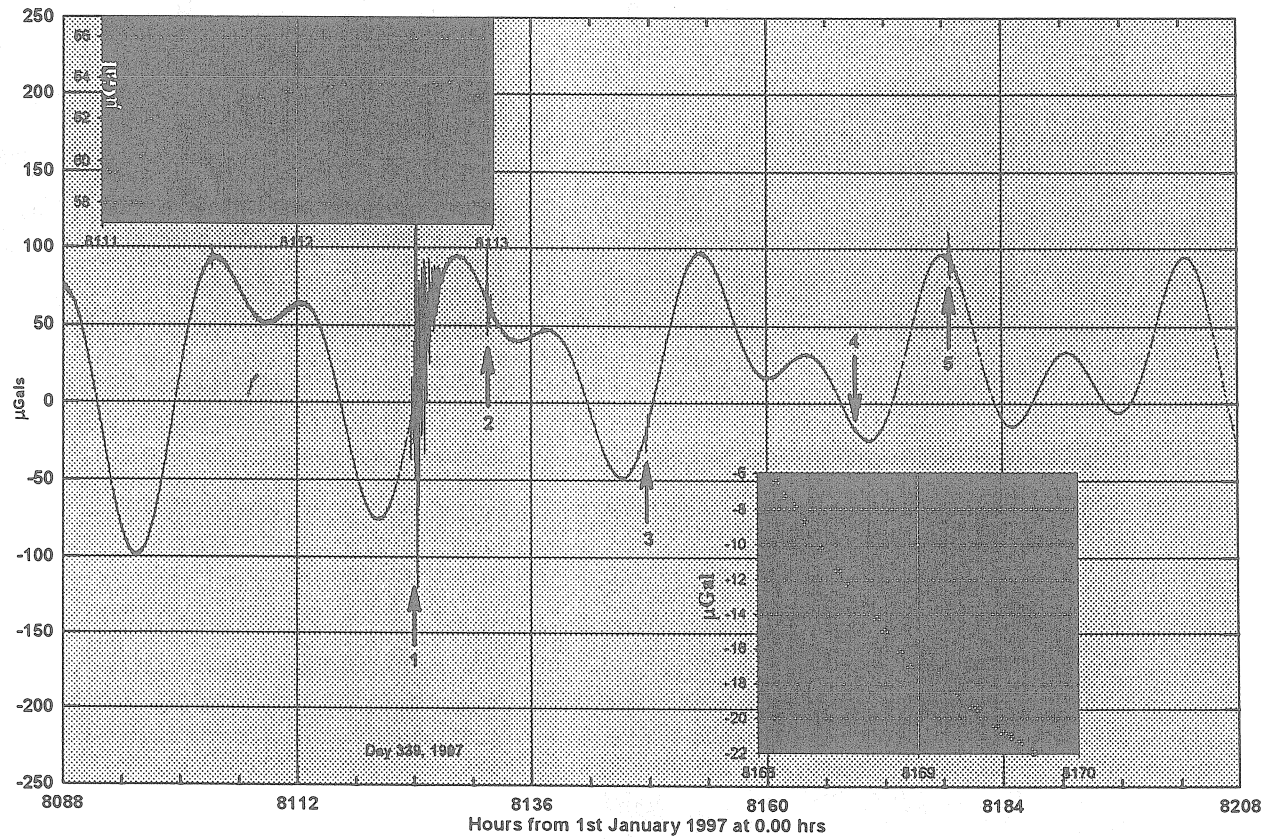

Fig. 2. A five-day data segment, produced from the original, 1s data, by applying a Parzen window with *lag*=29s. The series is unequally spaced with variances derived from rigorous error propagation of the window variance to the filtered data value. Sampling interval varies at random, between 1-6 minutes. The blue panels show details of the series. Red arrows indicate the location of possible offsets to be considered in the analysis. At t=8169 h (arrow 4) an artificial offset of +1μGal was introduced.

other arrows signify the times of possible offsets to be investigated in this analysis.

The original 1s data are filtered in the time domain, using a Parzen window (Jenkins and

Watts, 1968) with *lag*=29s (total width of 1 minute). This window is used as a weighting function throughout the whole segment, centred at random times with no overlap between successive windows to avoid correlation. Each series value that is included in the window is assumed to have a variance equal to that of the segment been filtered. This variance is propagated through the filtering algorithm to the filtered value. In Fig. 2, the blue panels show details of the series under investigation. Note the variable error bars and the unequal sampling, which in this particular case varies at random between 1-6 minutes. The choice of the Parzen window with *lag*=29s is somewhat arbitrary and it is selected here for illustration purposes only. The researcher may experiment with different weighting functions, such as boxcar, triangular, Gaussian, Tukey (e.g. Jenkins and Watts, 1968), or none at all, and with lags other than the one used above. The variable-sampling rate introduced in this analysis eliminates any aliasing arising from the filtering procedure. This is highly desirable in any time series analysis, and the LSSA is the only method that can handle unequally spaced series.

To illustrate the importance of the proper weighting of the time series values, we produce two spectra for the series. The first spectrum is calculated by choosing equal weights for the series values and it is shown in Fig. 3a, with its respective least-squares PSD (μGal^2/cpd) in Fig. 3b (cf. Eq. 7). Consequently, assigning variable weights to the series values (inverse of their variance) produces the second spectrum, which is shown in Figures 3c and 3d. It is obvious that the semidiurnal/diurnal peak ratios are different. However, the unequally weighted spectrum reproduces more accurately the theoretical ratios for this location. The interested reader can also refer to Pagiatakis (1999) for a similar example from VLBI series analyses.

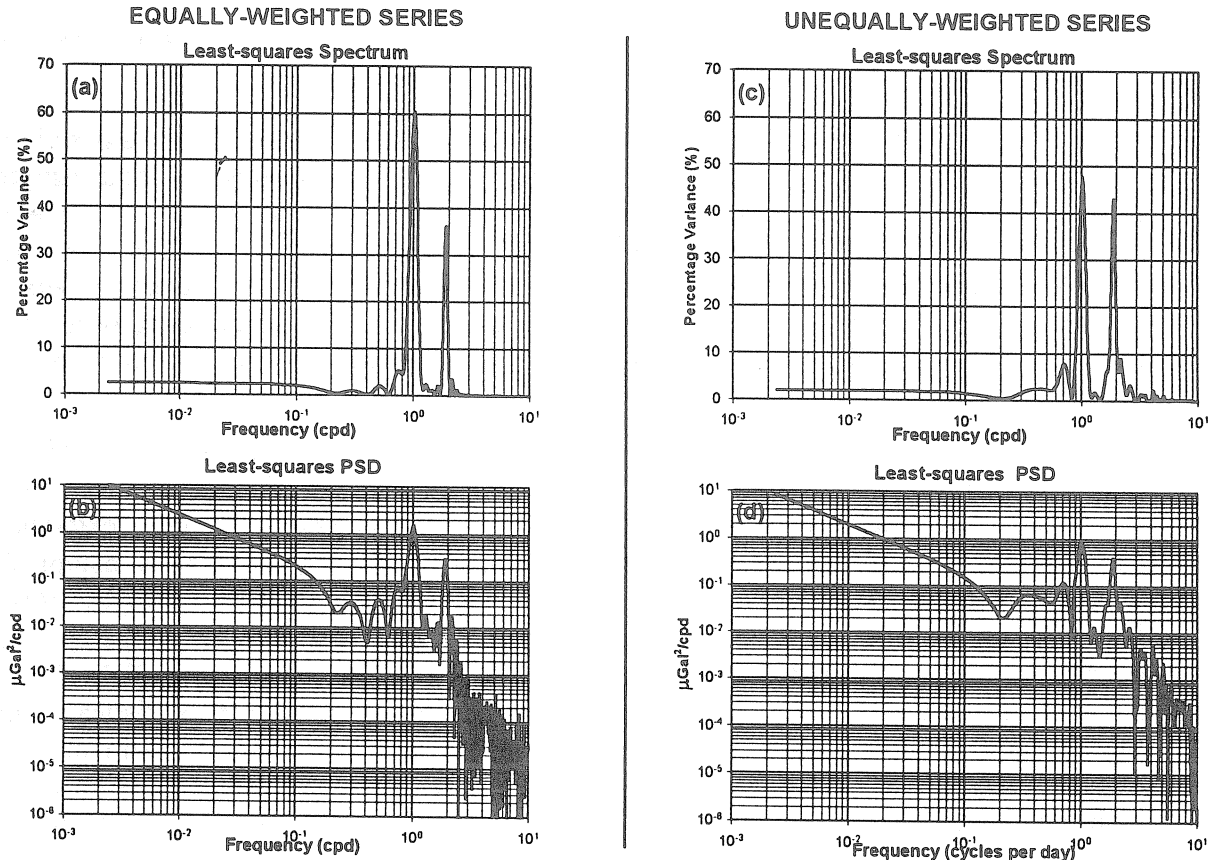

Fig. 3. Effect of weighing of time series values in the spectrum. Panels (a) and (b) show the spectrum of the time series in percentage variance (%) and in μGal^2/cpd, respectively, when the series values are equally weighted. Panels (c) and (d) show the spectrum of the time series in percentage variance (%) and in μGal^2/cpd, respectively, when the series values are weighted with the inverse of their variance. Note the difference in the ratios of the diurnal/semi-diurnal peaks.

The next step concerns the analysis of the five-day segment shown in Fig. 2. In this analysis, we are not interested in the tidal constituents; we suppress the tidal waves that are separable within the 5-day span, using their theoretical, well-defined frequencies. We cast the series in a least squares spectral analysis scheme, focusing our attention to the detection and suppression of other significant spectral peaks, as well as to the determination of the five datum shifts indicated by the arrows in Fig. 2. Significant peaks are identified by using **Theorem 3** and **Theorem 4** from Pagiatakis (1999), assuming a 99% confidence level. Following a meticulous identification of spectral peaks, all tidal and non-tidal constituents (15 in total) along with the five offsets are suppressed simultaneously to produce a residual series shown in Fig. 4. The residual series possesses a weighted RMS scatter of 0.18 μGal and the error bars signify 1-σ formal errors. Note the increased error bars during the earthquake.

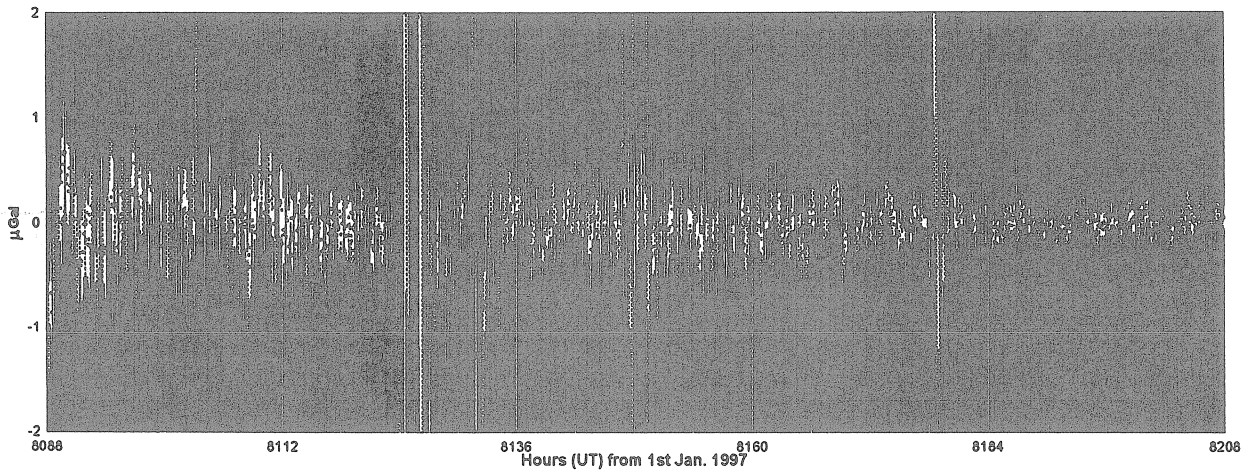

Fig. 4. Residual series after the suppression of 15 significant constituents (including tidal) and the five (5) offsets indicated by the arrows on Fig. 2. Error bars are 1σ formal errors. Residual series possesses a weighted RMS of 0.18 μGal.

Following the completion of the analysis and evaluation of all the parameters describing the significant constituents of the series, we step back to rerun the analysis without suppressing the five datum shifts. The residual series is shown in Fig. 5 (upper panel). The five arrows indicate, again, the points where offsets may be present. Other than the artificial offset at t=8169h, it is nearly impossible to conclude whether the other offsets exist, or even more importantly, whether they are significant or not, just by visually inspecting the series. We will revisit this "identification" issue after we discuss the evaluation of the determined parameters as obtained from the least squares analysis.

In the geodetic methodology of parameter determination using least squares procedures, it is important to evaluate statistically the various steps of the analysis. The application of rigorous, well-established statistical tests can be found in many classical geodetic textbooks (e.g. Mikhail, 1976; Vaní□ek and Krakiwsky, 1986). LSSA software v5.0 is equipped with numerous statistical tests, such as the *goodness-of-fit* test of the residual series, the *chi-square* test of the variance factor, the statistical tests on the significance of peaks in the spectrum (F, or hypergeometric distribution) and the statistical tests on the significance of the determined parameters (F, or *chi-square* distribution). We wish to focus here on the statistical evaluation of the vector of determined parameters, including the offsets. It is well known that the vector of determined parameters can be checked for statistical significance with respect to a set of expected or assumed values. These tests are very well documented and applied on a routine

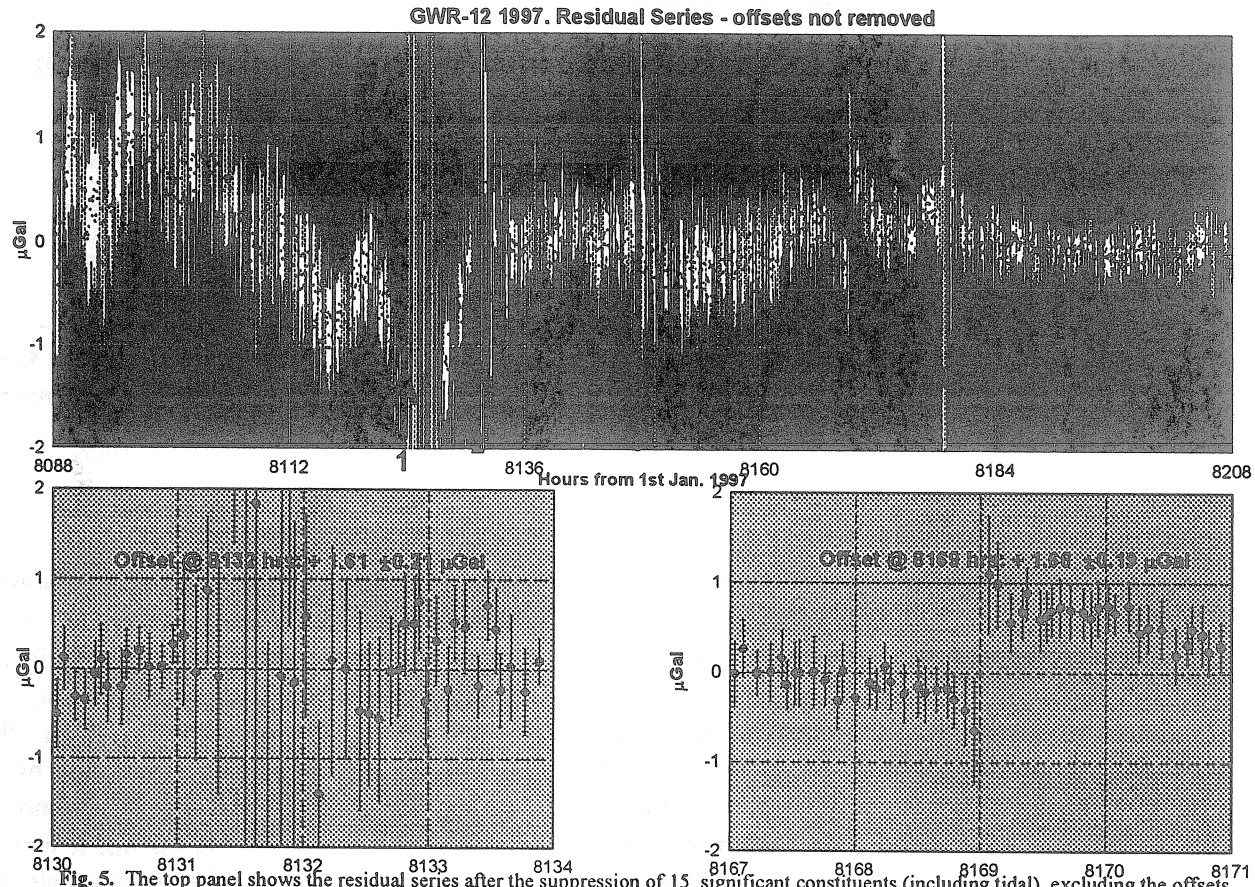

Fig. 5. The top panel shows the residual series after the suppression of 15 significant constituents (including tidal), excluding the offsets indicated by the arrows. Green arrows show offsets that are statistically significant, while red arrows indicate statistically insignificant offsets. The two bottom panels show details of the residual series at two significant offsets (#2 and #4), (see also Table 1).

basis in

geodetic problems (e.g. Vanícek and Krakiwsky, 1986, p.239). Often, however, we wish to test the statistical significance of a sub-vector of parameters, or even a single element of it. This is a slightly more involved but well established procedure (e.g. Vaní□ek and Krakiwsky, 1986; p. 241).

In the case of the present SG data analysis, we test whether the determined offsets are significantly different from zero. This is achieved by comparing the absolute value of each offset separately to its standard error, multiplied by an expansion factor C_α (see Vaní□ek and Krakiwsky, 1986; p.241). If the absolute value of the offset is less than the product $C_\alpha\sigma$, then the offset will be declared insignificant. The results from the evaluation of all five offsets are summarised in Table 1. In Table 1, column 1 gives the times of the offsets (hours), column 2 is the least-squares estimate of the offsets, whereas their standard error given in column 3. Columns 4 and 5 provide the product of the standard error with the expansion factor $C_{0.05}$=2.89, when the *a-priori* variance factor is known, or with $C_{0.05}$=3.04 when the *a-priori* variance factor is unknown, respectively. Note that the offset at t=8149hr, is marginally significant. When using a more stringent significance level, i.e., α=0.01, then this offset becomes insignificant. In Fig. 5, the green arrows show the times where the offsets are significant, while the red arrows indicate insignificant offsets.

Time (hours)	Offset (μGal)	σ (μGal)	$\lvert 2.89\sigma \rvert$ (μGal)	$\lvert 3.04\sigma \rvert$ (μGal)
8124	+0.41	±0.22	+0.64 *Insignificant*	+0.67 *Insignificant*
8132	+1.61	±0.21	+0.61 ***Significant***	+0.64 ***Significant***
8149	+0.73	±0.23	+0.66 ***Significant***	+0.70 ***Significant***
8169	+1.66	±0.19	+0.55 ***Significant***	+0.58 ***Significant***
8178	-0.23	±0.21	+0.61 *Insignificant*	+0.64 *Insignificant*

Table 1. Least-squares estimates of the offsets and their standard error (columns 2 and 3). Columns 4 and 5 show the upper limits of the offsets above which they are statistically significant at α=0.05 for known, or unknown *a-priori* variance factor, respectively.

5. Discussion and Conclusions

SG time series, like any other experimental series, possess trends, spikes, gaps, atmospheric and earthquake disturbances, as well as variable noise levels. Most importantly, SG series comprise very useful information on various physical processes, such as atmospheric and hydrological phenomena, sea level variations, tides, ocean loading, free oscillations and core motions. Many of these processes are at the nanogal or microgal level (at the most) and they can be easily obscured by the presence of noise in the series. Series editing is dictated by the FFT techniques because all the unwanted disturbances mentioned above simply cannot be handled by this method. Editing may produce artistic and well-composed series but it may, at the same time, obliterate useful information (signal), or even introduce new artificial signals. More importantly, editing is often performed at different non-rigorous pre-analysis stages and the determination of the parameters (e.g. offsets) is merely achieved in a non-simultaneous fashion, that is, the offsets are treated separately from each other and separately from the other parameters.

LSSA can be ápplied directly to the experimental series without the need of editing or filtering. All unknown parameters are determined simultaneously, whilst rigorous statistical testing is applied to evaluate the residual series and the significance of the determined parameters, either as a vector, or as individual elements. The statistical significance of the peaks is evaluated rigorously (Pagiatakis, 1999) leaving very little room for wrong decisions to be made by the researcher.

The identification and evaluation of offsets in a series is very important. LSSA can evaluate the offsets alongside other parameters. This is achieved by identifying the times at which offsets are suspected and letting the least squares procedure evaluate them. It is imperative to mention here that those offsets, which seem to recover slowly after a few or several hours need not be treated separately from the others. Simply the LSSA solution will show no offset at all, as the best fit of the sinusoid and the other base functions (trends, offsets, etc.) will result in larger residuals in the segment of the offset recovery. In fact, the offset recovery will show perfectly in the residuals.

References

Crossley D, Hinderer J, Casula G., Francis O., Hsu H.-T., Imanishi Y., Jentzsch G., Kääriänen J., Merriam J., Meurers B., Neumeyer J., Richter B., Shibuya K., Sato T., van Dam T., (1999) Network of Superconducting Gravimeters Benefits a Number of Disciplines. Eos Transactions, Vol. 80, No. 11, p.121,125-126.

Gelb A (ed.) (1974) *Applied Optimal Estimation*. The M.I.T. Press, Cambridge, Massachusetts.

Jenkins GM, Watts DG (1968) *Spectral Analysis and its applications*. Holden-Day, San Francisco.

Kay SM, Marple SL (1981) Spectrum Analysis - A Modern Perspective. *Proceedings of the IEEE, 69 (11):*1380-1419.

Maul GA, Yanaway A (1978) Deep sea tides determination from GEOS-3. NASA Contractor Report 141435, NOAA Atlantic Oceanographic and Meteorological Laboratories, Miami, FL.

Merry CL, Vaníček P (1981) The Zero Frequency Response of Sea Level to Meteorological Influences. Technical Report No. 82, Department of Surveying Engineering, University of New Brunswick, Fredericton, Canada.

Mikhail EM (1976) *Observations and Least Squares*. Thomas Y. Crowell Company, New York, 1976.

Oden JT (1979) *Applied Functional Analysis*. Prentice-Hall.

Pagiatakis SD, (1999) Stochastic significance of peaks in the least-squares spectrum. *Journal of Geodesy 73*: 67-78.

Press WH, Teukolsky SA, Vetterling WT, Flannery BP (1992) *Numerical Recipes in FORTRAN: The Art of Scientific Computing*. Cambridge University Press, New York (Second Edition).

Steeves RR (1981) A statistical test for significance of peaks in the least-squares spectrum. Collected Papers, Geodetic Survey, Department of Energy, Mines and Resources. Surveys and Mapping Branch, Ottawa, 149-166.

Taylor J, Hamilton S (1972) Some tests of the Vanicek method of spectral analysis. *Astrophysics and Space Science 17*:357-367.

Vanícek P (1969) Approximate Spectral Analysis by Least-squares Fit. *Astrophysics and Space Science 4*:387-391.

Vanícek P (1971) Further Development and Properties of the Spectral Analysis by Least-Squares. *Astrophysics and Space Science 12*:10-33.

Vaníček P, Krakiwsky EJ (1986) *Geodesy: The Concepts*. North Holland, Amsterdam (Second Edition).

Wells DE, Vaníček P. (1978). Least Squares Spectral Analysis. Report Series /BI-R-78-8/December 1978, Bedford Institute of Oceanography, Dartmouth, Nova Scotia, Canada.

Wells DE, Vaníček P, Pagiatakis SD (1985) Least Squares Spectral Analysis Revisited. Technical Report 84, Department of Surveying Engineering, University of New Brunswick, Fredericton, Canada.

Long-term and Tidal variation observed by tiltmeters and extensometers at the Ala-Archa Observatory (Tian Shan)

Timofeev V.Y.*, Ducarme B., Yakovenko V.S.***, Duchkov A.D.*, Saricheva Y.K*, Kuchai O.A.*, Vandercoilden L.**, Revtova E.***

***Institute of Geophysics UIGGM SB RAS, Koptiug pr.,3,630090 Novosibirsk, Russia**
e-mail: sari@uiggm.nsc.ru

****Observatoire Royal de Belgique, Avenue Circulaire 3,**
1180 Bruxelles,Belgium
e-mail: ducarme@oma.be

*****Institute of Seismology NAS, Alanbai, Bishkek, Kyrgyzstan**

Introduction

The deformation of the crust is studied in many tectonically active parts of our planet. The measurements with tiltmeters and extensometers are useful in geodynamic investigation. Such measurements are performed in the northern part of the Tian Shan mountain system (Central Asia) at Ala-Archa seismological station (30 km to south from Bishkek, Kyrgyzstan) since 1985. The Underground Laboratory of Ala-Archa is located in an underground gallery specially escavated at almost 50 m under ground level. First seismological observation started at 1982. Tilt and strain instruments were installed at October of 1985. Long series of tilt and strain data have been observed at this station. These experimental data give an opportunity to estimate the tidal deformations and the level of long-term variation of tilt and strain for this region with high seismic activity. The goals of our study were the tidal analysis of these data and the analysis of long-term deformation in connection with regional seismic activity. When possible we have also evaluated and separated the local effects from the global tidal deformation model.

Ala-Archa Observatory and its tectonic surroundings

The North Tian Shan mountain region is an active deformation zone of Central Asia. Modern space geodetic data show that the southern part of this region is indenting into the northern part with a speed of 2cm/year [1].This intracontinental tectonic system is associated with strong seismic activity and surface deformations. The main tectonic feature for this region is compression. Thrust fault systems are connected with these compressive stresses. This stress mechanism is generated by the India-Eurasia convergence spreading northwards fan-shaped and affects a large part of the Asian plate [2]. Observations and measurements on special geophysical stations contributes to the knowledge of the intracontinental deformation

processes, supply the field constraints necessary to test and validate theoretical deformation models and provide new data that will contribute to seismic hazard assessment in that region.

The measurements were made in the geodynamic observatory Ala-Archa (coordinates 42°38'13''N, 74°29'43''E, altitude 1700m) situated on the northern slope of the Kirgizskogo mountain range in northern Tian Shan, 33 km south from Bishkek – the capital of Kyrgyzstan. This underground observatory is located near the North end of the North-South Chonkurchatskii thrust fault. The fault plane is dipping to the South with a 30° dip angle[3]. Surrounding territory is covered by complex fault systems and the boundary of a sedimentary basin lays 10 km to the North. This region presents an high seismic activity. Strong earthquakes occurred during the observation period.

The underground laboratory Ala-Archa is shown on Figure 1. It has a U shaped form with two 80m long entrance galleries and a 33m perpendicular gallery. The entrances are protected by 3 successive doors to increase thermal stability. Along the galleries there are side rooms for the installation of geophysical instruments. The ceiling, walls and floor of the galleries were covered with a special cement layer so that we have an hard core surrounded by fracturated rock. The pillars placed in the side caves are not connected with the floor of the gallery. We can consider the whole underground laboratory as a long-base instrument located inside the mountain. The entrances of Laboratory are located 40 meters above the level of the small Ala-Archa river. The annual thermal stability in the underground gallery is close to 0.25°C (Figure 2). In this region the frozen layer is 17cm thick during the winter. An important feature of this gallery is the strong seasonal effect connected with spring snow melting and raining. In winter period the gallery is practically dry but in spring or summer time there can be even water in the gallery. This feature affects the observation results especially for tilt and strain measurements.

Long-term observation with tiltmeters and extensometers from 1985 to 1997.

As shown on Figure 1 the tiltmeters were installed on a special basement in a side vault($3.4 \times 3.4 m^2$) at 23m from the entrance. To measure tilt in north-south and east-west directions we use ASNS type tiltmeters developed at the Institute of Physics of the Earth (Moscow). This instrument is similar to the Ostrovsky metallic tiltmeters but is equipped with a capacititive transducer. An electromagnetic step function is used for calibration. The scale of record is of the order of 5mm/mas.

A dual quartz tube (diameter 45mm) extensometer developed at the Institute of Physics of the Earth (Moscow) was installed along the axis of the 33m and 80m long galleries with two extremities in North-South and East-West directions respectively. The instrument has base lengths of 30m. The ends of the extensometer and the support systems are installed on special basements placed on the floor of gallery. Capacitive sensors are used for registration. The sensitivity of the instrument is at least 0.05 μmeter/mm(1.6 nanostrain/mm) on the recording paper. Piezoelectric crystals are used for calibration. The calibration is performed usually once per week. The recorders room is located in the seismological station building at 300m from the gallery entrances. The connection to the sensors is insured by a special buried line crossing the Ala-Archa river.

To estimate the regional stresses we can use the information given by the local earthquakes. During the observation period strong earthquakes happened near the observatory. On Figures 3,4,5 and Table 1,2,3 one can find the solutions for the following earthquakes: 13h30m 17.06.1988, coordinates 43.00°N, 77.42°E, M= 5.0, R=200 km; Tash-Bashatskoe 13h48m 05.03.1989, coordinates 42.57°N, 74.73°E, M=4.6, R=20 km; Susamskoe 02h04m19.08.1992, coordinates 42.07°N, 73.63°E, M=7.2, R=110 km.

TABLE 1.
The solution for the 13h30m 17.06.88 earthquake
(43.00°N, 77.42°E, M=5.0, R=200 km)

T (extension)		P (compression)	
PL	AZM	PL	AZM
90	239	22	150

TABLE 2.
The solution for the 13h48m 05.03.89 earthquake
(42.57°N, 74.73°E, M=4.6, R=20 km)

T (extension)		P (compression)	
PL	AZM	PL	AZM
33	356	90	264

TABLE 3.
The solution for the 02h04m 19.08.92 earthquake
(42.07°N, 73.63°E, M=7.2, R= 110 km)

T (extension)		P (compression)	
PL	AZM	PL	AZM
31	352	59	165

According to the Figures 3, 4, & 5 one can see that for the M=7.2 strongest earthquake we had a compressive stress in a near North-South direction which is typical for this region. For the smaller ones we had different situations with compressive or extensive stress in a near East-West direction reflecting the complex fault situation in the region.

The observed long-term curves of tilts in North-South and East-West directions are shown on Figure 6. First of all one can see the strong seasonal effect during the 1987 spring. In this period surface water infiltrated the gallery and produced tilts up to 7". In the following years this effect corresponds to a step in the curve with amplitude varying between 0.1" and 3". The step is always to the North and to the East.

Long term tilt during the period 1985-1997 reached nearly 2" to South in the meridian and near 7" to West in the prime vertical. It is more correct to consider the results only after the middle of year 1987 as in this case we have a lower seasonal effect on the curves. For this

ten-years period a systematic drift to South was observed reaching 5". For the second component we see that the tilt returned in 1997 to the middle 1987 level. We observe two different periods : during the first two years we have 3" drift to West and in the second part a tilt to East returning to the middle 1987 level. The inversion of the tilt coincide with the M=4.6 earthquake with epicenter at 20km from the station. In 1992 the strongest earthquake with magnitude 7.2 affected the tilt in both directions but did not change the sign of tilt rate. A small earthquake (M=4.6, R=20 km) with epicenter near the observatory had a stronger effect than the M=7.2, R=110 km earthquake at a larger distance.

Figure 7 shows the observed curves of the extensometers. As already mentioned for the tiltmeters one can see the strong seasonal effect ($2x10^{-6}$) during the spring 1987, but we can see other variations at this level during the observation period. It is no more the most important effect. The different reactions to spring water influence may be connected with the different base-lengths of the instruments. For the tiltmeters we have either the base of instrument (20cm) or the size of the basement (2.5m) and for the extensometers we have a longer base (30m). Long-term variation of strain had a systematic character for the east-west direction reaching $10x10^{-6}$ during the 1985-1997 period with different annual rates. For the North-South component an extension up to $3.5x10^{-6}$ is observed during the first three years. A compression of $7x10^{-6}$ is observed during the second part, after the large M=7.2 earthquake in 1992. This effect may be connected with the typical stress situation of the region: a compression along the NS direction and an extension along the EW direction.

Steps in strain variation are observed at pre- and post-earthquake period. The effect reaches $1x10^{-6}$ as well for the small M=4.6 earthquake as for the strong M=7.2 earthquake. The step amplitude is nearly constant at the μstrain(10^{-6}) level and we can create an equation connecting the magnitude and the distance for equal strain release:

$$M=A.\log R \qquad (1)$$

where M is magnitude and R is the distance in km from the epicenter to the observation point. We find the constant A when we use the information given by two earthquakes: M=7.2 and R=110 km ; M=4.6 and R=20km. The value of A is equal 3.51 and we have :

$$M = 3.51.\log R. \qquad (2)$$

It means that if we observe a strain level $1x10^{-6}$ for M=7.2 at 110 km distance , we should obtain the same level of deformation for M=6 at distance $R=10^{(6/3.51)} = 10^{1.709} = 51$ km .

This equation for equal strain level reflects the properties of the region.

The tilt and strain components reflected the air pressure variation (Figures 8 & 9).The first figure shows short period variations in strain and tilt at the tidal deformation level. The second figure shows long-term changes in tilts for different seasons. The high level of correlation with air pressure reflects the fracturation of the rock surrounding the underground laboratory.

Earth Tide Analysis of Tilts and Strain.

The earth tide analysis of the tiltmeters and extensometer data set 1993-1996 has been carried out with program ETERNA 3.0 using the Tamura tidal potential catalogue and numerical band pass filtering. The adjusted tidal parameters are given in Table 4 for North-South component and in Table 6 for East-West component. The standard deviation for

TABLE 4.

Tidal Analysis Results for tilt NS

```
##########################################################################
# STATION 1281 ALA-ARCHA/BISHEK                KYRGYZSTAN                #
#  42.6333 N    74.5  E  H 1680 M    P 40 M   D 3000 KM                  #
# TILTMETER NAKL NS                                                      #
# INSTALLATION       : V.S.YAKOVENKO                                     #
# MAINTENANCE        : V.S.YAKOVENKO                                     #
# DATA PROCESSING    : V.TIMOFEEV                                        #
# DATA ANALYSIS      : L.VANDERCOILDEN                                   #
##########################################################################

 Latitude: 42.6330 deg, longitude: 74.5000 deg, azimuth:    .000 deg.

 Summary of observation data :

 19940101     0...19940131230000  19940201     0...19940228230000
 19940301     0...19940331230000  19940401     0...19940430230000
 19940501     0...19940831230000  19940901     0...19940930230000
 19941001     0...19941231230000  19950101     0...19950131230000
 19950201     0...19950731230000  19950801     0...19950831230000
 19950901     0...19951130230000  19951201     0...19951231230000
 19960101     0...19960331230000

 Initial epoch for tidal force     : 1994. 1. 1. 0

 Number of recorded days in total :   821.00
 TAMURA 1987   tidal potential used.
 UNITY window used for least squares adjustment.
 Numerical filter is PERTSEV 1959 with  51 coefficients.

 Estimation of noise by FOURIER-spectrum of residuals
 0.1 cpd band99999.9990  mas          1.0 cpd band     .1826  mas
 2.0 cpd band     .1466  mas          3.0 cpd band     .0658  mas
 4.0 cpd band     .0446  mas          white  noise     .0774  mas

 adjusted tidal parameters :

 from      to       wave   ampl. ampl.fac.    stdv. ph. lead    stdv.
 [cpd]     [cpd]     [ mas    ]                        [deg]     [deg]

  .721500  .906315 Q1       .165   1.53795  1.45344  49.5504  83.2784
  .921941  .940487 O1       .326    .57988   .20924  26.2831  11.9895
  .958086  .974188 M1       .103    .88610   .65190 -59.9667  37.3538
  .989049  .998028 P1       .241    .92143   .39839  77.9136  22.8315
  .999853 1.000147 S1      1.342 217.12922 24.41069-100.17171396.9401
 1.001825 1.003651 K1       .663    .83896   .14694  58.9040   8.4195
 1.005329 1.005623 PSI1     .606  98.11834 17.31441  72.9773 992.0143
 1.007595 1.011099 PHI1     .200  17.77697  9.16958 102.3772 525.3247
 1.013689 1.044800 J1       .142   3.21736  4.71855 111.5723 270.4408
 1.064841 1.216397 OO1      .321  13.26770  5.64110 142.4527 323.2030
 1.719381 1.872142 2N2      .264   1.09743   .27052  11.5911  15.4996
 1.888387 1.906462 N2       .816    .54049   .05520   2.9113   3.1626
 1.923766 1.942753 M2      5.084    .64515   .01043    .1168    .5974
 1.958233 1.976926 L2       .461   2.06933   .28889  49.5509  16.5529
 1.991787 2.002885 S2      2.249    .61342   .02310  32.1431   1.3236
 2.003032 2.182843 K2       .478    .47987   .10511  17.6322   6.0217
 2.753244 3.081254 M3       .064    .55725   .30175  33.5775  17.2885
 3.791964 3.937897 M4       .012   7.81528 14.80396-135.4555 848.2051

 Standard deviation of weight unit:     4.364
```

TABLE 6.

Tidal Analysis Results for tilt EW

```
#########################################################################
# STATION 1281 ALA-ARCHA                              KYRGYZSTAN        #
#  42.6333 N    74.5  E      H 1680 M    P 40 M   D 3000 KM            #
#                                                                       #
# TILTMETER NAKL EW                                                     #
# INSTALLATION       : V.S.YAKOVENKO                                    #
# MAINTENANCE        : V.S.YAKOVENKO                                    #
# DATA PROCESSING    : V.TIMOFEEV                                       #
# DATA ANALYSIS      : L.VANDERCOILDEN                                  #
#########################################################################
```

Latitude: 42.6330 deg, longitude: 74.5000 deg, azimuth:270.000 deg.

Summary of observation data :

19930101 0...19930630230000 19940101 0...19960331230000

Initial epoch for tidal force : 1993. 1. 1. 0

Number of recorded days in total : 1002.00
TAMURA 1987 tidal potential used.
UNITY window used for least squares adjustment.
Numerical filter is PERTSEV 1959 with 51 coefficients.

Estimation of noise by FOURIER-spectrum of residuals

0.1 cpd band	99999.9990 mas		1.0 cpd band	.1490	mas
2.0 cpd band	.1334 mas		3.0 cpd band	.0568	mas
4.0 cpd band	.0374 mas		white noise	.0699	mas

adjusted tidal parameters :

from [cpd]	to [cpd]	wave	ampl. [mas]	ampl.fac.	stdv.	ph. lead [deg]	stdv. [deg]
.721500	.906315	Q1	.469	.55522	.09794	27.1206	5.6114
.921941	.940487	O1	2.963	.67134	.01892	24.0789	1.0841
.958086	.974188	M1	.365	1.05049	.20455	35.5823	11.7195
.989049	.998028	P1	1.132	.55103	.03603	22.2854	2.0642
.999853	1.000147	S1	1.204	24.78015	2.22676	-6.8147	127.5639
1.001825	1.003651	K1	4.096	.65971	.01323	17.8775	.7581
1.005329	1.005623	PSI1	.353	7.26295	1.57633	148.8108	90.3123
1.007595	1.011099	PHI1	.197	2.22577	.83650	156.6404	47.9260
1.013689	1.044800	J1	.370	1.06549	.23999	26.5073	13.7507
1.064841	1.216397	OO1	.069	.36410	.52741	-40.4250	30.2182
1.719381	1.872142	2N2	.312	.87679	.14359	33.8510	8.2270
1.888387	1.906462	N2	1.157	.51946	.02961	8.3951	1.6966
1.923766	1.942753	M2	6.629	.56969	.00551	7.8143	.3159
1.958233	1.976926	L2	.181	.54965	.13876	33.2107	7.9502
1.991787	2.002885	S2	4.204	.77663	.01215	15.2377	.6963
2.003032	2.182843	K2	.899	.61086	.05350	16.5197	3.0660
2.753244	3.081254	M3	.109	.64692	.15101	15.4841	8.6524
3.791964	3.937897	M4	.013	5.55445	7.20463	137.2538	412.7924

Standard deviation of weight unit: 3.778

different components and for different periods is large of the order of 3 to 4 mas. As the results for the three years series and for partial analysis of one year series do agree within the RMS errors, we can conclude that the main problem is not to be found in temporal variations of the calibration factor but most probably in temporal variations of signal cable resistance. This last effect is also responsible of the large S1 amplitude. This situation is typical for a long signal cable with analog registration devices.

For comparison with the observed tidal parameters, the tilt tide parameters have been predicted from the Wahr-Dehant (1987)[4] model and the oceanic tidal load vector L computed using the Schwiderski model for the North-South and East-West components. If we call B the difference between the observed tidal vector and the predicted body tides according to [4], the discrepancy in amplitude and phase is given by the final residual vector X=B-L (Tables 5 & 7).

For North-South component the amplitudes of the diurnal waves are very small and we consider only the main semi-diurnal wave M2. The residual vector B for M2 is close to the oceanic load correction L in amplitude but has a large phase discrepancy. Consequently the discrepancy in amplitude of the anomalous vector X reaches 6.5 percents of the M2 amplitude. It corresponds roughly to a 10% attenuation of the strain amplitude. The observed amplitude factor $\gamma = 0.645$ is low compared to $\gamma_{md} = 0.705$.

For the East-West component we observe a stronger effects in amplitude and phase for the different tidal waves. The anomalous vector B reaches 1.5 mas for the main waves. It is ten times more than the oceanic correction. Strong phase anomalies reach 16°-22° for diurnal waves (0.7°-1.0° is the RMS error level) and 7-14° for semi-diurnal waves (0.3°-0.7° is the RMS error level). Here also a negative amplitude discrepancy is observed for all waves. For diurnal components X amplitude reaches 25 percent of the observed tidal amplitudes. For the strongest wave M2 it is 13 percents with RMS error level 1 percent.

The anomaly for tidal tilt parameter may be due to cavity and topographic effects as well as to the regional geological conditions.

The earth tide analysis of the strain data set 1993-1996 has been carried out with programs VEN66 with CTE550 potential and ETERNA 3.0 with the Tamura tidal potential catalogue and numerical filtering. The adjusted tidal parameters are given in Table 8 & 9 for North-South component and in Table 10 & 11 for East-West component. The following results are not yet corrected for the air pressure or ocean loading. The standard deviations for different components and for different periods are at the 2-5 nstrain level. The error level reaches 2 percents for M2 in NS component and is higher for the other waves. The results of tidal analysis by two methods are similar as well in amplitude as in phase except for the semi-diurnal waves in EW. The residues with respect to a theoretical model with given Love (h=0.621) and Shida(l=0.090) are presented in the last columns of Tables 8 & 10. The negative discrepancy in amplitudes reaches 30-60 percents for the largest waves. For the main diurnal and semi-diurnal waves in NS as wel as for the diurnal waves in EW the observed amplitude factor is close to 0.6. The semi-diurnal waves have a negligible amplitude in EW. The discrepancy in phases is only 1-4 degrees and corresponds to the RMS error level.

These large anomalies are probably due to the installation conditions as we get strong cavity effect when the fixed point of the dual instrument is placed at the angle of two perpendicular galleries (Figure 1). A second reason may be the surrounding rock fracturation. A third reason may be the complex fault conditions and the compressive stress in the area. Practically we are close to the model, with a 6.5 percents discrepancy, only for tilt wave M2 in North-South direction.

TABLE 5.

Results for tilt in North-South
$X(X,\chi) = B(B,\beta) - L(L,\lambda)$

Wave	Theor. Ampl.	B	β	L	λ	X	χ
N2	1.51	0.22	169.4	0.08	66.1	0.25	-173.4
M2	7.88	0.33	178.2	0.28	61.2	0.52	-152.7
S2	3.66	1.34	117.1	0.13	25.5	1.35	122.7

TABLE 7.

Results for tilt in East-West
$X(X,\chi) = B(B,\beta) - L(L,\lambda)$

Wave	Theor. Ampl.	B	β	L	λ	X	χ
O1	4.41	1.25	105.3	0.09	64.9	1.18	108.3
K1	6.21	1.41	117.3	0.16	47.2	1.37	123.5
N2	2.23	0.42	156.3	0.04	167.1	0.38	155.1
M2	11.63	1.68	147.6	0.17	164.7	1.52	145.7
S2	5.41	1.16	72.9	0.06	160.4	1.15	69.7

Conclusions.

The observations in the underground observatory Ala-Archa show interesting long term effects. These variations reflected the pre- and post-earthquake regional deformation. We observed changes in the E-W tilt curve and in the N-S strain curve after a M=4.6 earthquake at 20km from the station. After it the extensometers reflected the typical stress situation of the region – a compression along the North-South direction and a extension along the East-West axis. For a given $1x10^{-6}$ deformation(1μstrain) observed with the extensometers we found a relation between the magnitude of earthquakes and the distance from the epicentre:

$M = 3.51 \log R$,

where R is in km.

For tidal amplitude we found negative anomalies for tilt and strain. It means that the amplitudes are systematically reduced compared to the models. Only the M2 wave in tilt NS is close to the model. For the other components we have anomalies in amplitude of more than 10 percents. For tilt the phase differences are generally large. For strain phase the discrepancy is at the RMS error level. Cavity and geological effects may explain these discrepancies [5].

Acknowledgement

Our cooperation work was supported by INCO-COPERNIKUS project no PL 96-3202 "Landslides triggered by earthquakes in Kyrgyzstan, Tian Shan" and partly by the Belgo-Russian agreements for Scientific and Technical Cooperation and by the Russian Fund for Scientific Research (98-05-65227, 98-05-65278).

References

1.Abdrakhmatov K.Ye., Aldazhanov S.A., Hager B.H. et al. Relatively recent construction of the Tien Shan inferred from GPS measurements of present-day crustal deformation rates // Letter to Nature, 1996, v.384, pp.450-453.

2.Avoac J.P., Tapponnier P. Kinematic model of deformation in central Asia // Geophys. Res. Lett., 1993, v.20(10), pp.895-898.

3. Chedia O.K. Morpho-structures and modern tectonic of Tian Shan. (in Russian) "Ilim", Frunze, 1986.

4. Dehant, V. Tidal parameters for an inelastic Earth. Physics of the Earth and Planetary Interior, vol. 49, 97-116, 1987.

5. Harrison, J.C. Cavity and topographic effects in tilt and strain measurements. Journal of Geophysical Research, vol.81, 319-328, 1976

TABLE 8.

Tidal Analysis Results for strain NS
VEN66 method

STATION 1281 ALA-ARCHA/BISHEK COMPOSANTE EXTENSOMETRIQUE KYRGYZSTAN

42.6333 N 74.5 E H 1680 M P 40 M D 3000 KM
EXTENSOMETER NS
INSTALLATION : V.S.YAKOVENKO
MAINTENANCE : V.S.YAKOVENKO
DATA PROCESSING : V.TIMOFEEV
LEAST SQUARE ANALYSIS / VENEDIKOV FILTERS ON 48 HOURS / PROGRAMMING B.DUCARME
POTENTIAL CARTWRIGHT-TAYLER-EDDEN / COMPLETE DEVELOPMENT
COMPUTING CENTER INTERNATIONAL CENTER FOR EARTH TIDES/FAGS/ BRUSSELS
DATA PROCESSING BY L.VANDERCOILDEN ON 99/11/23
COMPUTER HP-UX 9000/819
AZIMUT .00S-E

VALEUR DES NOMBRES DE LOVE :
ORDRE 2 H=.6206 L=.0904
ORDRE 3 H= .289 L= .015
E 0 94 1 2/94 1 4 94 1 8/94 530 94 6 2/94 622 94 626/94 630 94 7 4/94 7 6
E 0 94 710/94 722 94 726/9412 1 9412 5/9412 5 9412 9/941225 941229/95 128
E 0 95 2 1/95 211 95 215/95 3 3 95 3 7/95 311 95 315/95 4 8 95 414/95 516
E 0 95 520/95 6 7 95 613/95 629 95 7 3/95 7 9 95 713/96 1 5 96 1 9/96 131
E 0 96 2 4/96 331

TIME INTERVAL 821.0 DAYS 18672 READINGS 21 BLOKS EFFICIENCY 0.95

WAVE GROUP ARGUMENT	N	WAVE	ESTIMATED AMPL. R.M.S.		AMPL. FACTOR	R.M.S.	PHASE DIFF.	R.M.S.	RESIDUE AMPL.	PHASE
127.-129.	11	SIGMA1	0.23	0.19	1.8399	1.5211	-70.875	47.355	0.22	-102.6
133.-136.	20	Q1	0.21	0.19	0.2700	0.2395	-7.849	50.859	0.57	-177.1
137.-139.	10	RO1	0.19	0.18	1.2578	1.1912	-132.473	54.327	0.31	-153.2
143.-145.	16	O1	2.52	0.18	0.6158	0.0443	4.573	4.121	1.53	172.5
152.-155.	15	NO1	0.16	0.18	0.5063	0.5595	65.754	63.305	0.29	149.0
161.-163.	10	P1	1.54	0.15	0.8114	0.0805	-20.473	5.680	0.59	-114.1
164.-164.	3	S1	0.50	0.22	11.1754	4.8065	109.701	25.023	0.52	113.6
165.-168.	20	K1	3.08	0.17	0.5370	0.0294	-2.616	3.140	0.42	-160.5
175.-177.	14	J1	0.28	0.18	0.8731	0.5623	-55.008	36.898	0.28	-126.1
184.-186.	11	OO1	0.20	0.28	1.1411	1.5814	-18.317	79.392	0.06	-78.3

WAVE GROUP ARGUMENT	N	WAVE	ESTIMATED AMPL. R.M.S.		AMPL. FACTOR	R.M.S.	PHASE DIFF.	R.M.S.	RESIDUE AMPL.	PHASE
233.-236.	10	2N2	0.37	0.20	1.1992	0.6581	-21.745	31.459	0.14	-75.6
237.-23A.	10	MU2	0.35	0.20	0.9453	0.5228	176.341	31.694	0.73	178.2
243.-245.	13	N2	1.36	0.19	0.5767	0.0825	2.970	8.198	1.00	176.0
246.-248.	11	NU2	0.26	0.19	0.5759	0.4237	113.442	42.115	0.60	156.7
252.-258.	26	M2	7.09	0.19	0.5775	0.0152	0.223	1.503	5.19	179.7
265.-265.	9	L2	0.60	0.15	1.7243	0.4361	17.540	14.486	0.29	38.9
267.-272.	5	T2	0.77	0.19	2.2993	0.5620	73.405	14.016	0.75	98.9
273.-273.	4	S2	3.90	0.19	0.6818	0.0333	-3.916	2.784	1.85	-171.7
274.-277.	12	K2	1.01	0.23	0.6477	0.1492	-28.384	13.196	0.82	-144.4

WAVE GROUP ARGUMENT	N	WAVE	ESTIMATED AMPL. R.M.S.		AMPL. FACTOR	R.M.S.	PHASE DIFF.	R.M.S.	RESIDUE AMPL.	PHASE
327.-375.	17	M3	0.06	0.06	0.8644	0.9424	103.203	62.600	0.09	144.9

STANDARD DEVIATION D 13.48 SD 16.42 TD 5.31 10E-9

QUALITY FACTORS : Q1= 1.3 Q2= 5.2

TABLE 9.

Tidal Analysis Results for strain NS
ETERNA method

```
##########################################################################
# STATION 1281 ALA-ARCHA/BICHKEK                    KYRGYZSTAN           #
#  42.6333 N    74.5  E      H 1680 M    P 40 M   D 3000 KM             #
# INSTITUTE OF SEISMOLOGY                                                #
# DEFNS : 30 M QUARTZ TUBE EXTENSOMETER                                  #
#                                                                        #
# INSTALLATION       : V.S.YAKOVENKO                                     #
# MAINTENANCE        : V.S.YAKOVENKO                                     #
# DATA PROCESSING    : V.TIMOFEEV                                        #
# DATA ANALYSIS      : L.VANDERCOILDEN                                   #
##########################################################################
```

Latitude: 42.6330 deg, longitude: 74.5000 deg, azimuth: .000 deg.

Summary of observation data :

19940101	0...19940430230000	19940501	0...19940531230000
19940601	0...19940731230000	19940801	0...19940930230000
19941001	0...19941031230000	19941101	0...19941130230000
19941201	0...19941231230000	19950101	0...19950531230000
19950601	0...19950731230000	19950801	0...19951231230000
19960101	0...19960331230000		

Initial epoch for tidal force : 1994. 1. 1. 0

Number of recorded days in total : 821.00
TAMURA 1987 tidal potential used.
UNIT window used for least squares adjustment.
Numerical filter is PERTSEV 1959 with 51 coefficients.

Estimation of noise by FOURIER-spectrum of residuals

0.1 cpd band	99999.9990 nstr	1.0 cpd band	.2096 nstr
2.0 cpd band	.2643 nstr	3.0 cpd band	.1068 nstr
4.0 cpd band	.0717 nstr	white noise	.1077 nstr

adjusted tidal parameters :

from [cpd]	to [cpd]	wave	ampl. [nstr]	ampl.fac.	stdv.	ph. lead [deg]	stdv. [deg]
.721500	.906315	Q1	.397	.48342	.15638	-8.4703	8.9654
.921941	.940487	O1	2.668	.62220	.02995	.2886	1.7165
.958086	.974188	M1	.249	.73698	.37563	28.1704	21.5236
.989049	.998028	P1	1.652	.82777	.05505	-23.5917	3.1547
.999853	1.000147	S1	.587	12.43825	3.36000	110.4823	192.3304
1.001825	1.003651	K1	3.089	.51219	.02030	-2.9063	1.1632
1.005329	1.005623	PSI1	.706	14.96270	2.38066	-26.4031	136.4016
1.007595	1.011099	PHI1	.275	3.20756	1.28621	-83.3491	73.7086
1.013689	1.044800	J1	.320	.95021	.37812	-64.9799	21.6639
1.064841	1.216397	OO1	.266	1.44348	.95619	-47.7255	54.7841
1.719381	1.872142	2N2	.140	.37359	.28731	-125.9918	16.4621
1.888387	1.906462	N2	1.351	.57747	.05849	.9812	3.3511
1.923766	1.942753	M2	7.201	.58940	.01108	-.0169	.6346
1.958233	1.976926	L2	.555	1.60633	.31551	24.2582	18.0776
1.991787	2.002885	S2	3.952	.69530	.02455	-2.9868	1.4064
2.003032	2.182843	K2	.941	.60875	.11182	-23.8510	6.4067
2.753244	3.081254	M3	.032	.48340	.77975	72.6861	44.6772
3.791964	3.937897	M4	.020	40.67599	68.09736	122.05173	901.4860

Standard deviation of weight unit: 5.565

TABLE 10.

Tidal Analysis Results for strain EW
VEN66 method

STATION 1281 ALA-ARCHA/BISHEK COMPOSANTE EXTENSOMETRIQUE KYRGYZSTAN

42.6333 N 74.5 E H 1680 M P 40 M D 3000 KM
EXTENSOMETER EW
INSTALLATION : V.S.YAKOVENKO
MAINTENANCE : V.S.YAKOVENKO
DATA PROCESSING : L.VANDERCOILDEN
LEAST SQUARE ANALYSIS / VENEDIKOV FILTERS ON 48 HOURS / PROGRAMMING B.DUCARME
POTENTIAL CARTWRIGHT-TAYLER-EDDEN / COMPLETE DEVELOPMENT
COMPUTING CENTER INTERNATIONAL CENTER FOR EARTH TIDES/FAGS/ BRUSSELS
DATA PROCESSING BY L.VANDERCOILDEN ON 99/11/23
COMPUTER HP-UX 9000/819
AZIMUT 90.00S-E

VALEUR DES NOMBRES DE LOVE :
ORDRE 2 H=.6206 L=.0904
ORDRE 3 H= .289 L= .015
E230 95 1 2/95 530 95 6 2/95 730 95 8 2/951230

TIME INTERVAL 364.0 DAYS 8688 READINGS 3 BLOKS EFFICIENCY 0.99

WAVE GROUP ARGUMENT	N	WAVE	ESTIMATED AMPL. R.M.S.		AMPL. FACTOR	R.M.S.	PHASE DIFF.	R.M.S.	RESIDUE AMPL.	PHASE
133.-136.	20	Q1	0.88	0.17	0.6660	0.1287	5.185	11.079	0.45	169.7
143.-145.	16	O1	4.06	0.16	0.5850	0.0236	-2.057	2.313	2.83	-177.0
152.-155.	15	NO1	0.46	0.20	0.8418	0.3738	-7.164	25.433	0.10	-145.2
161.-163.	10	P1	1.65	0.14	0.5117	0.0420	3.908	4.701	1.38	175.3
164.-168.	23	S1K1	4.22	0.15	0.4331	0.0155	-2.006	2.056	3.37	-177.5
175.-177.	14	J1	0.25	0.16	0.4594	0.2999	5.959	37.423	0.30	175.1
184.-186.	11	OO1	0.33	0.31	1.0906	1.0341	54.744	54.344	0.29	112.9

WAVE GROUP ARGUMENT	N	WAVE	ESTIMATED AMPL. R.M.S.		AMPL. FACTOR	R.M.S.	PHASE DIFF.	R.M.S.	RESIDUE AMPL.	PHASE
233.-23A.	20	2N2	0.17	0.05	2.4210	0.7044	1.399	16.659	0.10	2.4
243.-248.	24	N2	0.37	0.06	0.8543	0.1338	1.002	8.977	0.06	174.1
252.-258.	26	M2	2.17	0.05	0.9704	0.0229	3.204	1.354	0.14	119.9
265.-265.	9	L2	0.09	0.03	1.4969	0.4688	50.775	17.945	0.07	92.6
267.-273.	9	S2	1.11	0.05	1.0658	0.0499	2.415	2.685	0.08	34.7
274.-277.	12	K2	0.21	0.07	0.7277	0.2315	20.864	18.225	0.12	141.0

WAVE GROUP ARGUMENT	N	WAVE	ESTIMATED AMPL. R.M.S.		AMPL. FACTOR	R.M.S.	PHASE DIFF.	R.M.S.	RESIDUE AMPL.	PHASE
327.-375.	17	M3	0.01	0.03	0.7231	1.6194	179.779	128.205	0.03	179.9

STANDARD DEVIATION D 8.17 SD 3.10 TD 1.69 10E-9

QUALITY FACTORS : Q1= 4.0 Q2= 10.8

TABLE 11.

Tidal Analysis Results for strain EW
ETERNA method

```
##########################################################################
# STATION 1281 ALA-ARCHA/BICHKEK                    KYRGYZSTAN           #
#  42.6333 N    74.5  E      H 1680 M    P 40 M   D 3000 KM              #
#                                                                        #
# EXTENSOMETER DEF EW                                                    #
# INSTALLATION       : V.S.YAKOVENKO                                     #
# MAINTENANCE        : V.S.YAKOVENKO                                     #
# DATA PROCESSING    : V.TIMOFEEV                                        #
# DATA ANALYSIS      : L.VANDERCOILDEN                                   #
##########################################################################

 Latitude: 42.6330 deg, longitude: 74.5000 deg, azimuth:-90.000 deg.

 Summary of observation data :

 19950101      0...19950531230000  19950601      0...19950731230000
 19950801      0...19951231230000

 Initial epoch for tidal force     : 1995. 1. 1. 0

 Number of recorded days in total :   365.00
 TAMURA 1987   tidal potential used.
 UNIT window used for least squares adjustment.
 Numerical filter is PERTSEV 1959 with  51 coefficients.

 Estimation of noise by FOURIER-spectrum of residuals
 0.1 cpd band99999.9990  nstr         1.0 cpd band      .1811  nstr
 2.0 cpd band      .0958  nstr         3.0 cpd band      .0521  nstr
 4.0 cpd band      .0325  nstr         white  noise      .0677  nstr

 adjusted tidal parameters :

 from       to       wave   ampl.  ampl.fac.     stdv.  ph. lead     stdv.
 [cpd]      [cpd]      [ nstr   ]                          [deg]      [deg]

  .721500   .906315  Q1      1.031    .77620    .08640    5.4427    4.9531
  .921941   .940487  O1      3.927    .56611    .01640   -1.5815     .9394
  .958085   .974188  M1       .359    .65827    .25678   13.3265   14.7062
  .989049  1.011099  PSK1    4.271    .43778    .01024    -.8490     .5871
 1.013689  1.044800  J1       .298    .54652    .20888  -20.8092   11.9717
 1.064841  1.216397  OO1      .345   1.15482    .62868   23.5363   36.0163
 1.719381  1.872142  2N2      .158   1.75190    .47685    5.6104   27.3325
 1.888387  1.906462  N2       .370    .65516    .09415    9.9580    5.3940
 1.923766  1.942754  M2      2.154    .73034    .01665    3.6503     .9544
 1.958233  1.976926  L2       .067    .80365    .37027   46.0564   21.2145
 1.991787  2.182843  SK2     1.079    .78638    .03604    2.7478    2.0649
 2.753244  3.081254  M3       .008    .47600   1.42516 -133.5711   81.6561

 Standard deviation of weight unit:      2.352
```

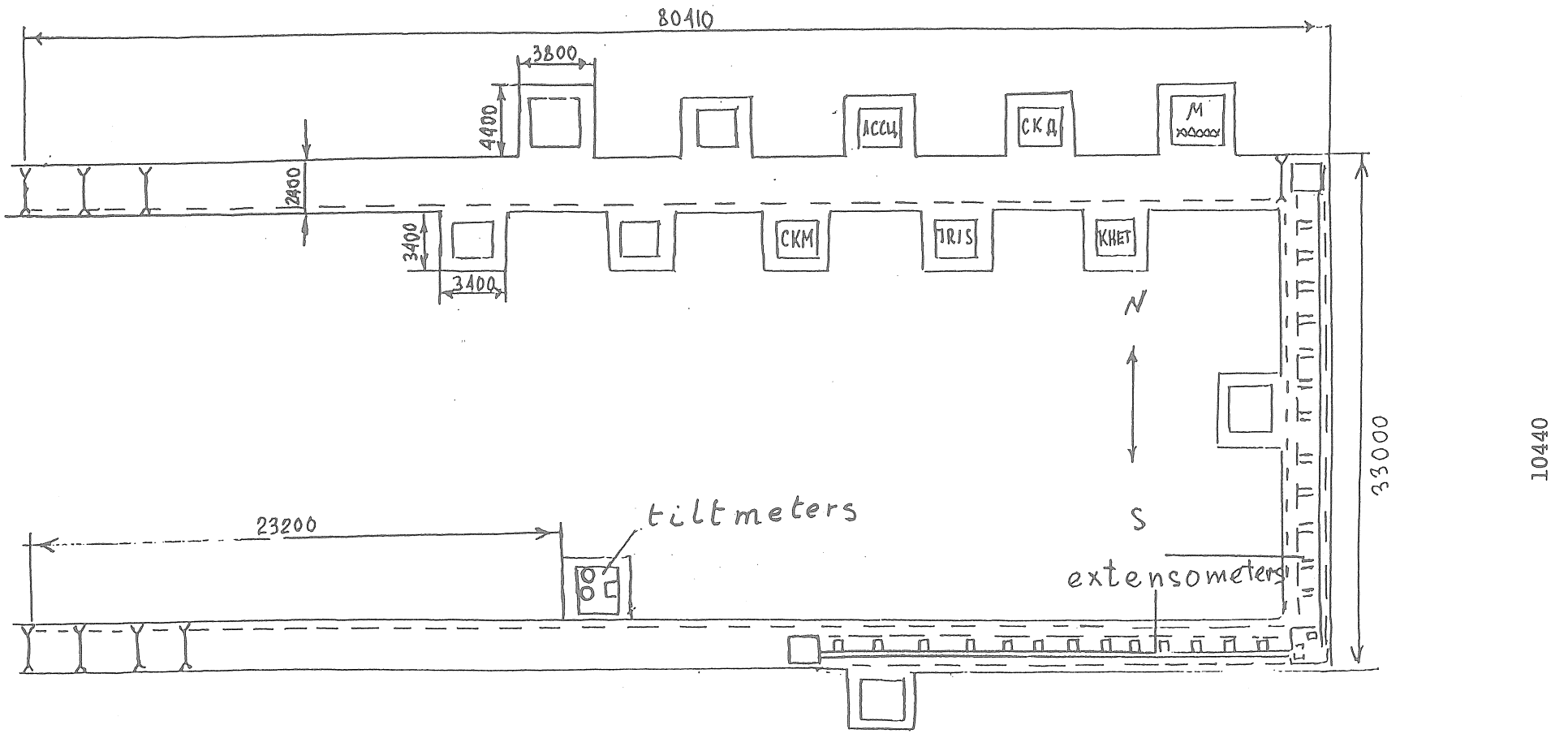

Figure 1: Sketch of Ala-Archa underground laboratory

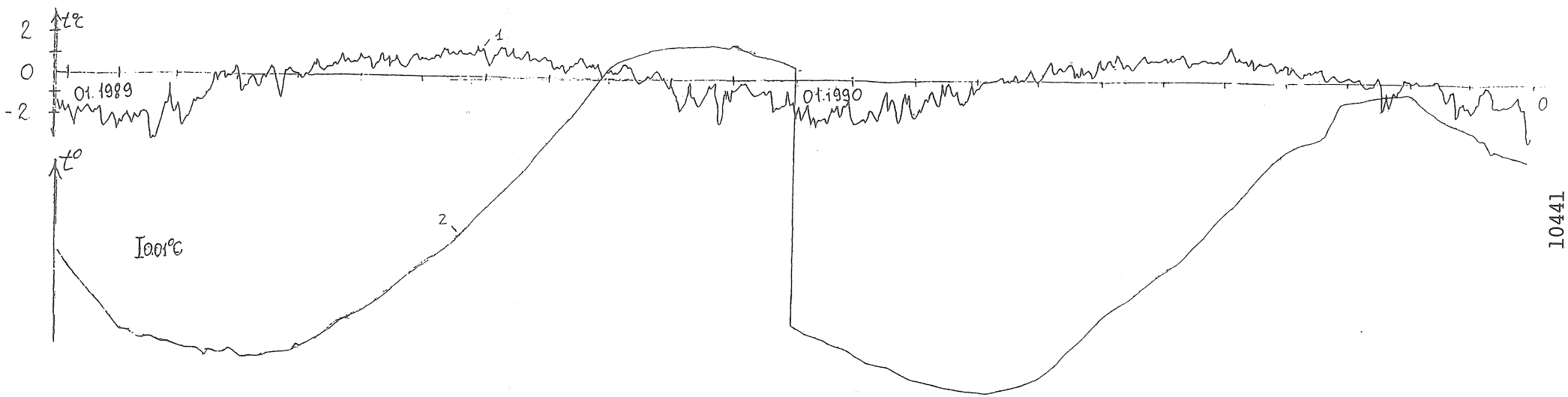

Figure 2: Temperature variations at Ala-Archa in 1989 and 1990 showing the annual variation

1- ground temperature

2- temperature inside the laboratory

Please note the scale difference. The lag of the annual wave in the laboratory is close to three months. An offset has been applied on curve 2 on January first 1990 to avoid superposition.

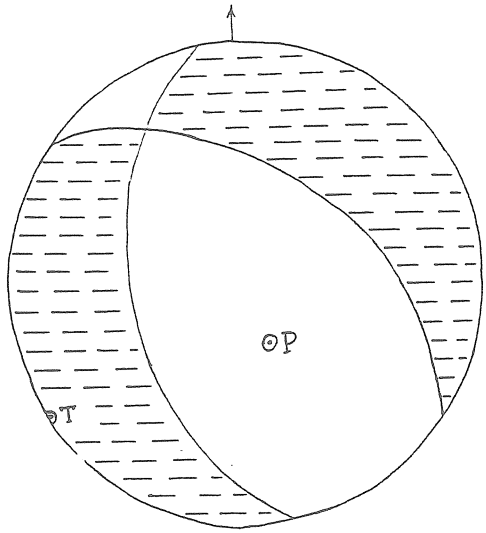

Figure 3: Focal mechanism of the 17/06/88 M=5.0 earthquake

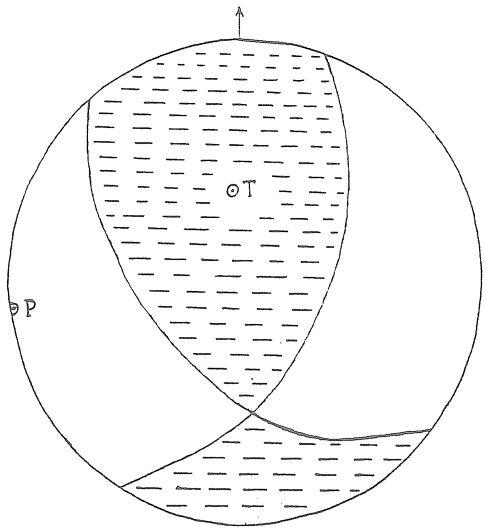

Figure 4: Focal mechanism of the 05/03/89 M=4.6 earthquake

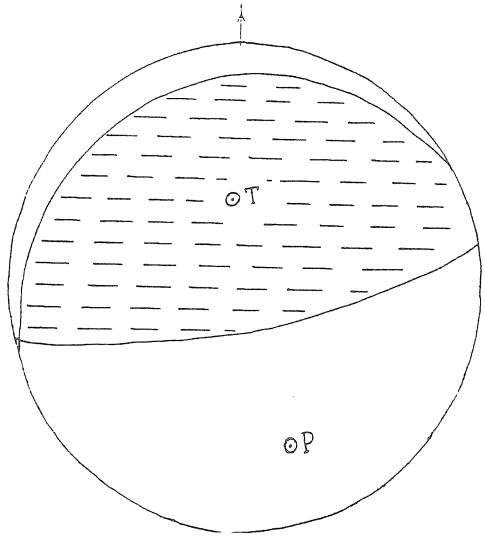

Figure 5: Focal mechanism of the 19/08/92 M=7.2 earthquake

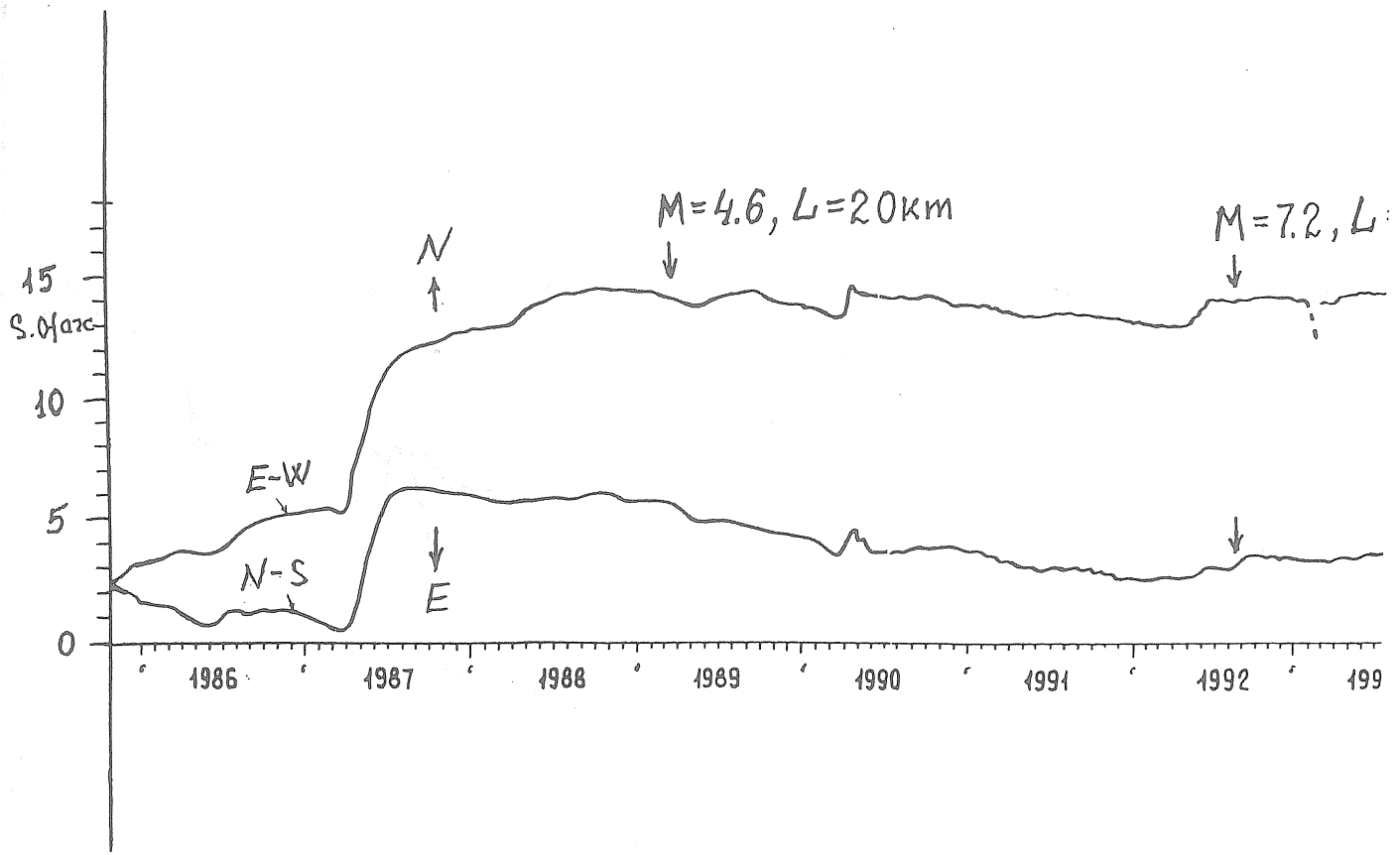

Figure 6: Non tidal tilt variations in NS and EW components

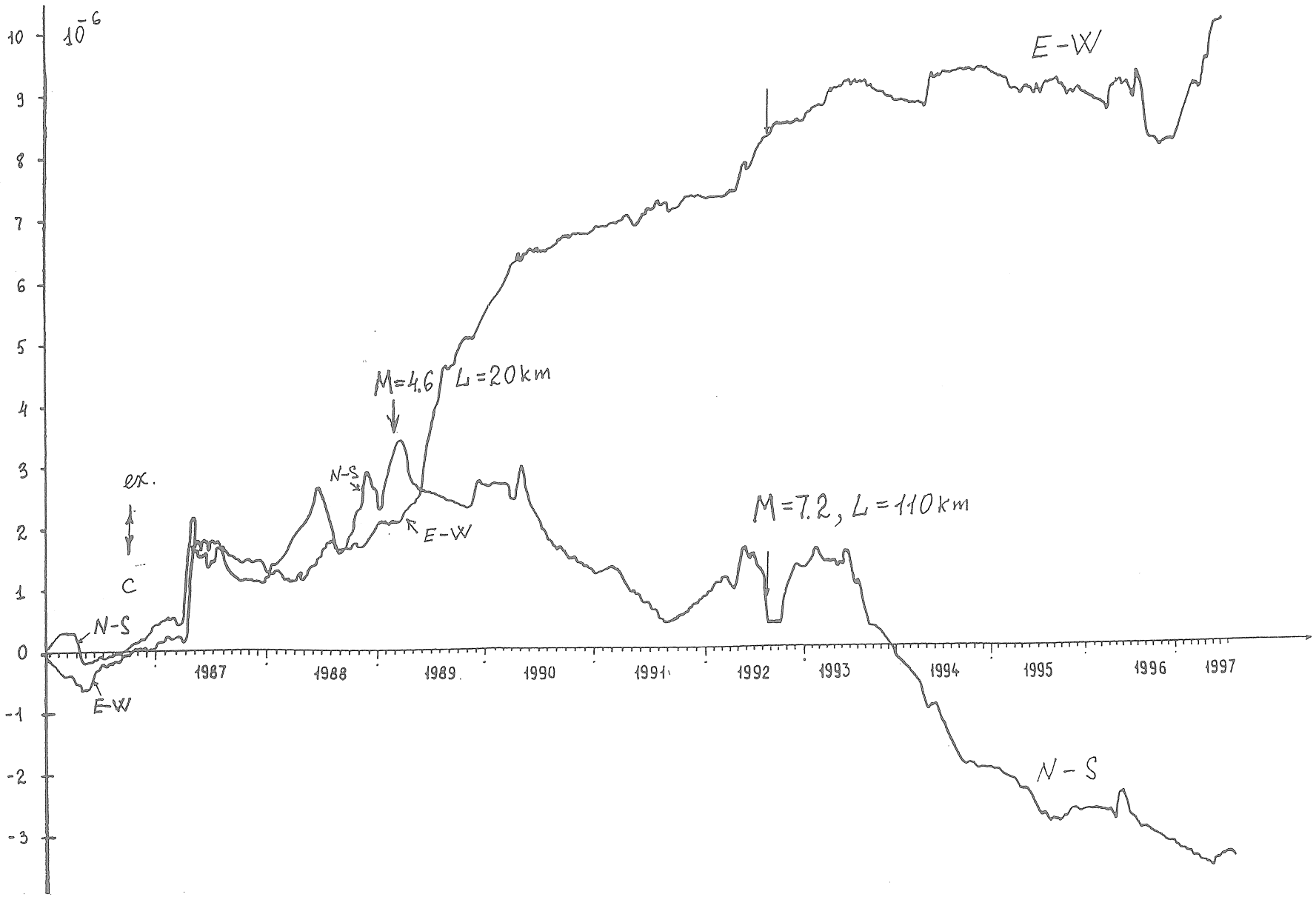

10444

Figure 7: Non tidal strain variations in NS and EW components

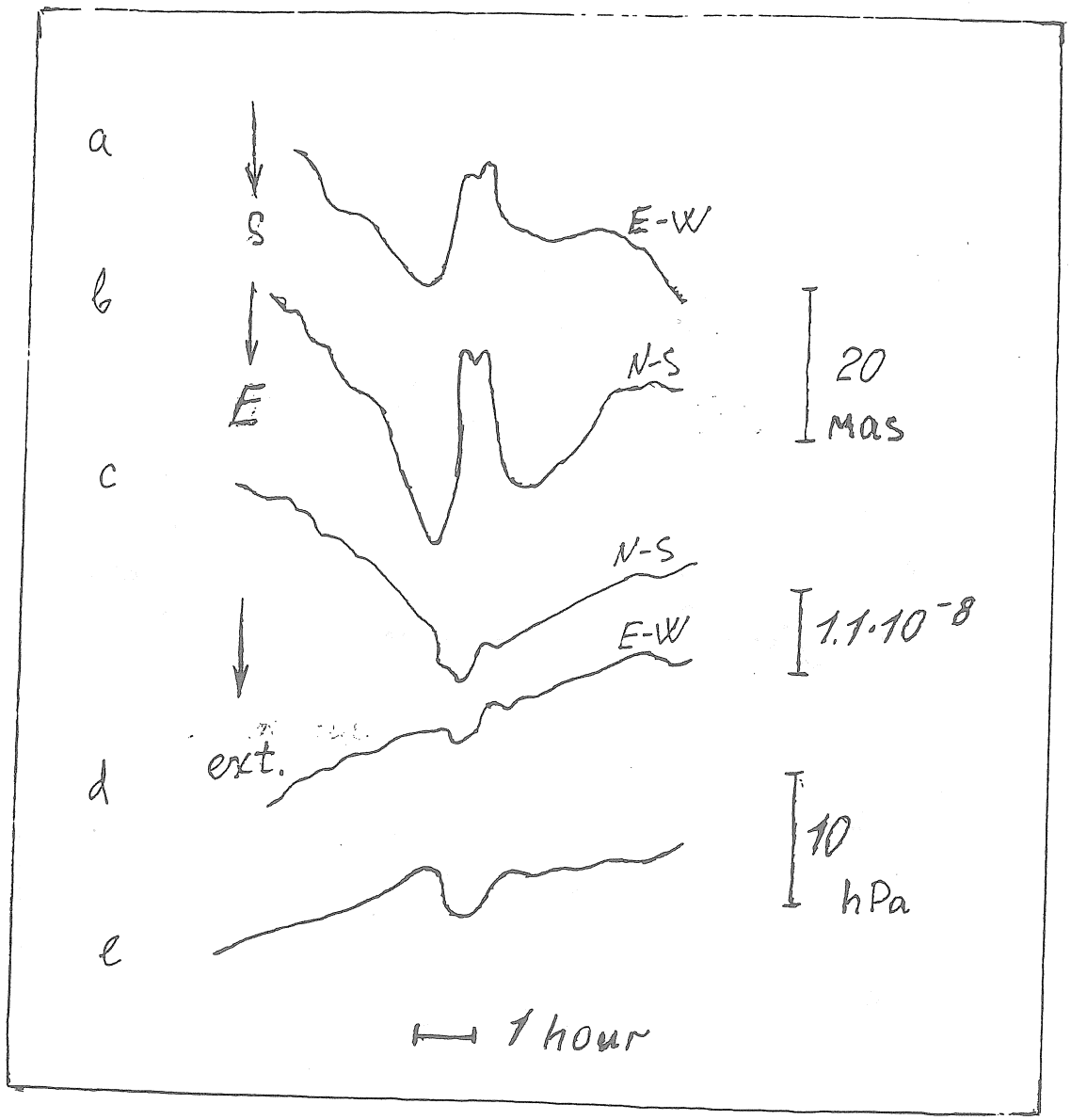

Figure 8: Typical short term correlation between tilt(a,b), strain(c,d) and pressure changes(e)

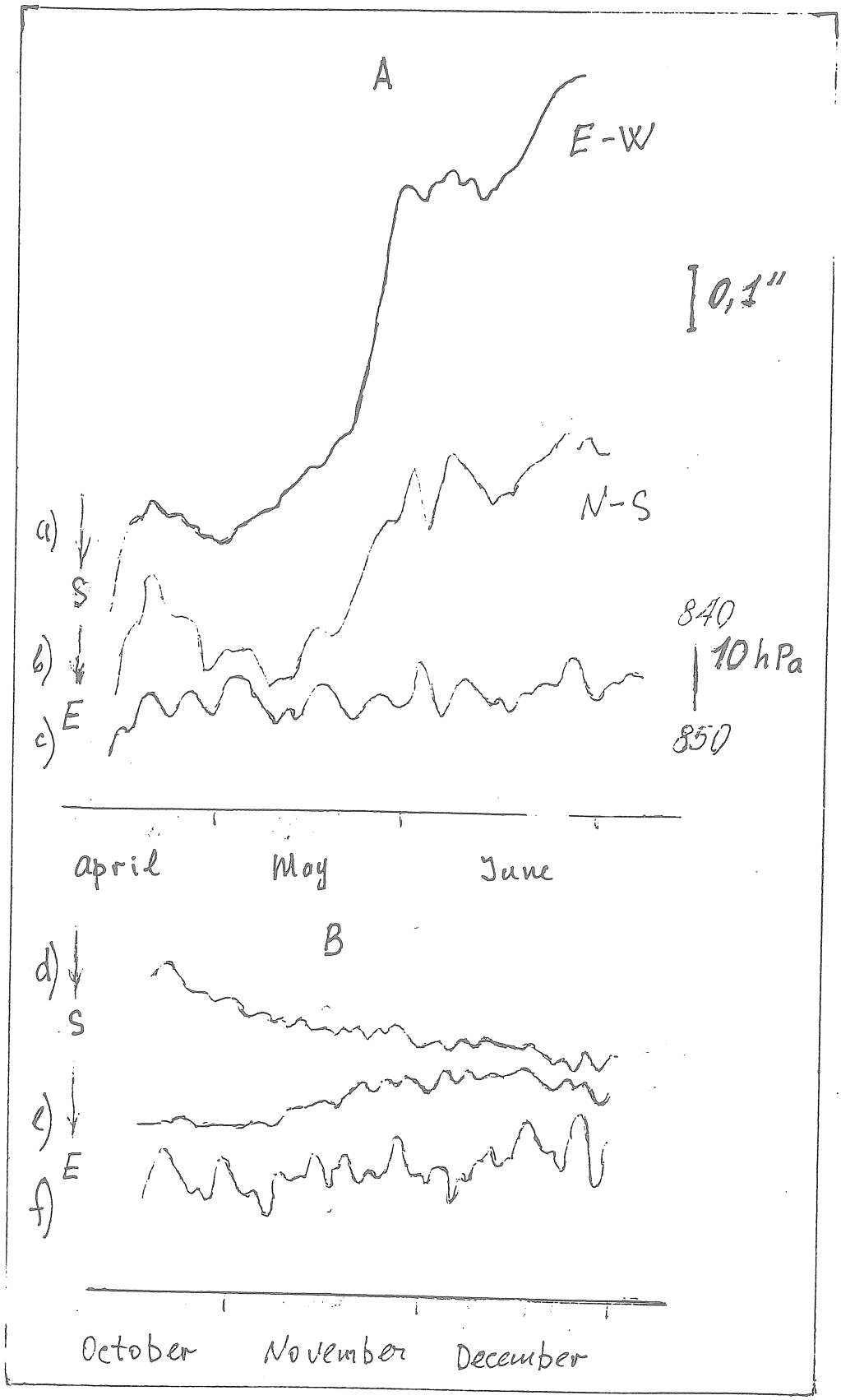

Figure 9: Typical correlation between long term A Tilt variations(a,b) and air pressure(c)
B Strain variations(d,e) and air pressure(f)

Tidal Analysis of Quartz-Tiltmeter Observations 1988-1998 at the Talaya Observatory (Baikal rift)

Timofeev V.Y.*, Ducarme B., Saricheva Y.K*, Vandercoilden L.*****
***Institute of Geophysics UIGGM SB RAS, Koptiug pr.,3,630090 Novosibirsk, Russia**
e-mail: sari@uiggm.nsc.ru
****Chercheur Qualifié FNRS**
Observatoire Royal de Belgique, Avenue Circulaire 3,
1180 Bruxelles,Belgium
e-mail: ducarme@oma.be
*****Observatoire Royal de Belgique, Avenue Circulaire 3**

Introduction

For many years on the former USSR territory ,the standard sensor to determine the tilt response of the Earth to the tidal forces was a short baseline metallic tiltmeter named Ostovsky, usually installed in underground stations as an high stability of environmental parameters was required. Another type of sensor was the quartz tiltmeter constructed by D.Gridnev. It was used some years in Garm and Poltava stations [1]. Long series were obtained with this instrument in Siberian stations for different purposes [2, 3]. Such quartz tiltmeters has been operated in the Talaya underground gallery since 1985. Preliminary result of short series of tidal tilts have been presented in [4]. Long series of tidal tilts have been observed at this station between 1988 and 1998. The station is installed in the centre of the Eurasian continent and the oceanic tidal loading is thus very low: 0.15mas for O1 and 0.06mas for M2 in North-South component and 0.22mas for O1 and 0.26mas for M2 in East-West component. The data processing and tidal analysis of these long series is described in this paper.

Installation of the tiltmetes.

Talaya station is an underground station primarily devoted to seismology. The station is situated in the South-West part of the Baikal rift. The Main Sayan fault is located a few kilometers to the North. It has an East-West orientation in the vicinity of Talaya observatory. Continuous observations of tilts were made in the 90 m underground gallery. This gallery is cut horizontally in the marble and granite-gneiss rock massif in the 332° N azimuth. It has six side galleries (drifts) 20-25 m long. Drifts are oriented perpendicular the main gallery. The gallery is cut in the steep slope of a valley. According to geological data, the rock massif is old, of Archean age. It is generally monolithic. a fractured zone is noticed in the more distant drift, along its axis. A set of tiltmeters was installed on a special basement built on the bedrock. Tilts are measured in North-South and East-West directions. The azimuth of the tiltmeters can be accidentally changed during servicing e.g. when changing the lamp illuminating the photocells. This procedure is required once every three or five years. The tiltmeter's basement are placed in a 10 m drift at 47m from the gallery entrance (Figure 1). The cross section of the drifts and the gallery is nearly 2x2 m^2. The average temperature in the gallery is +1 °C, with an annual variation in the range of one degree. The humidity is high during the summer season(July-September) with condensation and water infiltrating from the surface. From October to June there is a long frost period and the depth of frozen ground reaches up to 2 m in this region. Snow covers the surface at the end of October and disappears in the beginig of May.

Gridnev quartz tiltmeters have a Zollner suspension. Calibration is possible using either the torque of a spring or an electromagnetic coil system. The elements of tiltmeters construction - beam, base and spring, are prepared from melted quartz. Instrumental period is asjusted between 5 and 10 second. Small deviation angles are measured by a photoelectric sensor with a resolution of 0.1nanorad. The photoelectric sensor consists of two photocells, designed for space solar batteries assembly, and a 0.3 Watt light source. The beam displacement change the photocell illumination (Figure 2). The current is registered without amplification on the photorecorder with the speed 10 mm per hour. The galvanometer period being 16s, the short period noise between 2 and 6 seconds is attenuated. The recording system, including galvanometers, is located in a building at 30 m from the gallery entrance. The signal cable is suspended close to the ground surface (from 0 to 4 m). An analog recording system was used until the end of 1998. Hourly readings were taken on the curves.

Observation and calibration.

Two different calibration methods are possible either by an electromagnetic system or by a micrometric screw driving a quartz spring. Both systems act directly on the lower fixation point of the beam(Figure 2). We keep the beam position close to zero to reduce the non-linearity of the registration system. The long term drift of the beam is compensated by the quartz spring only for the N-S component and by the spring and the electromagnet(up to end of 1988 only) for the E-W one. Calibrations were performed by moving the micrometric screw of 6 divisions and by injecting a stable current in the coils. Results obtained with the two methods are presented in Table 1.

Table 1.

Comparison of Calibration Methods
EW component from 87/02/05 to 87/07/06

Calibration with Micrometer (mm/arc second)	Electromagnetic Calibration (mm/arc second)
1556.3	1551.5
1546.1	1556.9
1591.5	1519.4
1467.7	1530.1
1647.8	1470.2
1488.2	1470.2
1520.0	1587.9
1564.3	1605.0
1600.1	1545.1
1584.7	1620.0
1601.8	1596.4
	1632.8
	1583.6
	1585.7
	1583.6
	1557.9
Mean 1560.8 ± 16.0 (±1.0%)	Mean 1562.3 ± 11.8 (±0.7%)

TABLE 2

Tidal Analysis Results for NS Component
VEN66 Method

STATION 1301 TALAYA COMPOSANTE NORD-SUD SIBERIE - RUSSI

51.68 N 103.65 E H 600 M D 2000 KM
TIME LAG -60 SEC.
PENDULE HORIZONTAL

LEAST SQUARE ANALYSIS / VENEDIKOV FILTERS ON 48 HOURS / PROGRAMMING B.DUCARME
POTENTIAL TAMURA COMPLETE DEVELOPMENT
COMPUTING CENTER INTERNATIONAL CENTER FOR EARTH TIDES/FAGS/ BRUSSELS
DATA PROCESSING BY L. VANDERCOILDEN ON 00/06/16
COMPUTER HP-UX 9000/819
AZIMUT .00N-E
DATA ARE GIVEN IN LOCAL TIME=UT+ .0HOUR

P 0	88 7 5/88 7 9	88 724/88 8 3	88 831/88 831	88 921/88 927	881024/881028
P 0	8811 9/881125	8812 2/8812 6	881217/881227	89 1 2/89 114	89 128/89 227
P 0	89 3 2/89 326	8911 2/891128	8912 3/891221	90 6 2/90 626	90 8 3/90 815
P 0	90 821/90 827	90 9 5/90 9 5	90 9 9/90 919	901011/901011	901015/901017
P 0	901022/901026	901111/901115	901118/901128	901229/91 1 2	91 6 4/91 624
P 0	91 7 4/91 716	91 8 4/91 814	91 821/91 831	91 9 5/91 913	91 922/91 928
P 0	9111 5/911123	9112 4/911212	911217/911229	92 1 2/92 120	92 124/92 128
P 0	92 214/92 224	92 3 2/92 330	92 512/92 522	92 6 6/92 620	92 7 2/92 728
P 0	92 8 3/92 821	92 9 3/92 921	9210 5/921013	921017/921029	9211 1/921121
P 0	9212 2/921220	93 1 3/93 226	93 3 2/93 3 8	93 316/93 322	93 4 2/93 420
P 0	93 514/93 530	93 6 2/93 620	93 7 2/93 7 2	93 7 6/93 7 8	93 717/93 729
P 0	93 8 2/93 820	93 9 8/931024	9311 2/931112	931121/931211	94 1 2/94 124
P 0	94 2 3/94 227	94 3 2/94 316	94 320/94 326	94 4 2/94 418	94 5 2/94 512
P 0	94 523/94 529	94 6 2/94 626	94 7 2/94 720	94 811/94 821	94 9 3/94 913
P 0	9410 3/9410 5	9411 2/941130	9412 3/95 130	95 2 2/95 226	95 312/95 312
P 0	95 316/95 330	95 4 2/95 512	95 519/95 523	95 612/95 628	95 7 2/95 730
P 0	95 8 5/95 829	95 9 7/9510 5	9511 2/951112	951216/96 1 1	

TIME INTERVAL 2738.0 DAYS 33456 READINGS 84 BLOKS EFFICIENCY 0.51

WAVE GROUP ARGUMENT	N	WAVE	ESTIMATED AMPL. R.M.S.	AMPL. FACTOR	R.M.S.	PHASE DIFF.	R.M.S.	RESIDUE AMPL.	PHASE
127.-12A.	20	SIGMA1	0.0440.070	0.96870	1.54619	141.2662	91.3271	0.071	157.22
133.-136.	33	Q1	0.2850.069	0.99945	0.24233	-4.6830	13.9099	0.091	-14.82
137.-13A.	18	RO1	0.0180.068	0.32603	1.26368	-76.4406	222.0138	0.037	-152.59
142.-145.	32	O1	1.5950.067	1.07139	0.04522	1.8145	2.4189	0.572	5.06
152.-155.	30	NO1	0.1510.054	1.29082	0.46316	43.3338	20.5735	0.108	74.26
160.-163.	17	P1	0.8950.066	1.29200	0.09467	8.2282	4.2075	0.421	17.71
164.-164.	4	S1	0.5140.096	31.38272	5.86006	128.1098	10.5467	0.521	129.11
165.-169.	35	K1	2.2180.066	1.05904	0.03170	-3.4938	1.7166	0.693	-11.25
174.-177.	25	J1	0.1520.066	1.29793	0.56108	10.8254	24.7693	0.075	22.42
184.-187.	23	OO1	0.1250.060	1.95226	0.93649	89.6972	27.4861	0.132	109.07
233.-236.	23	2N2	0.1040.048	0.53401	0.24862	37.4395	26.6714	0.081	128.95
237.-23A.	21	MU2	0.1060.048	0.44995	0.20377	4.7704	25.9776	0.057	171.07
242.-245.	25	N2	1.0840.047	0.73597	0.03193	10.3743	2.4836	0.203	74.19
246.-249.	25	NU2	0.2200.047	0.78796	0.16647	23.0521	12.1065	0.087	82.86
252.-259.	56	M2	5.4150.046	0.70389	0.00593	9.3758	0.4827	0.884	85.96
264.-268.	32	L2	0.1310.042	0.60202	0.19162	-10.9876	18.2185	0.032	-129.75
270.-273.	9	T2	0.1990.045	0.95135	0.21554	28.5602	13.0002	0.100	71.84
273.-273.	7	S2	2.8510.045	0.79655	0.01258	4.9783	0.9203	0.456	32.83
274.-278.	28	K2	0.6940.045	0.71292	0.04655	1.2063	3.7479	0.030	29.66
315.-3A5.	82	*M3	0.1050.018	1.11972	0.19225	3.4174	9.8232	0.030	12.05

STANDARD DEVIATION D 7.631 SD 5.246 TD 2.100 MSECA

QUALITY FACTORS : Q1= 1.6 Q2= 9.2
O1/K1 1.0117 1-O1/1-K1 1.2093 M2/O1 0.6570
CENTRAL EPOCH TJJ= 2448715.5

TABLE 3
Tidal Analysis Results for NS Component
ETERNA Method

```
##########################################################################
# STATION 1301 TALAYA                                                    #
#  51.68 N     103.644 E      H 550 M   D  2000 KM                       #
# TILTMETER N-S, REGULATED                                               #
# INSTALLATION       : TIMOFEEV  V.Y.                                    #
# MAINTENANCE        : TIMOFEEV, PANIN                                   #
# AZIMUTH 00.00                                                         #
##########################################################################

 Latitude: 51.6800 deg, longitude:103.6440 deg, azimuth:   .000 deg.

 Summary of observation data :

 19880704     0...19880709230000  19880723     0...19880803230000
 ..............
 19951215     0...19960101230000

 Initial epoch for tidal force    : 1988. 7. 4. 0.

 Number of recorded days in total :  1455.50
 TAMURA 1987   tidal potential used.
 UNITY window used for least squares adjustment.
 Numerical filter is PERTSEV 1959 with  51 coefficients.

 Estimation of noise by FOURIER-spectrum of residuals
 0.1 cpd band99999.9990  mas          1.0 cpd band     .0857  mas
 2.0 cpd band     .0671  mas          3.0 cpd band     .0321  mas
 4.0 cpd band     .0239  mas          white  noise     .0407  mas

 adjusted tidal parameters :

 from      to       wave   ampl. ampl.fac.    stdv. ph. lead    stdv.
 [cpd]     [cpd]      [ mas    ]                      [deg]     [deg]

  .721500  .906315 Q1      .257    .90110   .14740  -5.2028   8.4505
  .921941  .940487 O1     1.588   1.06761   .02929   2.5178   1.6804
  .958086  .974188 M1      .191   1.63242   .29616  43.9514  16.9686
  .989049  .998028 P1      .885   1.27846   .06204   8.6385   3.5525
  .999853 1.000147 S1      .448  27.33261  3.79534 127.4763 217.3017
 1.001825 1.011099 K1     2.202   1.05245   .02079  -4.0804   1.1909
 1.013689 1.044800 J1      .168   1.43825   .35717  22.8649  20.4645
 1.064841 1.216397 OO1     .092   1.44107   .58750  90.9964  33.6754
 1.719381 1.872142 2N2     .092    .38933   .10511  18.7923   6.0228
 1.888387 1.906462 N2     1.097    .74515   .02220  10.8423   1.2716
 1.923766 1.942753 M2     5.409    .70363   .00433   9.5730    .2482
 1.958233 1.976926 L2      .129    .59166   .13507  -7.6152   7.7410
 1.991787 2.002885 S2     2.866    .80134   .00939   5.4323    .5358
 2.003032 2.182843 K2      .699    .71845   .03472   1.4398   1.9889
 2.753244 3.081254 M3      .082    .87432   .15599  15.3596   8.9361
 3.791964 3.937897 M4      .015  14.06653 10.01068 -83.4717 573.7007

 Standard deviation of weight unit:     2.504
 degree of freedom:                     30480
 Standard deviation:                    2.504   mas
```

TABLE 4
Tidal Analysis Results for EW Component
VEN66 Method

STAION 1301 TALAYA COMPOSANTE EST - OUEST SIBERIE - RUSSIE

51.68 N 103.65 E H 600 M D 2000 KM
PENDULE HORIZONTAL GRIDNEV
LEAST SQUARE ANALYSIS / VENEDIKOV FILTERS ON 48 HOURS / PROGRAMMING B.DUCARME
POTENTIAL TAMURA COMPLETE DEVELOPMENT
COMPUTING CENTER INTERNATIONAL CENTER FOR EARTH TIDES/FAGS/ BRUSSELS
DATA PROCESSING BY L. VANDERCOILDEN ON 00/03/16
COMPUTER HP-UX 9000/819
AZIMUT .00E-S

P 0 8810 4/8810 4 881026/881026 8811 9/881127 8812 2/881212 881217/881227
P 0 89 1 4/89 118 89 124/89 126 89 2 7/89 325 89 913/89 923 8910 9/891128
P 0 8912 3/8912 9 90 3 7/90 311 90 319/90 329 90 4 2/90 5 6 90 5 9/90 517
P 0 90 521/90 521 90 525/90 529 90 9 2/901030 9011 4/901128 9012 2/901212
P 0 901218/91 1 3 91 7 5/91 729 91 8 2/91 8 6 91 810/91 814 91 822/91 830
P 0 9111 2/911118 911217/911229 92 3 2/92 523 92 611/92 629 921010/921016
P 0 9211 1/9211 5 9212 2/921220 93 1 3/93 226 93 3 2/93 3 8 93 314/93 324
P 0 93 4 2/93 420 93 5 2/93 5 8 93 514/93 530 93 6 2/93 620 93 7 2/93 710
P 0 93 717/93 729 93 8 2/93 820 93 9 8/931024 9311 2/9311 8 931121/9312 1
P 0 9312 8/931210 931222/931226 94 1 2/94 120 94 523/94 529 94 6 2/94 624
P 0 94 7 2/94 728 94 8 3/94 819 9410 6/941010 9411 9/941125 9412 2/941230
P 0 95 1 2/95 130 95 2 2/95 218 95 315/95 325 95 4 2/95 524 95 612/95 628
P 0 95 7 2/95 730 95 8 5/95 829 95 9 7/95 919 9510 2/9510 8 951021/9511 6
P 0 951110/951124 9512 5/951229 96 1 3/96 127 96 2 9/96 227 96 317/96 323
P 0 96 4 2/96 420 96 511/96 628 96 711/96 727 96 8 2/96 8 6 96 9 3/96 919
P 0 9610 3/961023 9611 9/961121 97 4 1/97 4 3 97 4 8/97 424 97 5 2/97 6 9
P 0 97 612/97 630 97 7 3/97 830 97 9 2/971030 9711 2/9711 2 971116/971118
P 0 971122/971130 9712 3/971211 971216/971230

TIME INTERVAL 3376.0 DAYS 41424 READINGS 88 BLOKS EFFICIENCY 0.51

WAVE GROUP ARGUMENT	N	WAVE	ESTIMATED AMPL. R.M.S.	AMPL. FACTOR	AMPL. R.M.S.	PHASE DIFF.	PHASE R.M.S.	RESIDUE AMPL.	RESIDUE PHASE
127.-12A.	20	SIGMA1	0.0720.073	0.45816	0.46918	-40.4623	58.6661	0.070	-138.73
133.-136.	33	Q1	0.6870.072	0.70212	0.07309	1.2945	5.9623	0.021	47.90
137.-13A.	18	RO1	0.2220.071	1.19415	0.38226	-15.2376	18.3445	0.104	-34.04
142.-145.	32	O1	3.1300.070	0.61215	0.01374	0.7841	1.2861	0.391	173.71
152.-155.	30	NO1	0.2610.059	0.64792	0.14783	14.1158	13.0747	0.068	111.09
160.-163.	17	P1	1.3850.066	0.58204	0.02773	-13.0068	2.7256	0.443	-135.33
164.-164.	4	S1	0.6450.095	11.46028	1.69238	42.0313	8.3230	0.616	44.51
165.-169.	35	K1	4.6310.068	0.64401	0.00949	2.7613	0.8429	0.679	160.82
174.-177.	25	J1	0.3290.068	0.81776	0.16987	13.8536	11.9073	0.090	60.65
184.-187.	23	OO1	0.2150.067	0.97933	0.30680	-31.9728	17.9620	0.118	-74.34
233.-236.	23	2N2	0.1530.053	0.61770	0.21328	20.0737	19.7557	0.059	116.61
237.-23A.	21	MU2	0.1540.052	0.51218	0.17458	21.0227	19.5186	0.083	138.59
242.-245.	25	N2	1.2730.051	0.67797	0.02722	2.8599	2.2974	0.066	105.33
246.-249.	25	NU2	0.2000.050	0.56128	0.14100	7.9817	14.3834	0.054	149.16
252.-259.	56	M2	6.9720.050	0.71111	0.00505	-0.1393	0.4067	0.243	-4.00
264.-268.	32	L2	0.3050.042	1.10115	0.15007	7.7365	7.8094	0.119	20.12
270.-273.	9	T2	0.1790.049	0.66983	0.18491	48.3715	15.8482	0.148	115.74
273.-273.	7	S2	2.9940.050	0.65643	0.01098	-2.3966	0.9398	0.187	-138.06
274.-278.	28	K2	0.9540.052	0.76916	0.04187	-8.6456	3.1189	0.170	-57.37
315.-3A5.	82	*M3	0.0920.015	0.77231	0.12253	-8.4609	9.0907	0.014	-109.88

STANDARD DEVIATION D 8.545 SD 6.398 TD 1.903 MSECA

QUALITY FACTORS : Q1= 1.4 Q2= 8.7
RESIDUALS ARE GIVEN IN THE TRUE AZIMUT
O1/K1 0.9505 1-O1/1-K1 1.0895 M2/O1 1.1617
CENTRAL EPOCH TJJ= 2449125.5

TABLE 5
Tidal Analysis Results for EW Component
ETERNA Method

```
##########################################################################
# STATION 1301 TALAYA                                                    #
#  51.68 N     103.644 E      H 550 M   D  2000 KM                       #
# TILTMETER E-W,  GRIDNEV TYPE                                           #
# INSTALLATION       : TIMOFEEV  V.Y.                                    #
# MAINTENANCE        : TIMOFEEV, PANIN                                   #
# 1988 - 1993 AZIMUTH FROM NORTH (DEGREE) -92.30                         #
# 1994 - 1996 AZIMUTH FROM NORTH (DEGREE) -84.00                         #
##########################################################################

 Latitude: 51.6800 deg, longitude:103.6440 deg, azimuth:-90.000 deg.

 Summary of observation data :

 19881003     0...19881005230000  19881025     0...19881027230000
 .......
 19961002     0...19961024230000  19961108     0...19961122230000

 Initial epoch for tidal force    : 1988.10. 3. 0

 Number of recorded days in total :  1541.50
 TAMURA 1987   tidal potential used.
 UNITY window used for least squares adjustment.
 Numerical filter is PERTSEV 1959 with  51 coefficients.

 Estimation of noise by FOURIER-spectrum of residuals
 0.1 cpd band99999.9990  mas          1.0 cpd band     .0867  mas
 2.0 cpd band     .0791  mas          3.0 cpd band     .0274  mas
 4.0 cpd band     .0157  mas          white  noise     .0366  mas

 adjusted tidal parameters :

 from      to       wave   ampl. ampl.fac.    stdv. ph. lead    stdv.
 [cpd]     [cpd]     [ mas    ]                        [deg]    [deg]

  .721500  .906315 Q1       .627    .64059   .04519   6.2082   2.5856
  .921941  .940487 O1      3.213    .62879   .00898    .8249    .5144
  .958086  .974188 M1       .195    .48637   .09818  10.5327   5.6255
  .989049  .998028 P1      1.372    .57707   .01868 -11.1577   1.0704
  .999853 1.000147 S1       .748  13.31137  1.13935  32.8035  65.2164
 1.001825 1.011099 K1      4.639    .64567   .00633   2.1735    .3628
 1.013689 1.044800 J1       .246    .61306   .10931  -6.9221   6.2619
 1.064841 1.216397 OO1      .201    .91609   .18666  -8.4578  10.6918
 1.719381 1.872142 2N2      .171    .57028   .10105  11.1027   5.7912
 1.888387 1.906462 N2      1.285    .68509   .02115   4.1424   1.2125
 1.923766 1.942753 M2      6.947    .70901   .00409    .0253    .2344
 1.958233 1.976926 L2       .306   1.10465   .11767  11.9735   6.7425
 1.991787 2.002885 S2      2.997    .65743   .00889  -1.8207    .5112
 2.003032 2.182843 K2       .951    .76730   .03342  -6.1431   1.9150
 2.753244 3.081254 M3       .092    .76520   .10746 -10.9006   6.1568
 3.791964 3.937897 M4       .019  13.83821  5.30845  -8.5677 304.2713

 Standard deviation of weight unit:      2.405
 degree of freedom:                      32964
 Standard deviation:                     2.405   mas
```

TABLE 6
Tidal Analysis of the Atmospheric Pressure
VEN66 Method

STATION 1301 TALAYA BAROMETER SIBERIE - RUSSIE

51.68 N 103.65 E H 600 M D 2000 KM G 980 981
LAC BAIKAL
INSTITUTE OF GEOLOGY AND GEOPHYSICS, NOVOSIBIRSK, J.K. SARITCHEVA
INSTALLATION TIMOFEEV
MAINTENANCE TIMOFEEV
RECORDING SENSITIVITY 0.0147058 mbar PER MM (931202 -960420)

LEAST SQUARE ANALYSIS / VENEDIKOV FILTERS ON 48 HOURS / PROGRAMMING B.DUCARME
POTENTIAL CARTWRIGHT-TAYLER-EDDEN / COMPLETE DEVELOPMENT
COMPUTING CENTER INTERNATIONAL CENTER FOR EARTH TIDES/FAGS/ BRUSSELS
DATA PROCESSING BY L.VANDERCOILDEN ON 99/11/04
COMPUTER HP-UX 9000/819

P 1 90 9 2/901030 9011 2/901122 9012 2/901230 91 1 2/91 130 91 2 7/91 225
P 1 91 3 9/91 319 91 4 2/91 430 9312 3/931215 931221/94 130 94 2 3/94 211
P 1 94 3 7/94 329 94 412/94 418 94 5 2/94 530 94 6 2/94 730 94 8 3/94 930
P 1 9410 4/941022 941110/941230 95 1 2/95 223 95 3 3/95 327 95 5 2/95 520
P 1 95 6 2/95 626 95 720/95 730 95 8 5/95 829 95 9 5/95 915 9510 3/951027
P 1 9511 2/951212 96 1 9/96 131 96 2 5/96 2 7 96 212/96 224 96 312/96 326
P 1 96 4 4/96 420 96 430/96 524 96 529/96 7 2 96 711/96 923 961017/961029
P 1 9611 9/961117 961123/97 215 97 310/97 4 9 97 5 9/97 519 97 531/97 730
P 1 97 8 2/97 927

TIME INTERVAL 2584.0 DAYS 30144 READINGS 41 BLOKS EFFICIENCY 0.49

WAVE GROUP ARGUMENT	N	WAVE	ESTIMATED AMPL. R.M.S.	AMPL. FACTOR	R.M.S.	PHASE DIFF.	R.M.S.	RESIDUE AMPL.	RESIDUE PHASE
127.-129.	11	SIGMA1	0.035	0.058		139.1	93.4		
133.-136.	20	Q1	0.064	0.057		-61.0	51.1		
137.-139.	10	RO1	0.037	0.054		-140.4	83.4		
143.-145.	16	O1	0.103	0.055		100.2	30.6		
152.-155.	15	NO1	0.030	0.048		-62.5	90.8		
161.-163.	10	P1	0.063	0.048		-89.3	43.5		
164.-164.	3	S1	0.488	0.068		82.4	8.0		
165.-168.	20	K1	0.147	0.052		-65.0	20.2		
175.-177.	14	J1	0.061	0.054		-32.8	50.9		
184.-186.	11	OO1	0.031	0.069		-17.5	129.2		
233.-236.	10	2N2	0.013	0.017		36.8	76.7		
237.-23A.	10	MU2	0.018	0.016		136.5	51.2		
243.-245.	13	N2	0.006	0.016		85.6	161.2		
246.-248.	11	NU2	0.011	0.016		13.1	80.4		
252.-258.	26	M2	0.012	0.015		-178.1	75.6		
265.-265.	9	L2	0.013	0.011		-135.1	46.7		
267.-272.	5	T2	0.011	0.015		11.2	80.8		
273.-273.	4	S2	0.388	0.016		-92.5	2.3		
274.-277.	12	K2	0.080	0.018		-129.5	12.7		
327.-375.	17	M3	0.008	0.007		-76.7	52.8		

STANDARD DEVIATION D 5.35 SD 1.70 TD 0.81 MBAR

QUALITY FACTORS : Q1= 3.2 Q2= 16.8
O1/K1 0.9821 1-O1/1-K1 1.0001 M2/O1 0.1177
CENTRAL EPOCH TJJ= 2449427.0

The agreement on the mean value is excellent but with a large scattering.

The error of calibration was on 1-3 percents level. The main problem is that we have to approach the instrument for manual calibration so that there is a thermal effect during some hours. We tried to calibrate always in the same position of the elecro-optical transducer. The time between the calibration steps was 10-15 minutes for the electro-magnetic method and from half an hour to one day for the quartz spring. To determine the phase shift we used the decay curve following each step of micrometer or each change of the current. This value varied from 1 to 3 minutes during the observation period. This variation is connected to changes of the input resistance of the galvanometer.

After 1988 we used only the micrometer for calibration. The scale coefficients during ten years varied from 500 mm per arc second up to 3000 mm per arc second according to the different free periods of the pendulums. Usually this value was kept around 1000-1500 for North-South direction and 1500-2500 for East-West direction, depending on photocells characteristics.

The annual meteorological effect was estimated to be in the 10^{-7} - 10^{-8} radian limits. Rain effect is only effective during the short summer season and reaches a similar amplitude. Long term seasonal effect, connected with the annual Baikal Lake level variation reaching 1.5 m, was near 0.1" for tilt in the E-W direction. A long term drift of the order of 0.1" per year up to 3" per year was observed and is related to the strong seismic and tectonic activity of the Baikal rift.

Earth Tide Analysis

The earth tide analysis of the quartz tiltmeters data set 1988-1998 has been carried out not only with method VEN66 using the CTE550 tidal potential and filtering on 48 hours blocks but also with ETERNA 3.0 using the Tamura tidal potential and Pertsev numerical filters. The adjusted tidal parameters are given in Tables 2 & 3 for North-South component and in Tables 4 & 5 for East-West component. The standard deviation of weight unit for different components and for different periods reaches 2 to 2.5 mas. The results of tidal analysis by the two methods are similar in amplitude and in phase. The discrepancies are due to the different filtering techniques interfering with the gaps.

Slight changes are observed between successive partial analysis. They can be due to temporal variations of the calibration factor and temporal variations of the signal cable impedance. This last effect is probably responsible of the large S1. Tidal analysis of barometric pressure (table 6) shows a diffuse effect in the diurnal band with a maximum at S1 frequency and only one peak on S2 in the semi-diurnal band.

Comparison of Observed and Predicted Tidal Parameters

For comparison with the observed tidal parameters, the tilt tide parameters have been modelled from the Wahr-Dehant model[5] and ocean-tide loading computed using the Farrell procedure and the Schwiderski ocean tide model (Tables 7 & 8). Tidal oceanic loading is below 0.15mas in NS but reaches 0.25mas in EW. The consideration of this effect in the modelling does not improve the fit with the observations.

In NS component we compare the results of the two analysis methods with the predicted tidal factors in table 7. For amplitude factors we have a positive anomaly for all the main waves. We observe a phase advance in semi-diurnal waves and a phase lag in diurnal ones. It should be pointed out that for this component the diurnal part of the tidal spectrum is very weak at the latitude of Talaya station.

In East-West component (Table 8) with the two analysis methods we observe a phase lag for all waves and a negative anomaly for amplitude factors with the exception of M2. The liquid core resonance effect is fairly well observed between O1 and K1. The instrumental phase lag cannot explain the phase discrepancy as this one has a similar amplitude for diurnal and semidiurnal waves.

Concerning the causes of these anomalies we tried to consider cavity effects[6] but the discrepancies between NS and EW directions remain unexplained. The installation of the tiltmeters in the drift gallery is similar as the angle with drift axis is similar in both cases from 35° to 50°. On the other hand the angle between main gallery direction and North direction is 22° - 24° and in this case according to the theory we should observe very weak influence, but we have opposite result. For topographic effect we have the similar situation as the mountain range near the station is oriented in azimuth 35°-50°N and we would have the same effect on the North-South and East-West components. Considering the effect of geological structures we have many geological boundaries around the station. However for wave M2 in E-W component the tilt-strain coupling effect is minimal as for this latitude the amplitude of semi-diurnal strain is minimal.

As a conclusion for North-South component we can use practically only M2 wave. Internal error on M2 reaches 0.5 percent. For this wave we have discrepancy at the level of 3 percents on the amplitude factor but nearly 10 degrees in phase which represent a 10% out of phase signal. It may be explained by the geological structure effect as we have 3 km to the North of the station the main Sayan fault oriented in EW direction.

In East-West component amplitude factors fits with modelling at the 4% level for M2 and O1. The phase lag reaches 2 degrees which represent a 4% perturbing signal in out of phase component. It may be due to cavity and topographic effect.

For S2 and K1 wave we do always have a larger discrepancy in amplitude and in phase probably caused by strong temperature effects changing the resistance of the 30m cable laid between gallery and building with recorder.

Table 7.

Comparison of predicted and observed tidal tilt parameters
NS component

Wave	ampl. theor.	ampl. fact. predict.	Ampl. Fact. Observ.	Ampl. Fact. Discrep.	Error ampl. Fact.	Phase predict.	phase observ.	Phase discrep.	error phase
VEN66									
O1	1.49	0.6159	1.0714	0.4555	0.0452	+6.36	+1.81	-4.55	2.42
K1	2.09	0.6922	1.0590	0.3668	0.0317	+4.04	-3.49	-7.53	1.72
M2	7.69	0.6792	0.7039	0.0247	0.0059	-0.16	+9.36	+9.52	0.48
S2	3.58	0.6849	0.7966	0.1117	0.0125	-0.33	+4.98	+5.31	0.92
ETERNA									
O1	1.49	0.6159	1.0676	0.4517	0.0293	+6.36	+2.52	-3.84	1.68
K1	2.09	0.6922	1.0557	0.4635	0.0209	+4.04	-3.97	-8.01	1.19
M2	7.69	0.6792	0.7036	0.0244	0.0043	-0.16	+9.57	+9.73	0.25
S2	3.58	0.6849	0.8013	0.1164	0.0094	-0.33	+5.43	+5.76	0.54

Table 8.

Comparison of predicted and observed tidal tilt parameters
EW component

Wave	ampl. theor.	ampl. fact. predict.	Ampl. Fact. Observ.	ampl. fact. discrep.	Error ampl. Fact	Phase predict.	phase observ.	Phase discrep.	error phase
VEN66									
O1	5.11	0.6528	0.6215	-0.0313	0.0137	+2.29	0.78	-1.51	1.29
K1	7.19	0.7172	0.6440	-0.0732	0.0095	+2.87	2.76	-0.11	0.84
M2	9.80	0.6657	0.7111	0.0454	0.0051	+1.36	-0.14	-1.22	0.41
S2	4.56	0.6708	0.6564	-0.0144	0.0110	+2.03	-2.40	-4.43	0.94
ETERNA									
O1	5.11	0.6528	0.6288	-0.0240	0.0090	+2.29	0.82	-1.47	0.51
K1	7.19	0.7172	0.6457	-0.0715	0.0063	+2.87	2.17	-0.70	0.36
M2	9.80	0.6657	0.7091	0.0434	0.0041	+1.36	0.03	-1.33	0.23
S2	4.56	0.6708	0.6574	-0.0134	0.0089	+2.03	-1.82	-3.85	0.51

Acknowledgement

This work has been supported by the Belgo-Russian agreement for Scientific and Technical Cooperation and by the Russian Fund for Scientific Research (98-05-65227, 98-05-65278). The authors wish to thank P. Melchior for interest of this work.

References

1. Boulanger Y.D., Gridnev D.G. et.al. Quarz tiltmeter NK-1. "Tidal deformation of the Earth". (in Russian) Moscow, Nauka, 1975, pp.149-157.
2. Gridnev D.G., Timofeev V.Y., Saricheva Y.K., Anisimova L.V. Inclinaison de la surface terrestre dans le Sud du lac Baikal (Talaya). Bull. d'informations Marées Terrestres, 114, 1993, pp. 8405-8415.
3. Timofeev V.Yu., Panin S.F., Saricheva Y.K., Anisimova L.V., Gridnev D.G., Masalskii O.K. Etude des inclinaisons et des déformations de la surface de la Terre dans la zone de Rift du Baikal (Talaya). Bull. d'informations Marees Terrestres, 1996, n 125. p.9588-9600.
4.Saricheva Yu.K., Timofeev V.Yu. Inclinaisons des marees à Talaya(zone de rift du Baikal). Bull. d'Informations Marees Terrestres.1994. n120. pp.8990-9001.
5. Dehant, V. Tidal parameters for an inelastic Earth. Physics of the Earth and Planetary Interior, vol. 49, 97-116, 1987.

6. Harrison, J.C. Cavity and topographic effects in tilt and strain measurements. Journal of Geophysical Research, vol.81, 319-328, 1976.

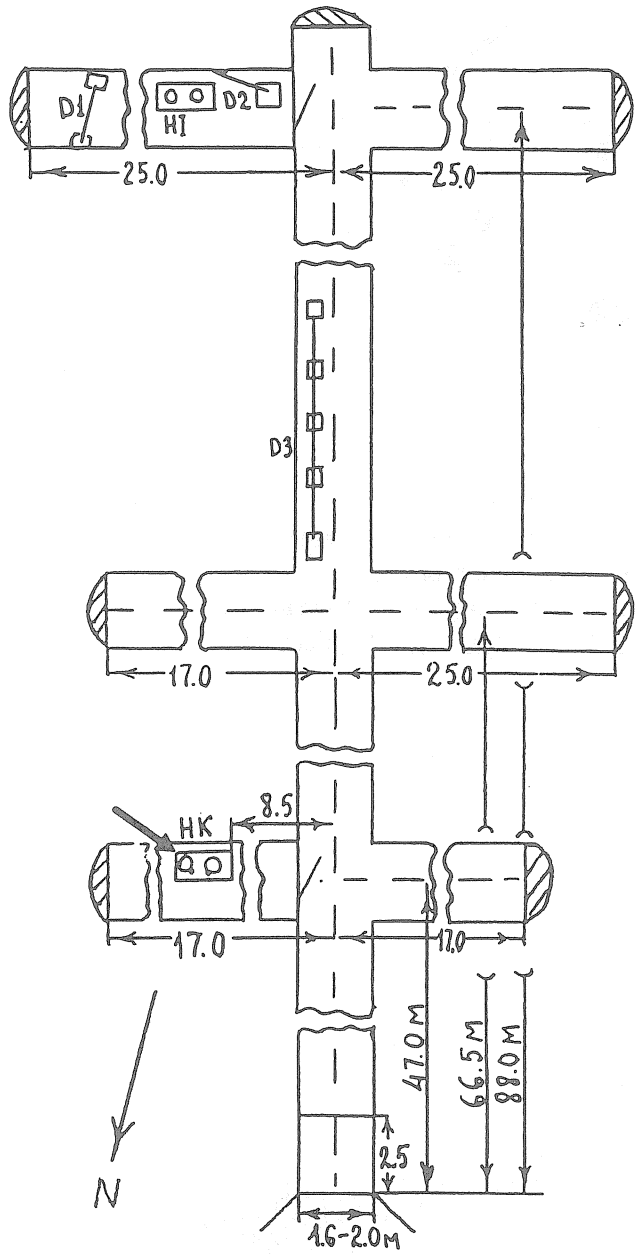

Figure 1. Sketch of the Talaya underground laboratory
The location of the tiltmeters is indicated by an arrow

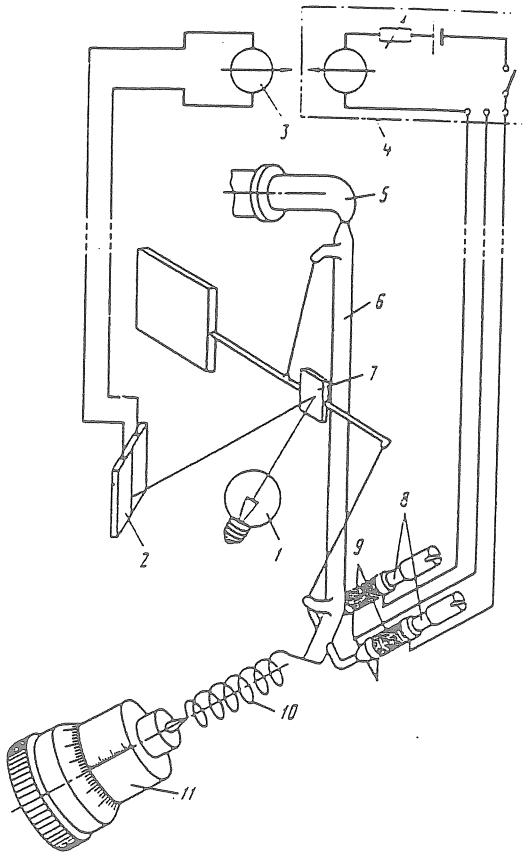

Figure 2a. Gridnev quartz tiltmeter
1- lamp, 2- differencial photocells, 3- galvanometer,
4- control panel for coils, 5- lever-spring(quartz),
6- support(quartz), 7- mirror of beam(quartz), 8- magnets,
9- coils on quartz tubes, 10- quartz spring, 11- micrometer

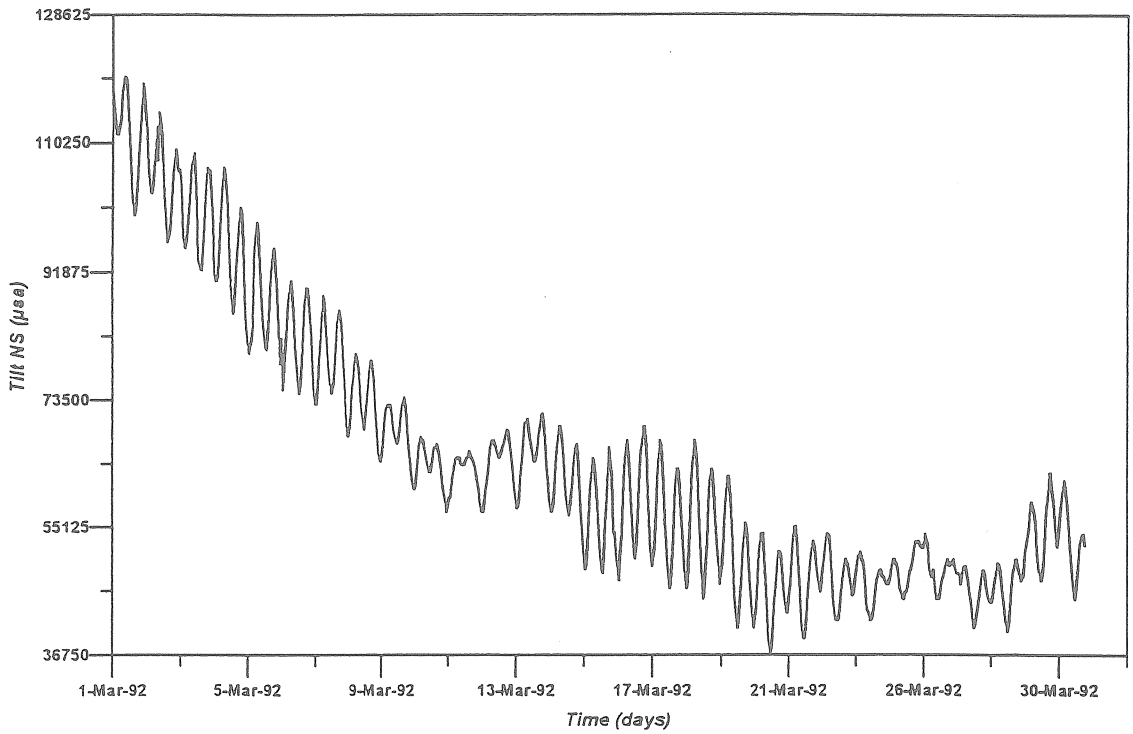

Figure 2b. Tidal recording in NS direction
Vertical scale is given in 10^{-6}" (5.10^{-12}rad) units
Tidal amplitude reaches 0.03" (0.15μrad)

Tidal analysis of strain measurements in southwest part of Baikal rift.

Timofeev Vladimir[1], Ducarme Bernard,[2] Semibalamut Vladimir[3], Ribushkin Aleksandr[3], Fomin Yurii[3], Vandercoilden Leslie[4] .

[1]*Institute of Geophysics UIGGM SB RAS, Koptiug pr.,3, 630090, Novosibirsk, Russia*
[2]*Chercheur Qualifié au Fonds National de la Recherche Scientifique*
Observatoire Royal de Belgique, Avenue Circulaire 3, 1180 Bruxelles, Belgium
[3]*Laser Experimental Laboratory SB RAS, Lavrentieva st.10, 630090, Novosibirsk, Russia*
[4]*Observatoire Royal de Belgique, Avenue Circulaire 3, 1180 Bruxelles, Belgium*

Introduction

The strain response of the Earth to the tidal forces has been observed in Talaya station on the Baikal rift territory. As usual the equipment is installed in an underground gallery. Different types of extensometers were used: quartz tube, invar rod and laser. Preliminary results of short series of tidal strain observations have been presented in [1,2]. Long series of tidal strains are now available at this station. The station being located in the hearth of the Eurasian continent has a very low level of ocean influence but some instrumental and cavity effects were observed in this gallery. We present here the data processing and tidal analysis of long series summarising the 1989-1996 period of measurements.

Installation of the extensometers and observation.

The measurements were made in the geodynamic observatory Talaya (coordinates 51.68° N, 103.65° E) located 7 km to the west of the Southwest extremity of the Baikal lake and 3 km to the South of the Main Sayan fault. Our measurements are carried out in the 90m long underground gallery of the Talaya seismic station. The main gallery and the six perpendicular drifts have a cross section of 2x2 m^2 (figure 1). The equipment consists primarily of two short quartz tube extensometers and an invar rod strainmeter with induction sensors. Later on a laser extensometer with two 25m orthogonal legs was also installed. This set of extensometers was installed in different drifts and directions (-24° N, -22.5° N, 0° N, 90° N, 66° N), as we need at least three different directions to calculate the main strain axes variations for long term study of the tectonic activity [3].

Continuous observations of strain were made in the underground gallery of Talaya observatory since 1989 in a distant drift by quartz tube extensometers in N-S (base 1.3 m) and E-W (base 2.0 m) components. An invar bar extensometer (base 8.3 m) is placed 70 m apart from the gallery entry, along the gallery axis since 1990. An inductive displacement gauge was used in these extensometers. The signal was recorded close to the zero position of sensor to insure the linearity. The strainmeters in north-south and –22.5°N directions were placed on basements installed on the bed rock. The height of these basements, situated on the floor of gallery, is near 20 cm. For the east-west direction one side of the tube was sealed in the wall of the gallery and the sensor was placed on a large basement. The height of the system was near 1/2 meter under the floor of gallery. The angle between the tube direction and the wall direction was near 25-30°. A narrow crack system, 1-3 cm wide, is located along the axis of this drift and runs under the basements.

The signals are registered at a distance of 50 m from the gallery entrance in the building of the seismic station by an analog recording system at a speed of 20 mm/h and with a sensitivity of $1\text{-}6\cdot10^{-9}$ per mm. For calibration we used small displacements of the sensor plate as well in the laboratory as in the underground gallery. With this method we obtain a precision

of 3 to 5 percents. In 1999 we started to use the μDAS digital system developed by the Royal Observatory of Belgium[4].

Since 1995 continuous laser extensometers observations (base 25 m, azimuths -24° N and 66° N) were performed in the underground gallery. The instrument has two light beams, perpendicular to each other. The instrument was developed at the Institute of Laser Physics SB-RAS (Novosibirsk, Russia) [2]. The mirror for first direction (-24°) is placed in a small cavity at the end of the main gallery. The mirror for second direction (66°) is placed near the axis of a big drift. Open laser light system is used in the gallery, as there are stable temperature conditions with mean temperature +1°C. The daily temperature stability is close to 0.001°C in the drifts which are far away from the entrance of the gallery. The annual stability is different: near the three entrance doors the variation reaches some degrees and in the longest drifts it is only one tenth of degree. Open laser system are sensitive to the air pressure variation. We tried to exclude this effect by additional laser measurements on one meter invar plate and extrapolating this result to the 25 meters bases. The main part of the air pressure effect has been excluded, but there is still some effect on the data.

The results of the laser strainmeter are registered in digital form on PC with one sample every 1 or 2 seconds.

Using the laser extensometer with two light beams is useful for the analysis of the temporal variations of the tidal amplitudes, as this instrument has a very stable scale coefficient connected with laser light wavelength. As already pointed out, the results are still slightly affected by air pressure. To solve this problem we make the difference between the two laser beams. In this case we have a minimum of air pressure influence and the results for the main semi-diurnal wave M2 showed high temporal stability and a low error level.

As it is well known strain results generally differ from global tidal deformation models [5] due to cavity effects, topography effects and the boundary conditions on a fault zone [6]. When possible we should thus try to evaluate and separate the global model and the local effects.

Earth Tide Analysis

The earth tide analysis of the strain data set 1989-1998 has been carried out with programs VEN66 and ETERNA 3.1 using respectively the Cartwright-Tayler-Edden and the Tamura tidal potential catalogue. As the results of tidal analysis by the two methods are very similar we give only the results obtained with VEN66. This method allows to compute the L/H ratio which is independent of the instrumental calibration. The results are not corrected for the air pressure or ocean loading.

The adjusted tidal parameters are given in Table 1 for the north-south component, in Table 2 for the east-west component and Table 3 for the –22.5°N component. The standard deviations for the different components are high. This can be due to temporal variations of the calibration factor and temporal variations of signal cable resistance. This last effect may explain the great S1 amplitude. This opinion is supported by the fact that the S1 amplification is much lower for the laser strainmeter.

For laser extensometer data the same methods of analysis were used and the results are shown in Tables 4 & 5. As expected we got lower standard deviations but not as small as expected with such an increase of length. We could suspect a residual influence of the air pressure variation.

Table 1
Tidal Strain Analysis
NS Component

STATION 1301 TALAYA COMPOSANTE EXTENSOMETRIQUE NS SIBERIE - RUSSIE

51.68 N 103.65 E H 600 M D 2000 KM
LAC BAIKAL
INSTITUTE OF GEOPHYSICS, UIGGM, NOVOSIBIRSK
QUARTZ TUBE EXTENSOMETER, LENGTH 1.3M
INSTALLATION V.Y.TIMOFEEV
MAINTENANCE TIMOFEEV, OSHEPKOV
LEAST SQUARE ANALYSIS / VENEDIKOV FILTERS ON 48 HOURS / PROGRAMMING B.DUCARME
POTENTIAL CARTWRIGHT-TAYLER-EDDEN / COMPLETE DEVELOPMENT
COMPUTING CENTER INTERNATIONAL CENTER FOR EARTH TIDES/FAGS/ BRUSSELS
DATA PROCESSING BY L.VANDERCOILDEN ON 95/12/20
COMPUTER HP-UX 9000/819
AZIMUT .00S-E

VALEUR DES NOMBRES DE LOVE :
ORDRE 2 H=.6206 L=.0904
ORDRE 3 H= .289 L= .015
E 13 89 3 5/89 327 89 331/89 428 89 5 2/89 524 89 6 2/89 630 89 8 2/89 828
E 13 8910 8/8911 1 891222/90 1 9 90 115/90 2 8 90 212/90 312 90 325/90 4 2
E 13 90 510/90 526 90 713/90 717 901029/9011 8 901117/901127 91 120/91 311

TIME INTERVAL 738.0 DAYS 8352 READINGS 15 BLOKS EFFICIENCY 0.47

WAVE GROUP ARGUMENT	N	WAVE	ESTIMATED AMPL. R.M.S.		AMPL. FACTOR	R.M.S.	PHASE DIFF.	R.M.S.	RESIDUE AMPL.	PHASE
127.-129.	11	SIGMA1	1.18	0.79	9.6212	6.4979	-132.734	38.654	1.26	-136.8
133.-136.	20	Q1	0.19	0.77	0.2456	1.0100	31.515	235.894	0.60	170.7
137.-139.	10	RO1	2.36	0.79	16.2755	5.4129	97.025	19.032	2.39	100.5
143.-145.	16	O1	4.56	0.77	1.1410	0.1920	-0.960	9.644	0.62	-7.0
152.-155.	15	NO1	0.46	0.71	1.4660	2.2545	-95.488	88.219	0.58	-127.4
161.-163.	10	P1	2.39	0.91	1.2847	0.4892	2.531	21.836	0.74	8.1
164.-164.	3	S1	5.64	1.41	128.3600	32.0307	151.294	14.011	5.68	151.5
165.-168.	20	K1	3.37	0.83	0.6010	0.1474	1.398	14.056	0.09	108.8
175.-177.	14	J1	1.39	0.74	4.4410	2.3497	-58.999	30.327	1.26	-71.6
184.-186.	11	OO1	0.27	0.55	1.5444	3.1909	20.199	118.291	0.12	50.4

WAVE GROUP ARGUMENT	N	WAVE	ESTIMATED AMPL. R.M.S.		AMPL. FACTOR	R.M.S.	PHASE DIFF.	R.M.S.	RESIDUE AMPL.	PHASE
233.-236.	10	2N2	1.13	1.10	4.1651	4.0653	121.595	55.876	1.29	131.9
237.-23A.	10	MU2	0.51	1.12	1.5519	3.4041	29.619	125.822	0.28	65.5
243.-245.	13	N2	1.65	1.09	0.8060	0.5299	12.880	37.642	0.57	140.0
246.-248.	11	NU2	4.18	1.09	10.7254	2.7843	93.169	14.855	4.22	98.5
252.-258.	26	M2	10.81	1.07	1.0077	0.0994	4.789	5.650	0.90	87.1
265.-265.	9	L2	1.03	1.17	3.4137	3.8638	16.210	65.059	0.75	22.7
267.-272.	5	T2	2.45	1.07	8.3913	3.6581	167.095	24.978	2.73	168.5
273.-273.	4	S2	5.39	1.07	1.0806	0.2148	15.405	11.509	1.45	81.7
274.-277.	12	K2	2.13	0.84	1.5682	0.6213	-9.137	22.658	0.82	-24.4

WAVE GROUP ARGUMENT	N	WAVE	ESTIMATED AMPL. R.M.S.		AMPL. FACTOR	R.M.S.	PHASE DIFF.	R.M.S.	RESIDUE AMPL.	PHASE
327.-375.	17	M3	0.23	0.14	4.9253	3.0569	-9.926	35.514	0.18	-12.4

STANDARD DEVIATION D 48.88 SD 58.80 TD 7.84 10E-9

QUALITY FACTORS : Q1= 0.2 Q2= 0.5
O1/K1 1.8987 1-O1/1-K1 -0.3534 M2/O1 0.8832

Table 2
Tidal Strain Analysis
EW Component

STATION 1301 TALAYA COMPOSANTE EXTENSOMETRIQUE E-W SIBERIE - RUSSIE

51.68 N 103.65 E H 600 M D 2000 KM
INSTITUTE OF GEOPHYSICS, UIGGM, NOVOSIBIRSK
QUARTZ TUBE EXTENSOMETER, LENGTH 2.0M
INSTALLATION TIMOFEEV V.Y.
INSTALLATION TIMOFEEV, OSHEPKOV
CALIBRATION 2.6879

LEAST SQUARE ANALYSIS / VENEDIKOV FILTERS ON 48 HOURS / PROGRAMMING B.DUCARME
POTENTIAL CARTWRIGHT-TAYLER-EDDEN / COMPLETE DEVELOPMENT
COMPUTING CENTER INTERNATIONAL CENTER FOR EARTH TIDES/FAGS/ BRUSSELS
DATA PROCESSING BY L.VANDERCOILDEN ON 99/11/29
COMPUTER HP-UX 9000/819
AZIMUT 90.00S-E

VALEUR DES NOMBRES DE LOVE :
ORDRE 2 H=.6206 L=.0904
ORDRE 3 H= .289 L= .015
E 20 89 7 7/89 812 89 821/89 9 6 89 9 9/8910 7 90 223/90 313 90 411/90 5 3
E 20 90 512/90 6 9 90 613/90 7 7 90 713/90 717 901029/9011 8 901117/901127
E 20 9012 2/901214 91 122/91 2 9 91 221/91 315 91 318/91 413 91 423/91 521
E 20 91 524/91 625

TIME INTERVAL 720.0 DAYS 8784 READINGS 16 BLOKS EFFICIENCY 0.51

WAVE GROUP ARGUMENT	N	WAVE	ESTIMATED AMPL.	R.M.S.	AMPL. FACTOR	R.M.S.	PHASE DIFF.	R.M.S.	RESIDUE AMPL.	PHASE
127.-129.	11	SIGMA1	0.36	0.34	1.7404	1.6370	52.621	53.889	0.29	87.5
133.-136.	20	Q1	1.14	0.32	0.8769	0.2501	-2.913	16.317	0.16	-159.4
137.-139.	10	RO1	0.19	0.33	0.7573	1.3241	22.647	100.074	0.10	135.3
143.-145.	16	O1	6.42	0.31	0.9471	0.0456	-24.448	2.761	2.80	-108.3
152.-155.	15	NO1	0.63	0.36	1.1847	0.6799	-71.913	32.917	0.68	-118.8
161.-163.	10	P1	3.15	0.37	0.9989	0.1170	2.544	6.705	0.24	35.8
164.-164.	3	S1	0.98	0.56	13.1147	7.5245	-169.225	32.780	1.05	-169.9
165.-168.	20	K1	5.84	0.34	0.6123	0.0353	-37.787	3.300	4.55	-128.1
175.-177.	14	J1	0.44	0.30	0.8182	0.5700	-63.886	39.960	0.52	-131.6
184.-186.	11	OO1	0.20	0.25	0.6782	0.8431	-158.013	71.128	0.48	-171.2

WAVE GROUP ARGUMENT	N	WAVE	ESTIMATED AMPL.	R.M.S.	AMPL. FACTOR	R.M.S.	PHASE DIFF.	R.M.S.	RESIDUE AMPL.	PHASE
233.-236.	10	2N2	0.19	0.44	18.6218	44.2914	48.300	136.710	0.18	50.7
237.-23A.	10	MU2	0.17	0.30	13.8177	25.2645	152.915	104.668	0.18	154.7
243.-245.	13	N2	1.68	0.40	22.3496	5.2618	-59.932	13.465	1.65	-62.2
246.-248.	11	NU2	0.63	0.28	44.0937	19.2942	-23.885	25.050	0.62	-24.4
252.-258.	26	M2	6.43	0.25	16.3481	0.6261	-73.986	2.197	6.33	-77.4
265.-265.	9	L2	0.06	0.06	5.1917	5.3826	12.510	59.472	0.05	15.5
267.-272.	5	T2	0.87	0.25	81.7096	23.1863	-169.215	16.235	0.89	-169.3
273.-273.	4	S2	2.51	0.25	13.7323	1.3691	-96.470	5.616	2.54	-100.6
274.-277.	12	K2	0.79	0.19	15.8512	3.9101	-97.507	14.122	0.80	-101.1

WAVE GROUP ARGUMENT	N	WAVE	ESTIMATED AMPL.	R.M.S.	AMPL. FACTOR	R.M.S.	PHASE DIFF.	R.M.S.	RESIDUE AMPL.	PHASE
327.-375.	17	M3	0.02	0.08	8.7331	30.4876	157.339	200.306	0.02	159.6

STANDARD DEVIATION D 20.13 SD 13.93 TD 4.41 10E-9

QUALITY FACTORS : Q1= 0.6 Q2= 1.8
RESIDUALS ARE GIVEN IN THE TRUE AZIMUT
O1/K1 1.5467 1-O1/1-K1 0.1365 M2/O1 17.2618
CENTRAL EPOCH TJJ= 2448073.0

Table 3
Tidal Strain Analysis
Azimuth –22°.5N

STATION 1301 TALAYA COMPOSANTE EXTENSOMETRIQUE SIBERIE - RUSSIE

51.68 N 103.65 E H 600 M D 2000 KM
INSTITUTE OF GEOPHYSICS, UIGGM, NOVOSIBIRSK
INVAR ROD STRAINMETER, LENGTH 8.3M
INSTALLATION TIMOFEEV V.Y.
INSTALLATION TIMOFEEV, OSHEPKOV
AZIMUTH FROM NORTH DIRECTION -22.500 DEG.

LEAST SQUARE ANALYSIS / VENEDIKOV FILTERS ON 48 HOURS / PROGRAMMING B.DUCARME
POTENTIAL CARTWRIGHT-TAYLER-EDDEN / COMPLETE DEVELOPMENT
COMPUTING CENTER INTERNATIONAL CENTER FOR EARTH TIDES/FAGS/ BRUSSELS
DATA PROCESSING BY L.VANDERCOILDEN ON 98/11/24
COMPUTER HP-UX 9000/819
AZIMUT 22.50S-E

VALEUR DES NOMBRES DE LOVE :
ORDRE 2 H=.6206 L=.0904
ORDRE 3 H= .289 L= .015

E 83 90 223/90 313 90 4 8/90 524 901118/9012 2 901212/901218 91 114/91 118
E 83 91 130/91 215 91 219/91 327 91 4 2/91 418 91 423/91 5 9 91 513/91 519
E 83 91 6 3/91 6 7 91 612/91 618 91 630/91 728 91 8 8/91 818 91 9 5/91 921
E 83 91 925/911013 911017/9112 8 911219/911231 92 1 4/92 2 9 92 216/92 311
E 83 92 530/92 6 3 92 6 7/92 617 92 8 2/92 816 92 829/92 9 2 92 910/92 918
E 83 92 923/921013 921027/921031 9211 6/921116 921120/921214 93 2 6/93 210
E 83 93 3 9/93 3 9 93 313/93 313 93 318/93 318 93 322/93 4 9 93 413/93 417
E 83 93 519/93 529 93 731/93 8 4 93 918/9310 6 931010/931016 931027/931120
E 83 94 216/94 310 94 6 7/94 617 94 7 5/94 717 94 811/94 817 94 822/94 915
E 83 94 919/941110 941114/941120 941125/941225 941231/95 1 8 95 111/95 2 6

TIME INTERVAL 1811.0 DAYS 20784 READINGS 50 BLOKS EFFICIENCY 0.48

WAVE GROUP ARGUMENT	N	WAVE	ESTIMATED AMPL. R.M.S.		AMPL. FACTOR	R.M.S.	PHASE DIFF.	R.M.S.	RESIDUE AMPL.	PHASE
127.-129.	11	SIGMA1	0.31	0.33	2.2159	2.3861	59.437	61.633	0.27	86.1
133.-136.	20	Q1	1.68	0.33	1.9125	0.3740	17.583	11.216	0.89	35.1
137.-139.	10	RO1	0.47	0.32	2.8362	1.9385	-44.916	39.175	0.37	-62.9
143.-145.	16	O1	6.34	0.32	1.3843	0.0707	6.463	2.933	1.92	22.6
152.-155.	15	NO1	0.62	0.33	1.7309	0.9079	9.433	30.021	0.28	22.1
161.-163.	10	P1	2.73	0.33	1.2809	0.1531	7.319	6.832	0.88	29.6
164.-164.	3	S1	2.62	0.48	51.9246	9.4418	-173.182	10.259	2.66	-170.4
165.-168.	20	K1	6.53	0.33	1.0144	0.0505	-1.592	2.845	2.24	20.5
175.-177.	14	J1	0.73	0.31	2.0319	0.8646	-27.263	24.405	0.44	-50.2
184.-186.	11	OO1	0.93	0.31	4.7314	1.5879	53.047	19.223	0.83	63.9

STATIC VALUE 12.1486 -15.97 L/H=0.1457

GROUP	SYMBOL	AMPLITUDE	PHASE	RATIO L/H OBS.	MSE.	THEOR.
66- 81	O1	16.8168	-9.51	0.1098	0.0205	0.1466
92-106	NO1	21.0282	-6.53	0.0862	0.2719	0.1473
114-123	P1	15.5605	-8.65	0.1037	0.0512	0.1533
127-146	K1	12.3237	-17.56	0.1524	0.0114	0.1756

WAVE GROUP ARGUMENT	N	WAVE	ESTIMATED AMPL.	R.M.S.	AMPL. FACTOR	R.M.S.	PHASE DIFF.	R.M.S.	RESIDUE AMPL.	PHASE
233.-236.	10	2N2	0.46	0.35	1.8210	1.4151	2.541	44.502	0.21	5.6
237.-23A.	10	MU2	0.43	0.35	1.4363	1.1559	11.596	46.146	0.15	35.4
243.-245.	13	N2	2.67	0.34	1.4138	0.1824	1.174	7.384	0.78	4.0
246.-248.	11	NU2	0.61	0.34	1.6972	0.9493	-23.605	32.105	0.31	-50.8
252.-258.	26	M2	12.36	0.33	1.2528	0.0340	-0.024	1.552	2.49	-0.1
265.-265.	9	L2	0.54	0.32	1.9259	1.1457	84.283	34.091	0.58	112.9
267.-272.	5	T2	0.49	0.33	1.8345	1.2287	-160.832	38.399	0.75	-167.6
273.-273.	4	S2	6.43	0.33	1.4022	0.0724	-7.764	2.992	1.99	-25.9
274.-277.	12	K2	2.18	0.32	1.7463	0.2591	13.839	8.507	1.01	31.0

STATIC VALUE 10.8596 22.76 L/H=0.1457

GROUP	SYMBOL	AMPLITUDE	PHASE	RATIO L/H OBS.	MSE.	THEOR.
227-236	2N2	19.7749	25.30	0.1640	0.3264	0.1457
247-259	N2	15.3533	23.93	0.1540	0.0531	0.1457
271-296	M2	13.6052	22.73	0.1455	0.0110	0.1457
316-319	S2	15.2273	14.99	0.0933	0.0194	0.1457

WAVE GROUP ARGUMENT	N	WAVE	ESTIMATED AMPL.	R.M.S.	AMPL. FACTOR	R.M.S.	PHASE DIFF.	R.M.S.	RESIDUE AMPL.	PHASE
327.-375.	17	M3	0.12	0.07	3.0458	1.7306	130.738	32.564	0.15	142.3

STATIC VALUE 3.3955 10.66 L/H=0.0502

STANDARD DEVIATION D 29.27 SD 30.11 TD 6.33 10E-9

QUALITY FACTORS : Q1= 0.3 Q2= 1.5
RESIDUALS ARE GIVEN IN THE TRUE AZIMUT
O1/K1 1.3646 1-O1/1-K1 26.6469 M2/O1 0.9051
CENTRAL EPOCH TJJ= 2448850.0

Table 4
Tidal Strain Analysis
Azimuth –24°N

STATION 1301 TALAYA COMPOSANTE EXTENSOMETRIQUE SIBERIE - RUSSIE

51.681 N 103.644 E H 550 M
INSTALLATION FOMIN, RIBUSHKIN
INSTALLATION OSHEPKOV
LASER EXTENSOMETER
INSTRUMENTAL TIME LAG CORRECTED
AZIMUTH FROM NORTH DIRECTION -24.000 DEG.

LEAST SQUARE ANALYSIS / VENEDIKOV FILTERS ON 48 HOURS / PROGRAMMING B.DUCARME
POTENTIAL CARTWRIGHT-TAYLER-EDDEN / COMPLETE DEVELOPMENT
COMPUTING CENTER INTERNATIONAL CENTER FOR EARTH TIDES/FAGS/ BRUSSELS
DATA PROCESSING BY L.VANDERCOILDEN ON 98/11/20
COMPUTER HP-UX 9000/819
AZIMUT 24.00S-E

VALEUR DES NOMBRES DE LOVE :
ORDRE 2 H=.6206 L=.0904
ORDRE 3 H= .289 L= .015
E 18 95 129/95 3 8 95 421/95 515 95 622/95 7 4 95 728/95 817 95 9 8/951026
E 18 951120/951230 96 221/96 4 7 96 414/96 420 96 831/9610 8 961014/9611 5
E 18 9611 9/961129 9612 2/961212 961227/961231

TIME INTERVAL 703.5 DAYS 8496 READINGS 13 BLOKS EFFICIENCY 0.50

WAVE GROUP ARGUMENT	N	WAVE	ESTIMATED AMPL. R.M.S.		AMPL. FACTOR	R.M.S.	PHASE DIFF.	R.M.S.	RESIDUE AMPL.	PHASE
127.-129.	11	SIGMA1	0.40	0.35	2.7859	2.4534	55.443	50.518	0.34	75.8
133.-136.	20	Q1	0.84	0.34	0.9394	0.3844	-19.351	23.455	0.29	-108.7
137.-139.	10	RO1	0.05	0.31	0.2853	1.8621	112.460	374.064	0.19	166.6
143.-145.	16	O1	3.20	0.32	0.6888	0.0686	-9.799	5.716	1.53	-159.7
152.-155.	15	NO1	0.51	0.32	1.4085	0.8867	108.024	36.009	0.71	136.8
161.-163.	10	P1	1.45	0.27	0.6707	0.1233	3.366	10.473	0.54	165.8
164.-164.	3	S1	0.73	0.37	14.3107	7.2784	-101.219	29.728	0.74	-101.6
165.-168.	20	K1	2.90	0.30	0.4439	0.0462	-7.078	5.940	1.59	177.3
175.-177.	14	J1	0.82	0.33	2.2407	0.9052	-60.895	23.117	0.72	-88.2
184.-186.	11	OO1	0.86	0.57	4.2784	2.8469	5.396	38.163	0.66	6.9

WAVE GROUP ARGUMENT	N	WAVE	ESTIMATED AMPL. R.M.S.		AMPL. FACTOR	R.M.S.	PHASE DIFF.	R.M.S.	RESIDUE AMPL.	PHASE
233.-236.	10	2N2	0.28	0.29	1.1184	1.1901	34.053	60.790	0.16	96.7
237.-23A.	10	MU2	0.45	0.28	1.4963	0.9562	26.168	36.707	0.22	62.5
243.-245.	13	N2	1.47	0.28	0.7861	0.1494	31.843	10.903	0.99	128.7
246.-248.	11	NU2	0.07	0.28	0.1939	0.7782	-8.850	229.698	0.29	-177.9
252.-258.	26	M2	6.90	0.25	0.7083	0.0259	9.992	2.098	3.18	157.9
265.-265.	9	L2	0.16	0.22	0.5790	0.7900	7.694	78.338	0.12	169.7
267.-272.	5	T2	0.89	0.26	3.3575	0.9928	-40.079	16.825	0.71	-54.0
273.-273.	4	S2	3.97	0.27	0.8753	0.0603	13.538	3.932	1.15	126.0
274.-277.	12	K2	1.60	0.34	1.2965	0.2753	-3.109	12.184	0.37	-13.4

WAVE GROUP ARGUMENT	N	WAVE	ESTIMATED AMPL. R.M.S.		AMPL. FACTOR	R.M.S.	PHASE DIFF.	R.M.S.	RESIDUE AMPL.	PHASE
327.-375.	17	M3	0.15	0.10	3.7665	2.5198	23.742	38.406	0.11	31.8

STANDARD DEVIATION D 14.81 SD 15.01 TD 5.96 10E-9
QUALITY FACTORS : Q1= 0.7 Q2= 1.8
RESIDUALS ARE GIVEN IN THE TRUE AZIMUT
O1/K1 1.5517 1-O1/1-K1 0.5596 M2/O1 1.0283
CENTRAL EPOCH TJJ= 2450098.0

Table 5
Tidal Strain Analysis
Azimuth 66°N

STATION 1301 TALAYA COMPOSANTE EXTENSOMETRIQUE SIBERIE - RUSSIE

51.681 N 103.644 E H 550 M
INSTALLATION FOMIN, RIBUSHKIN
INSTALLATION OSHEPKOV
LASER EXTENSOMETER
INSTRUMENTAL TIME LAG CORRECTED
AZIMUTH FROM NORTH DIRECTION 66.000 DEG.

LEAST SQUARE ANALYSIS / VENEDIKOV FILTERS ON 48 HOURS / PROGRAMMING B.DUCARME
POTENTIAL CARTWRIGHT-TAYLER-EDDEN / COMPLETE DEVELOPMENT
COMPUTING CENTER INTERNATIONAL CENTER FOR EARTH TIDES/FAGS/ BRUSSELS
DATA PROCESSING BY L.VANDERCOILDEN ON 98/11/20
COMPUTER HP-UX 9000/819
AZIMUT-66.00S-E

VALEUR DES NOMBRES DE LOVE :
ORDRE 2 H=.6206 L=.0904
ORDRE 3 H= .289 L= .015
E 98 95 129/95 3 8 95 421/95 515 95 622/95 7 4 95 728/95 817 95 9 8/951026
E 98 951120/951230 96 221/96 4 9 96 414/96 420 96 831/9610 8 961014/9611 5
E 98 9611 9/961213 961227/961231

TIME INTERVAL 703.5 DAYS 8592 READINGS 12 BLOKS EFFICIENCY 0.51

WAVE GROUP ARGUMENT	N	WAVE	ESTIMATED AMPL.	R.M.S.	AMPL. FACTOR	R.M.S.	PHASE DIFF.	R.M.S.	RESIDUE AMPL.	PHASE
127.-129.	11	SIGMA1	0.53	0.35	2.6993	1.7492	41.538	37.157	0.41	60.1
133.-136.	20	Q1	0.53	0.34	0.4292	0.2736	-20.723	36.553	0.76	-165.6
137.-139.	10	RO1	0.20	0.31	0.8660	1.3296	35.500	87.962	0.14	119.9
143.-145.	16	O1	1.92	0.32	0.2972	0.0489	1.150	9.431	4.49	179.6
152.-155.	15	NO1	0.49	0.33	0.9699	0.6490	85.579	38.275	0.67	133.2
161.-163.	10	P1	1.16	0.26	0.3872	0.0876	21.484	12.934	1.77	166.6
164.-164.	3	S1	0.61	0.37	8.5117	5.2328	-177.607	35.220	0.67	-179.2
165.-168.	20	K1	2.42	0.30	0.2663	0.0328	23.341	7.071	4.80	170.4
175.-177.	14	J1	0.62	0.33	1.2187	0.6429	-85.216	30.198	0.77	-126.8
184.-186.	11	OO1	0.57	0.56	2.0638	2.0299	-6.000	56.480	0.30	-11.5

STATIC VALUE 17.1334 11.83 L/H=0.1457

GROUP	SYMBOL	AMPLITUDE	PHASE	RATIO L/H OBS.	MSE.	THEOR.
66- 81	O1	5.0923	12.98	0.1550	0.0745	0.1466
176-186	OO1	35.3595	5.83	0.0860	0.6706	0.1451

WAVE GROUP ARGUMENT	N	WAVE	ESTIMATED AMPL.	R.M.S.	AMPL. FACTOR	R.M.S.	PHASE DIFF.	R.M.S.	RESIDUE AMPL.	PHASE
233.-236.	10	2N2	0.15	0.29	1.3627	2.6863	43.082	113.206	0.10	90.3
237.-23A.	10	MU2	0.30	0.28	2.2984	2.1427	73.974	53.289	0.29	99.4
243.-245.	13	N2	0.14	0.27	0.1772	0.3361	68.812	108.786	0.78	170.0
246.-248.	11	NU2	0.17	0.27	1.1280	1.7318	-32.047	88.103	0.09	-94.2
252.-258.	26	M2	3.86	0.25	0.9066	0.0578	19.202	3.655	1.41	115.8
265.-265.	9	L2	0.14	0.22	1.1571	1.8353	22.240	90.881	0.05	80.8
267.-272.	5	T2	0.86	0.26	7.3842	2.2152	39.948	17.064	0.77	45.5
273.-273.	4	S2	2.04	0.26	1.0284	0.1333	39.751	7.535	1.37	107.7
274.-277.	12	K2	1.11	0.33	2.0608	0.6143	48.062	17.088	0.85	76.2

STATIC VALUE 4.6927 -70.17 L/H=0.1457

GROUP	SYMBOL	AMPLITUDE	PHASE	RATIO L/H OBS.	MSE.	THEOR.
271-296	M2	4.2544	-50.97	0.1217	0.0047	0.1457
302-310	L2	5.4300	-47.93	0.1178	0.1198	0.1457

WAVE GROUP ARGUMENT	N	WAVE	ESTIMATED AMPL. R.M.S.		AMPL. FACTOR	R.M.S.	PHASE DIFF.	R.M.S.	RESIDUE AMPL.	PHASE
327.-375.	17	M3	0.11	0.10	8.6966	8.1985	-111.367	54.112	0.11	-117.2

STANDARD DEVIATION D 14.74 SD 14.73 TD 6.15 10E-9

QUALITY FACTORS : Q1= 0.7 Q2= 1.8
RESIDUALS ARE GIVEN IN THE TRUE AZIMUT
O1/K1 1.1161 1-O1/1-K1 0.9579 M2/O1 3.0503
CENTRAL EPOCH TJJ= 2450098.0

Comparison of Observed and Predicted Tidal Parameters

The "residue" given in the last column of tables 1 to 5 is computed as the vectorial difference between the observed tidal vector and a model using values h= 0.6206 and l= 0.0904.

For all components S2 is systematically higher than the other waves. Here also we can suspect the air pressure influence.

The discrepancy in amplitudes for the NS and –22.5°N instruments is at the 5-15 percents level for the main waves except for K1 NS. It should be noted the exceptional perturbation on S1 for this component. The discrepancy in phases reaches a maximum of six degrees.

Strong anomalies are registered in east-west component especially for the semi-diurnal waves where we should observe normally very low tidal amplitudes. It reflects probably the installation condition of the instrument as we get strong cavity effect when the instrument is fixed to the wall of a gallery. As we see the installation on the floor along the axis of the gallery was better.

The L/H ratios have been computed for the instrument with azimuth –22.5°. They are very close to the theory for all the semidiurnal waves except S2. In the diurnal band the values are systematically too low and the liquid core resonance can be hardly seen.

For the 66°N direction the observed main semi-diurnal wave M2 is close to the model in amplitude but with a large phase difference. The tidal factors are very low in the diurnal band. For the other component (-24°N) a negative anomaly is observed for all the waves of the tidal spectrum. It reaches from 10 to 30 percents for the semi-diurnal waves. It may be connected with the installation condition of this instrument as the end mirrors are installed in a small cavity in the gallery wall.

As we shall see in the next paragraph, the best results for laser instrument was obtained for differential strain. In this case we obtain for M2 a discrepancy of 8% in amplitude and 20^0 in phase.

The computed L/H ratios are not reliable for the component -24°N. An internal test in the program cancelled their computation for most of the waves. Only some strange results emerged such as L/H=0.23(diurnals). The results are slightly better for the other component.

Strain difference

The best results for the laser system have been observed for differential strain as in this case we obtain the best elimination of the air pressure influence. We used for tidal analyses of strain difference between two orthogonal directions the version "0" (gravity) of the ETERNA analysis programs with with a convenient renormalisation to convert it to strain evaluation i.e. potential divided by g (absolute gravity) and by R (radius in the point of the observation).

As known [7] for strain in two directions of azimuth $a1$ and $a2$ we have:

$$e_{d1} = \cos^2 a1 \cdot e_{\theta\theta} + \sin^2 a1 \cdot e_{\lambda\lambda} + \cos a1 \cdot \sin a1 \cdot e_{\theta\lambda},$$

$$e_{d2} = \cos^2 a2 \cdot e_{\theta\theta} + \sin^2 a2 \cdot e_{\lambda\lambda} + \cos a2 \cdot \sin a2 \cdot e_{\theta\lambda},$$

We have for strain difference:

$$\Delta e = e_{d1} - e_{d2}$$

$$= e_{\theta\theta} \cdot (\cos^2 a1 - \cos^2 a2) + e_{\lambda\lambda} \cdot (\sin^2 a1 - \sin^2 a2) - e_{\theta\lambda} \cdot (\cos a1 \cdot \sin a1 - \cos a2 \cdot \sin a2)$$

When the first direction is perpendicular to the second one:

$a2 = a1 + 90°$

and we can use only one angle $a1 = \alpha$ to express the strain difference:

$\Delta e = (e_{\theta\theta} - e_{\lambda\lambda}) \cdot (\cos^2\alpha - \sin^2\alpha) - 2\, e_{\theta\lambda} \cdot \sin\alpha \cdot \cos\alpha$

$= (e_{\theta\theta} - e_{\lambda\lambda}) \cdot \cos 2\alpha - e_{\theta\lambda} \cdot \sin 2\alpha$

For the different tidal waves we have:

Sectorial waves –

$e_{\theta\theta} = [h + 2((1-2\sin^2\theta)/\sin^2\theta) \cdot l] \cdot J_2/a \cdot g$

$e_{\lambda\lambda} = [h - 2((1+\sin^2\theta)/\sin^2\theta) \cdot l] \cdot J_2/a \cdot g$

$e_{\theta\lambda} = 4l[(\cos\theta / \sin^2\theta) \cdot \tan 2H] \cdot J_2/a \cdot g$

Tesseral waves -

$e_{\theta\theta} = (h - 4l) \cdot T_2/a \cdot g$

$e_{\lambda\lambda} = (h - 2l) \cdot T_2/a \cdot g$

$e_{\theta\lambda} = -2l \cdot (tgH/\cos\theta) \cdot T_2/a \cdot g$

where h and l are tidal number, J_2 and T_2 - tidal potential, a - radius of Earth, g – gravity, θ - colatitude, H - hour's angle.

Using these formulas for computing the strain difference, we get

Sectorial waves

$\Delta e_2 = \cos 2\alpha \cdot (e_{\theta\theta} - e_{\lambda\lambda}) - \sin 2\alpha \cdot e_{\theta\lambda} =$

$\{[2l \cdot \cos 2\alpha \cdot (2 - \sin^2\theta) / \sin^2\theta)] - [4l \cdot \sin 2\alpha \cdot (\cos\theta / \sin^2\theta) \cdot \tan 2H]\} \cdot J_2/a \cdot g$

Tesseral waves

$\Delta e_1 = \cos 2\alpha \cdot (e_{\theta\theta} - e_{\lambda\lambda}) + \sin 2\alpha \cdot e_{\theta\lambda} = \{(-2l \cdot \cos 2\alpha) + [2l \cdot \sin 2\alpha \cdot (tgH/\cos\theta)]\} \cdot T_2/a \cdot g$

After the calculation we obtain the theoretical values for amplitude factor and phase :

Sectorial waves

Amplitude factor $F2 = (2l/\sin^2\theta) \cdot \sqrt{[(2\cos\theta \cdot \sin 2\alpha)^2 + \cos^2 2\alpha \cdot (2 - \sin^2\theta)^2]}$

Phase $\Delta\varphi 2 = -\text{arctg}[2\tan 2\alpha \cdot \cos\theta / (2 - \sin^2\theta)]$

Tesseral waves

Amplitude factor $F1 = [2l/(\cos\theta)] \cdot \sqrt{(\cos^2 2\alpha \cdot \cos^2\theta) + \sin^2 2\alpha}$

Phase $\Delta\varphi 1 = \text{arctg}\,[\tan 2\alpha / \cos\theta)]$

After the calculation with Talaya parameters: $\alpha = -24°$N and the latitude $\phi = 51.68°$N we got:

F1 = 1.8197.l; $\Delta\varphi 1 = -54.76°$,

F2 = 8.2711.l; $\Delta\varphi 2 = 42.83°$

Taking tidal number l = 0.0904 we should obtain:

F1 = 0.1645 with a phase -54.76°;
F2 = 0.7477 with a phase 42.83°.

When we use the tidal program for gravity calculation we can adopt these values as reference values or compute apparent values of number l. We computed differential strain as well for the whole period(Table 6) as for consecutive three months periods. The results for M2 in consecutive three months series(Table 7) are very stable in amplitude as variations are within the error bars (0.5%). We got temporal variations in tidal phase up to 5° with error bars 0.2-0.4°.

Table 6
Comparison of predicted and observed tidal strain parameters:
Difference of the component (-24°N) and the component (+66°N)

Wave	Ampl. Observ (nstr)	Ampl. Factor Predict	Ampl. Factor Obser.	Apparent Value of L	Ampl. Factor Error	Phase Predict	Phase Observ	Phase discrep	Phase error
O1	3.256	0.1675	0.2154	0.118	0.0045	-54°.76	-62°.12	-7°.36	0°.26
P1	1.499	0.1675	0.2132	0.117	0.0065	-54°.76	-63°.77	-9°.01	0°.38
K1	3.705	0.1675	0.1719	0.094	0.0025	-54.76	-73°.62	-18°.86	0°.14
N2	1.625	0.7477	0.7471	0.090	0.0229	42°.83	59°.30	17°.47	1°.31
M2	9.991	0.7477	0.6915	0.084	0.0037	42°.83	64°.55	21°.72	0°.21
S2	5.173	0.7477	0.7696	0.093	0.0091	42°.83	65°.79	22°.96	0°.52

Table 7 .
Analyses on 3 months consecutive periods for laser strain difference between (-24°) and 66° beams for M2 wave.

Period	Ampl.factor	Ampl.Factor Error	Phase in degree	Phase error
01-03.1995	0.7046	0.0054	61.08	0.31
04-06.1995	0.6917	0.0099	63.31	0.57
07-09.1995	0.7039	0.0051	65.72	0.29
10-12.1995	0.7034	0.0044	63.03	0.25
01-03.1996	0.7078	0.0040	63.73	0.23
04-06.1996	0.7077	0.0081	63.99	0.46
07-09.1996	0.6940	0.0053	64.86	0.30
10-12.1996	0.7039	0.0039	65.91	0.22
01-03.1997	0.6826	0.0063	66.65	0.36
04-06.1997	0.6590	0.0087	64.21	0.40
07-09.1997	0.6915	0.0037	64.55	0.21
10-12.1997	0.6959	0.0060	63.31	0.34
01-03.1998	0.6771	0.0046	63.11	0.26
04-06.1998	0.6966	0.0073	61.66	0.42
07-09.1998	0.6628	0.0230	61.89	1.32
10-12.1998	0.6576	0.0102	58.84	0.58

Conclusions

For the wave with the strongest amplitude, the discrepancies in amplitude for every component are shown in Table 8. We can see a maximum discrepancy of 5% for the quartz tube instruments corresponding to the associated internal error level. For the invar rod instrument a systematic amplification of 14% is apparent. For the laser instrument we have the residual influence of air pressure along the light path. The amplitude factor of the component in the azimuth of the gallery is reduced of 30% but the attenuation is only 10% in the 66°N azimuth for the strain difference between these two components. The temporal variation of difference strain amplitude during period 1995-1998 was near the error level (0.5 %). For the phase we observed 3 to 5 degrees of variation with an associated error level of 0.2-0.4 degree. It may be connected with the seismic activity of the region.

The discrepancies are connected with instrumental and cavity effects. Maybe boundary condition and geological structure effect can play an effective role as we have the main Sayan fault 3 km to the north , extending in a EW direction.

Table 8

Observed parameters for the strongest wave for different instruments and directions

Type of Instrument	Baselength (m)	Azimuth N to E	Wave	Obs. Ampl. (nstrain)	Reference	Observed Ampl. Fact.	RMS Error
Quartz	1.3	North-South	M2	10.81	1.0000	1.0077	0.0944
Quartz	2.0	East-West	O1	6.42	1.0000	0.9471	0.0456
Invar	8.3	-22.5°	M2	12.36	1.0000	1.1364	0.0348
Laser	25.0	-24.0°	M2	6.90	1.0000	0.7083	0.0259
Laser	25.0	+66°	M2	3.86	1.0000	0.9066	0.0578
Laser difference	25.0	(-24°) – 66°	M2	9.99	0.7477	0.6915	0.0037

Acknowledgement

Our cooperation work is supported by the Scientific and Technical Agreements between Belgium and the Russian Federation on one hand and by the Russian Fund for Scientific Research (98-05-65227, 98-05-65278) on the other hand. The authors wish to thank P. Melchior for his interest to this work.

References

1. Timofeyev.V.Yu., Saritcheva You.K., Panin S.F., Anisimova L.V. et al. Effet dynamique du noyau liquide dans les observations de marees terrestres dans les stations de Siberie (Novosibirsk, Talaia, Irkoutsk). // J.Marees Terrestres, Bull.D'Informations, Belgium, 1994, n 120. pp.9344-9354.
2. Semibalamut V.M., Fomin Yu.N., Timofeev V.Yu. et al. Tidal parameters from the results of laser deformografic measurements in the South-West part of the Baikal rift, Talaya station. // J.Marees Terrestres, Bull.D'Informations, Belgium, 1995, n 123. p.9355-9364.
3. Timofeev V.Y. et al. Experimental models for the Earth's crust deformations in the south-west of the Baikal Rift Zone, Geologii i Geoficika, V. 40, 3, 1999, 387-394.
4. Timofeev V., Ducarme B., Van Ruymbeke M. Preliminary results of µDAS system for tilt strain monitoring at Baikal rift. Comptes-Rendus, 86th JLG meeting, M.Bonatz editor, Institut für Theoretische Geodäsie, Universität Bonn.

5. Dehant, V. Tidal parameters for an inelastis Earth. Physics of the Earth and Planetary Interior, vol. 49, 97-116, 1987.
6. Harrison, J.C. Cavity and topographic effects in tilt and strain measurements. Journal of Geophysical Research, vol.81, 319-328, 1976.
7. Melchior P. Physics and dynamics of planets. Pergamon Press.Oxford- London-Edinburgh-New York-Paris-Frankfurt, 1976, pp.483

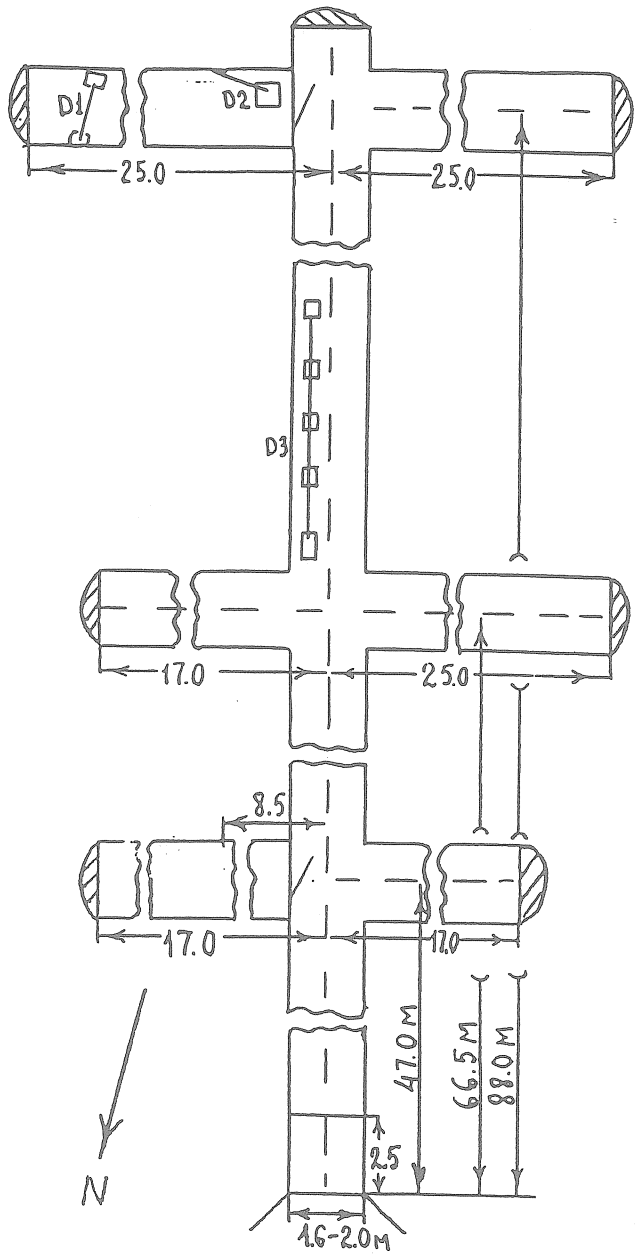

Figure 1
Sketch of the Talaya Underground Laboratory
D1 NS 1.3m, D2 EW 2.0m, D3 22.5° N 8.3m

MODELLING OF GRAVITATIONAL EFFECTS DUE TO NONSTANDARD ATMOSPHERIC CONDITIONS

Martin LEDERER

Department of Levelling and Gravimetry, Land Survey Office, Czech Republic

Antonín ZEMAN

Department of Advanced Geodesy, Czech Technical University, Prague, Czech Republic

Summary : Models for estimating the gravitational effects of the Earth's atmosphere on gravity observations are defined. The models from the simplest Bouguer plate to the numerically more complicated models of the spherical cap, divided into the layers in which density is distributed according to height and, simultaneously, by a grid defined by geographical coordinates. Data from the European Center for Medium-Range Weather Forecasts (ECMRWF) was used. The values, computed from the investigated models, were compared with the residual values of gravity acceleration after elimination of Earth's tides, polar motion (free nutation) and other trends from the records of continual gravity data of the tidal gravimeter at the Geodetic Observatory Pecný (Ond□ejov). The comparison is evidence that the Bouguer plate model with barometric pressure values, observed only at the places where gravity acceleration is observed, is sufficient. The correlations, however, indicate some advantages of the more sophisticated models.

1. INTRODUCTION

The atmosphere, surrounding the Earth, is a part there of from the point of view of gravitational effects. All geodetic observations, carried out within the atmosphere, are influenced both by direct gravitational effects of the atmosphere and by indirect (deformational) effects caused by variable loading of the Earth's surface by masses different from the masses of a normal atmosphere.

The atmosphere for which the values of the air temperature, pressure and density are expressed for individual heights above sea level by mean values, is referred to as the Standard Atmosphere. Static models of the density distribution of the atmosphere were proposed by different institutions, e.g., the C.I.R.A. model (Cospar International Reference Atmosphere) or U.S.S.A. (U.S. Standard Atmosphere) . Models are designed on the basis of observations and theoretical premises.

The effects of variable loading by the atmosphere were modelled by different authors using models ranging from extremely simple to considerably complicated, e.g., *Van Dam and Wahr (1987), Sun H.P. et al. (1995), Kostelecký and Zeman (1997).*

The deformations of the Earth's surface and gravity variations due to the variable part of the atmosphere are mainly computed for the surface of a spherical elastic Earth by performing a convolution between the real local or regional barometric pressure and Green functions according to *Farrell (1972).*

The problem arises when we want to check the derived models. The best method is to compare model values with observations. For this purpose we can use the values of gravity acceleration from the tidal station at the Geodetic Observatory Pecný (Ond□ejov) after eliminating tidal variations, the general drift of the observed values and variations caused by polar motion. Correlations between both values can then be used to determine the optimum variant of the model for computing the effects of anomalous atmospheric formations on the observed values of the gravity acceleration.

2. MODELS OF ATMOSPHERE

Bouguer plate model

To compute the direct gravitational effects of near atmospheric masses, one can use the model of an infinite cylindric plate with constant density σ_A and height b_A. Its gravitational effect is given as $\delta g = 2\pi G \sigma_A b_A$ (Bouguer plate), where G is the gravitational constant. If we also apply the relation for hydrostatic pressure of the atmosphere $p_N = \sigma_A g b_A$ ($p_N = 101\,325$ Pa), where g is the gravity acceleration, the local gravitational effect comes out as

$$\delta g_N^1 = 2\pi G p_N / g . \qquad (1)$$

For G = 6.672 x 10^{-11} kg^{-1} m^3 s^{-2} and g = 9.806 m s^{-2} the gravitational effect of pressure anomaly $\Delta p = p - p_N$ = 100 Pa = 1 hPa (1mbar) is

$$\delta g_N^1 = -0.43 \times 10^{-8} m\, s^{-2} / 1hPa . \qquad (2)$$

The minus sign expresses the decrease of the observed value of gravity acceleration for positive value of the atmospheric masses above the point where the gravity acceleration is observed.

An additional change of gravity acceleration is caused by elastic deformation of the Earth's surface due to its loading by atmospheric masses. If the masses are directly above the point at which the effects are being computed, it is necessary to reduce the Green functions of Farrell's solution to Lamé's parameters for the very surface layers of the given Earth model. This yields approximate value $\delta g_E^1 = 0.04 \times 10^{-8} m\, s^{-2} / 1hPa$. The total change of the gravity acceleration from the modelling with the Bouguer plate is then

$$\delta g^1 = -0.39 \times 10^{-8} m\, s^{-2} / 1hPa . \qquad (3)$$

Spherical cap model

This model takes into consideration, in contrast to the Bouguer plate model, the curvature of the Earth surface (the atmosphere is then modelled by a spherical layer).

To find the direct effect, we used the elementary relation for the intensity of the gravitational field but modified to read

$$\delta g_N^2 = -G \int_{m'} \frac{dm_i'}{D_i^2} \cos\alpha_i \quad , \qquad (4)$$

where quantities D_i (distances between the elements of mass dm_i and point P, where the effects are being computed) and α_i ($\cos\alpha_i$ are the projections of the intensity vectors on to the geocentric radiusvector of point P) are shown in Fig.1. and are defined by the following two relations using geocentric spherical coordinates ρ, Φ, Λ.

$$D_i = \left(R^2 + \rho_i^2 - 2R\rho_i \cos\vartheta_i\right)^{1/2} , \qquad (5)$$

$$\cos\alpha_i = \frac{\rho_i^2 - D_i^2 - R^2}{2D_i R} . \qquad (6)$$

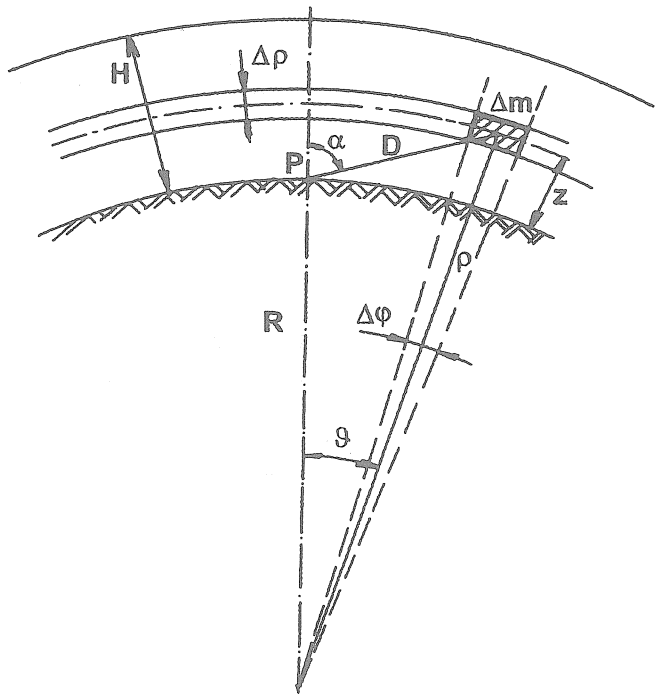

Fig.1.

In Eqs. (5) and (6) $\rho_i = R + z_i$ and $\vartheta_i = \sin\Phi \sin\Phi_i + \cos\Phi \cos\Phi_i \cos(\Lambda - \Lambda_i)$. The computation will be carried out as the sum of the effects of the finite elements of mass $\Delta m_i = \sigma_i \Delta\tau_i$, where $\Delta\tau_i$ are the finite elements of the volume which must be defined individually for a particular configuration. The density of the atmosphere can be modelled in two ways:

a) by a constant for the whole layer using the relation

$$\sigma_i = \Delta p_i / (gH), \qquad (7)$$

b) by a relation which takes into account that the barometric pressure decreases with increasing height. This relation can be expressed as an exponential function of the of density varying with height

$$\sigma_i = \sigma_0 e^{-z_i/H}, \qquad (8)$$

where σ_0 is the density reduced to the Earth's surface. H and z_i are symbols for the height of the whole layer and the heights of the individual layers, respectively – see Fig. 1.

The elastic effect δg_E^2 of mass Δm_i at angular distance ϑ_i from point P is given by *the Farrell (1972)* solution. In the computations we interpolate the tabulated values of the Green functions $G(\vartheta_i)$ and values Δm_i, now located at discrete points on the Earth's surface (z_i = 0)

$$\delta g_E^2 = \frac{\Delta m_i G(\vartheta_i)}{10^{18} R \vartheta_i}. \qquad (9)$$

Expression (9) is normalized by the numerical value of the term $10^{18} R\vartheta_i$ (R = 6.371 x 10^6m, ϑ_i in radians), hence the result is in units of m s^{-2}.

Models of the spherical cap in which the barometric pressure depends on height its surface is divided into a grid by geographical coordinates

To come even closer to reality we have used the air pressure data given in the $2.5^{\circ} \times 2.5^{\circ}$ grid of geographical coordinates (for practical computations we shall use data in the intervals from 10° to 80° in latitude and from -20° to 60° in longitude and with 12-hour time interval). The barometric pressure data for a grid of this extent are from the ECMWF (European Center for Medium-Range Weather Forecast). For the reason of data division we have used for the computation a modified spherical cap model which is not circularly symmetric but is represented by the area limited by geographical coordinates $\left(\varphi_{\min}, \varphi_{\max}; \lambda_{\min}, \lambda_{\max}\right)$.

The formulas will be the same as for the previous spherical cap model, only the following formula is used to compute the mass elements – see Fig. 2.

$$\Delta m_i = \sigma_i \rho_i^2 \cos\varphi_i \Delta\rho_i \Delta\varphi_i \Delta\lambda_i \quad , \Delta\rho_i = \Delta h_i \, . \qquad (10)$$

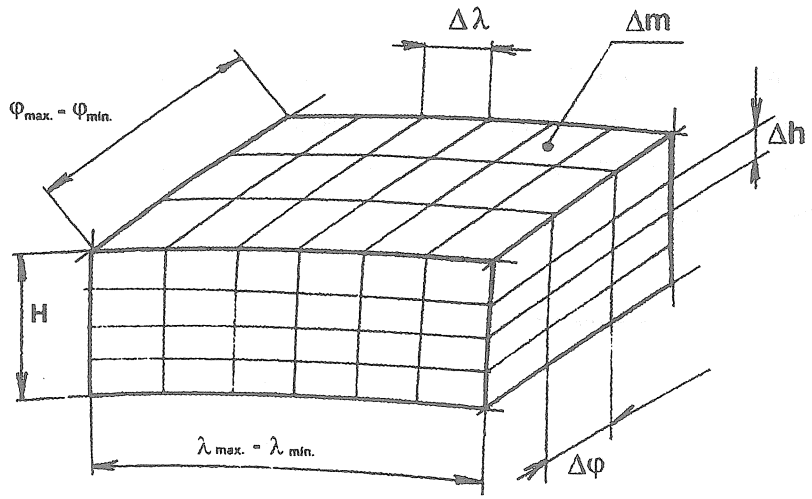

Fig. 2.

Densities σ_i are now computed for each mass element separately. Using the relation between density and barometric pressure, we can compute the densities from the interpolated values of the observed barometric pressure given by the ECMWF data. The resulting direct gravitational effect is again given by the formula

$$\delta g_N^3 = -G \frac{\Delta m_i}{D_i^2} \cos\alpha_i \, . \qquad (11)$$

The indirect effect is computed in the same way as for the previous spherical cap model.

3. RESIDUAL GRAVITY ACCELERATION AFTER ANALYSES OF TIDAL GRAVIMETER RECORDS

The tidal gravimeter Askania Gs 15 No. 228 (Geodetic Observatory Pecný) provides digital records of gravity acceleration observations at 1-hour intervals. The observations are, however, affected by different influences which have to be removed to be able to compare them with the computed model values of the gravity acceleration variations caused by variable barometric pressure.

The main effects are due to the Earth's tides and gravimeter drift. We can also judge the significance of eliminating other influences such as ocean tides and polar motion (free nutation).

After introducing all the corrections, we can assume that the most significant residual effect is (except for errors of observations and other negligible effects) the effect of the varying distribution of atmospheric masses.

■ Effect of the Earth's tides

The effect of tidal waves of synthetic tides was removed by theoretical reductions. Computations were made using the special software of the GO Pecný.

■ Gravimeter drift

The gravimeter drift was approximated by a polynomial of optimum degree for a given time interval of observations and then removed by reductions from the observed values. Fig. 3. shows the analyzed time interval (1.7.1994 – 27.11.1994) where the values were cleared of tidal effects and approximated by a 3rd degree polynomial.

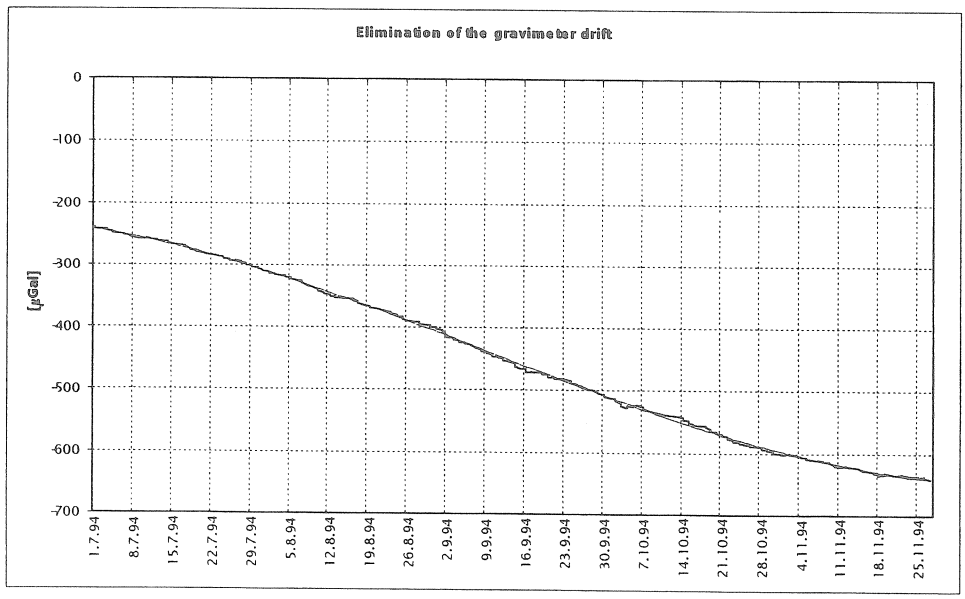

Fig. 3.

Polar motion (free nutation)

The effect was removed with the help of the following formula

$$\delta g_P = -18.9 \sin 2\vartheta \left(x \cos\lambda - y \sin\lambda \right) , \qquad (12)$$

where x, y are the pole coordinates in arc seconds , φ, λ are geographic coordinates of the point where the effect is being computed, $\vartheta = 90 - \varphi$. The coordinates of the CIO pole were taken from the IERS Bulletin. The resulting values are in $\mu Gal \left[10^{-8} m\, s^{-2} \right]$.

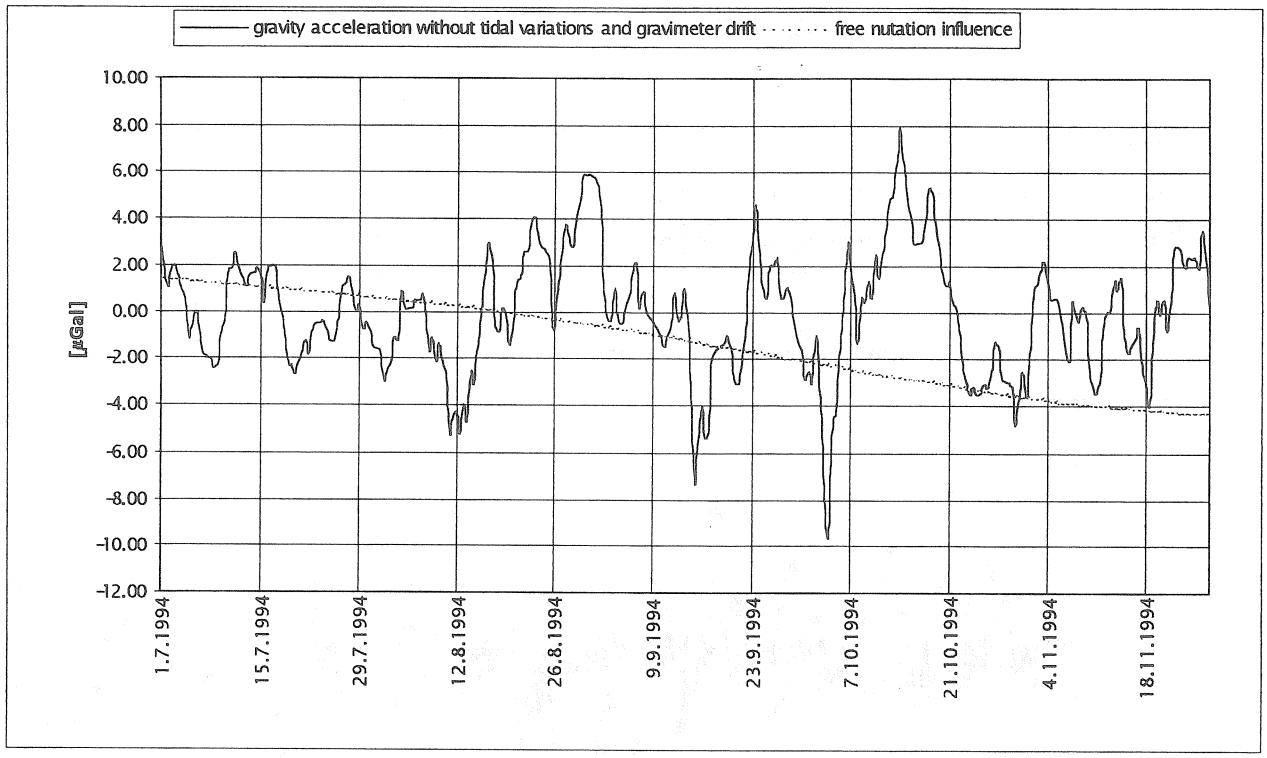

Fig. 4.

4. CORRELATIONS BETWEEN THE RESIDUAL VALUES OF GRAVITY ACCELERATION AND THE VALUES COMPUTED FROM DIFFERENT MODELS OF THE ATMOSPHERE

Correlation coefficients were computed for comparing the individual models with the observed (and reduced) values. The slopes of the regression lines were then computed. These values express the dependence of the variations of the gravity acceleration on the variations of barometric pressure. We used 146 days of observation i.e. 292 data altogether. The models are compared with the "observed" values in Table 1 and Fig. 5.

Table 1.

Model	Correlation r	Regression $\mu Gal / hPa$
Bouguer plate	0.45	0.39
Spherical cap – pressure varying with height	0.45	0.24
Spherical cap – pressure varying with height and position	0.62	0.23

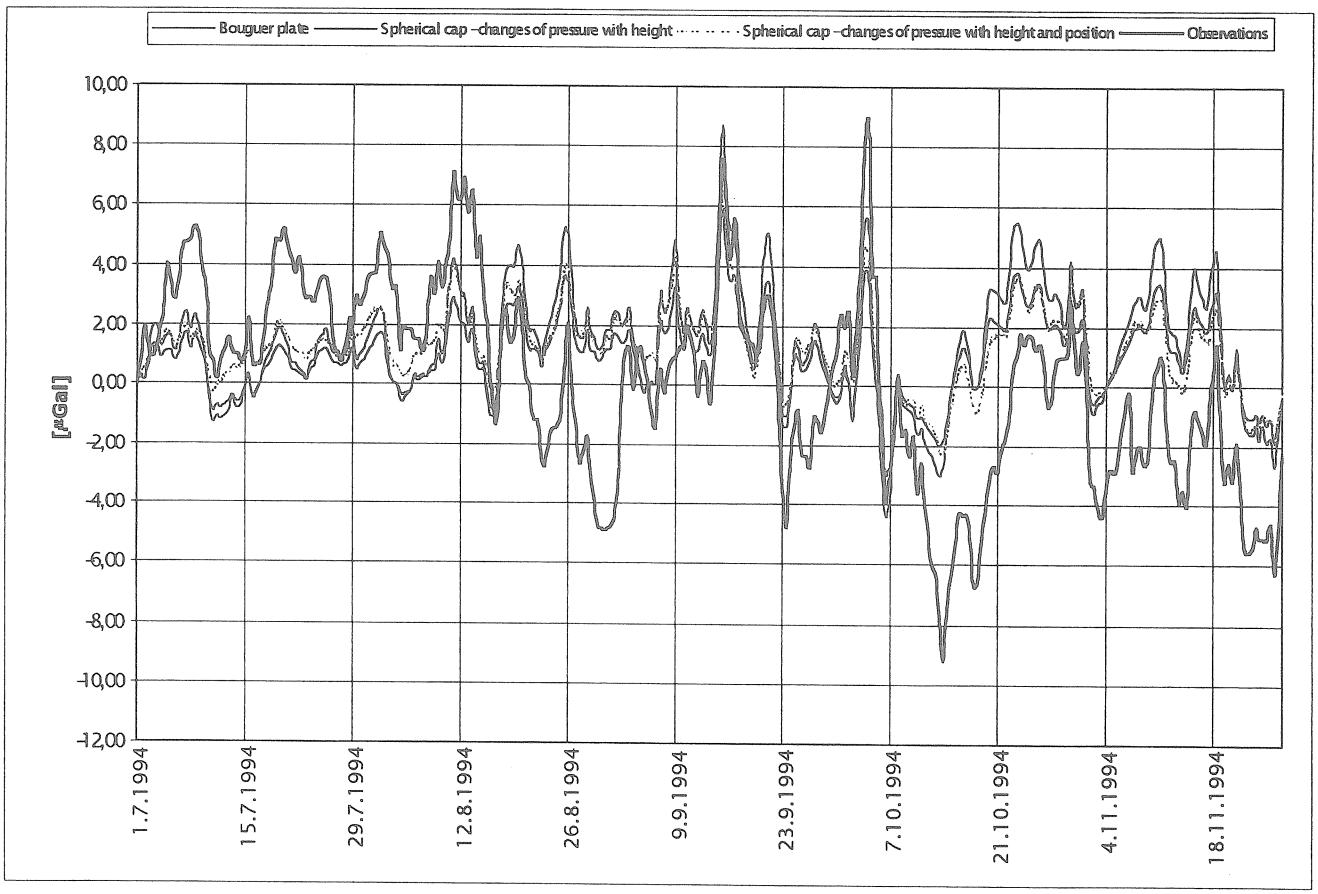

Fig. 5.: Comparisons of the models with "observed" values

The same comparisons for shorter time interval are in Fig. 6.

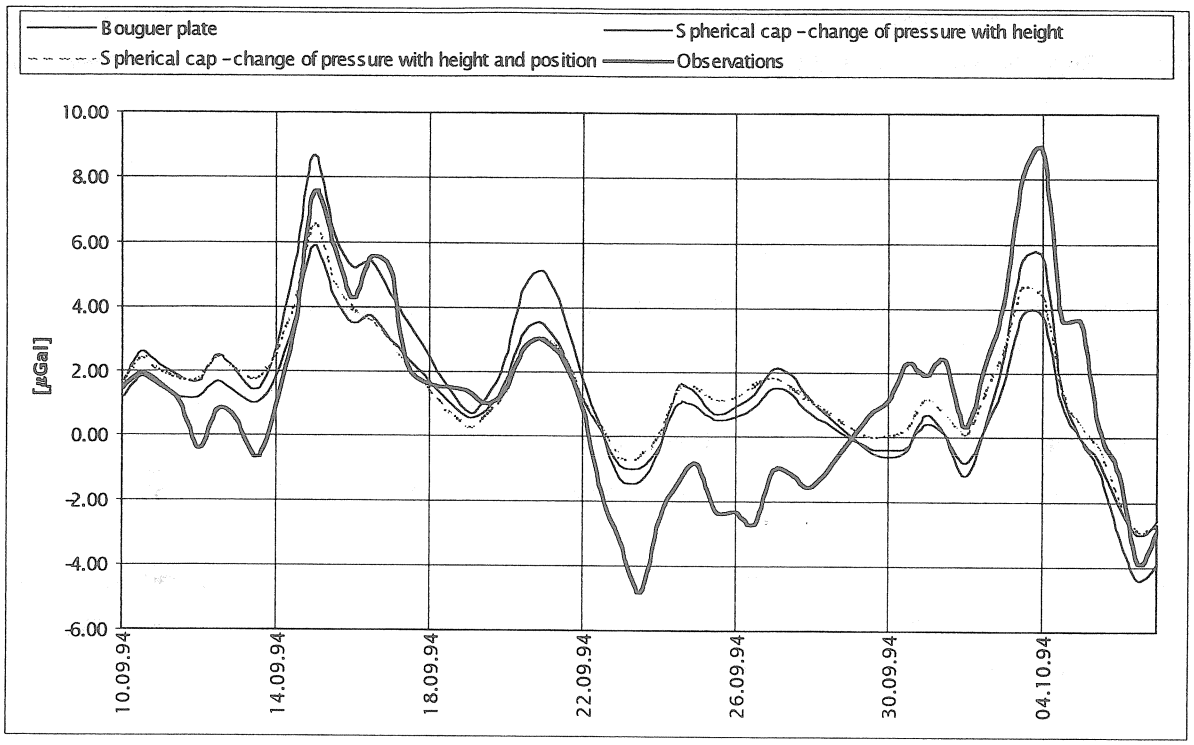

Fig. 6.: Comparisons of the models with "observed" values – detail

5. CONCLUSION

We have derived some mathematical models which can serve to compute the gravitational effects of nonstandard atmospheric conditions. The Bouguer plate model is very simple from the mathematical point of view. Other models come closer to reality. This means they take into consideration the real "shape" of the atmosphere, the variations of pressure with height and, in the last model, we are not restricted only to local barometric pressure but we have used data from a grid of larger extent. The computed results can then be compared with the real "observed" values.

Having compared the resulting values and correlation coefficients of all solutions, we can conclude that the models are not significantly different. Not even the model using interpolation in the grid of pressure data of larger extent represents a considerable improvement although the correlation has increased slightly. This supports the conclusion that the local anomalous barometric pressure has the greatest influence, and that, in most cases, the information on barometric pressure variations in a wider vicinity of the point where the effects are to be computed, does not need to be used.

For practical purposes, the Bouguer plate is the best model which is, moreover, very simple for computations. It is clear from this paper that the results from this model are very near to the real values of the effect.

Acknowledgments: The authors wish to thank Prof. Kostelecký from the CTU in Prague for his valuable help with exploiting the ECMWF data. This work was supported by the Grant Agency of the Czech Republic, Grant No. 103/99/1633. This work was also supported by the Research Project No.7 of the Faculty of Civil Engineering, Czech Technical University in Prague.

References

[1] Farrell W.E.,1972: Deformation of the Earth by Surface Loads. Rev. of Geoph. and Space Physics,10, 761 – 797.

[2] Van Dam T.M., Wahr J. M., 1987: Displacements of the Earth's Surface Due to Atmospheric Loading: Effects on Gravity and Baseline Measurements. J. Geophys. Res.,92,1281 – 1286.

[3] Sun H.P., Ducarme B. and Dehant V.,1993:Preliminary Investigations of the Atmospheric Pressure Effect on Vertical Displacement and Gravity Observations. B.I.M. (Marees Terrestres, Bulletin D'Informations), No. 114, 8334 – 8362.

[4] Sun H.P., Ducarme B. and Dehant V.,1995: Effects of the Atmospheric Pressure on Surface Displacements. J. Geodesy, 70, 131 – 139.

[5] Zeman A., 1978: Estimate of the Effect of Changes of Atmospheric Pressure on the Results of Levelling. Studia geoph. et geod.,22, 241 – 247.

[6] Kostelecký J., Zeman A., 1997: Study of the Influence of the Indirect Effect of Ocean Tides and of the Direct Deformation Effect of the Atmosphere on the Results of GPS Observations. Studia geoph. et. geod.,41, 93 – 102.